

Analytical Study of Light Propagation in Highly Nonlinear Media

Inaugural-Dissertation

zur Erlangung der
Doktorwürde der Naturwissenschaften
(Dr. rer. nat.)

vorgelegt beim Fachbereich Naturwissenschaften
der Universität Kassel

von

Larisa Tatarinova

aus Barnaul, Russland

Juni 2009

Supervisor Prof. Dr. Martin E. Garcia

Day of disputation is 8-th of July 2009

Contents

1	Introduction	2
2	Model equations	7
2.1	Propagation equations	7
2.2	Bound electron response	9
2.3	Free electron response	11
2.4	Back to the propagation equations. Nonlinear Schrödinger equation (NLSE)	14
2.5	Properties of the nonlinear pulse propagation equation	18
3	Model equations. The geometrical optics approximation.	22
4	Review of Analytical Results	27
4.1	Exact analytical solutions	27
4.1.1	Geometrical optics approximation	27
4.1.2	Exact solutions beyond the geometrical optic approximation .	28
4.2	Approximate Results. Quasi self-similar methods	32
4.2.1	Variational approach	32
4.2.2	Berge's variational approach	34
4.2.3	Fibich's quasi self-similar method	35
4.3	Renormalization group symmetry analysis	37
4.3.1	RGS results in (1+1) dimensions	37
4.3.2	RGS results in (1+2) dimensions	38
5	Renormalization group symmetry analysis. Exact solutions	41
5.1	Introduction	41
5.2	Renormgroup analysis: General scheme	43
5.3	Renormalization group solutions for the eikonal equations with a saturating nonlinearity	46
5.3.1	Recursion operators and Lie-Bäcklund symmetries of the second order	47
5.3.2	Invariant solutions	51

6	Approximate analytical results	57
6.1	Analytical solutions in case of (1+1) dimensions	58
6.1.1	An exact solution	59
6.1.2	Accuracy of the approximate solutions	59
6.1.3	Kerr nonlinearity	60
6.1.4	Power nonlinearity	61
6.1.5	Saturating nonlinearities	62
6.1.6	Two-terms nonlinearity	64
6.2	An example: influence of the Taylor series truncation	67
6.3	Propagation on the laser pulse with arbitrary initial intensity distribution	71
6.4	Generalization in (1+1) dimensions	73
6.5	Nonlinear models in (1+ ν) dimensions	74
6.5.1	Analytical solutions. Search for the best approximation	74
6.5.2	The parabolic beam profile	76
6.5.3	Gaussian beam profile. First consideration	76
6.5.4	Two-term nonlinearity	77
6.5.5	Gaussian beam profile. Second consideration	78
6.5.6	Power nonlinearity	79
6.5.7	Saturating nonlinearity	80
6.5.8	Two-term nonlinearity	80
6.6	Comparison with results of experiments and numerical simulations	82
7	Theoretical study of the fused silica ablation	86
7.0.1	Short review of the ablation results	86
7.0.2	Material processing below the diffraction limit with the help of the femtosecond laser pulse	89
7.0.3	Theoretical model	90
8	Conclusions	97
	Bibliography	99
	List of Publications	111
	Acknowledgments	113
	Erklärung	114
	Curriculum Vitae	115

Abstract

The present dissertation is devoted to the construction of exact and approximate analytical solutions of the problem of light propagation in highly nonlinear media. It is demonstrated that for many experimental conditions, the problem can be studied under the geometrical optics approximation with a sufficient accuracy. Based on the renormalization group symmetry analysis, exact analytical solutions of the eikonal equations with a higher order refractive index are constructed. A new analytical approach to the construction of approximate solutions is suggested. Based on it, approximate solutions for various boundary conditions, nonlinear refractive indices and dimensions are constructed. Exact analytical expressions for the nonlinear self-focusing positions are deduced. On the basis of the obtained solutions a general rule for the single filament intensity is derived; it is demonstrated that the scaling law (the functional dependence of the self-focusing position on the peak beam intensity) is defined by a form of the nonlinear refractive index but not the beam shape at the boundary. Comparisons of the obtained solutions with results of experiments and numerical simulations are discussed.

Chapter 1

Introduction

The problem of theoretical description of the light propagation in nonlinear media emerged in physics in the early 1960s. Already in experiments with first lasers such nonlinear effects as self-focusing and filamentation were discovered Refs. [38, 64], i.e. it was observed that the diameter of an intense laser light beam dramatically decreased upon propagation with the peak intensity strongly increasing. A first theoretical explanation of these effects was performed based on the assumption that the refractive index, representing the media response, becomes a function of light intensity Refs. [28, 3, 86]. Due to moderate light intensities available at that time, the material response could be modeled by the Kerr-type refractive index, that is a refractive index linearly depending on the laser beam intensity, $n(I) = n_0 + n_2 I$. If $n_2 > 0$, it leads to the spatial beam compression and its subsequent collapse at some point if the initial power of the beam exceeded a certain critical value. In the opposite case $n_2 < 0$ a beam broadening was predicted.

The effect of nonlinear self-focusing currently plays a key role in all scientific and technological applications related to the propagation of intense light beams [34] like material processing [35], environmental sciences [106, 30], femtochemistry in solutions [126], macromolecule chromatography [32], medicine [92] etc. Therefore, it is of great importance to have rather simple analytical formulae able to predict if the self-focusing takes place and if this is the case, its exact position.

The first results in this direction were obtained by Akhmanov *et. al.* in Ref. [4] from the exact solution of the eikonal equations for spatial boundary conditions and under the geometrical optics approximation. Later, an empirical expression for the nonlinear self-focusing position was derived by Marburger via fitting the results of extensive numerical simulations [86]. The latest analytical results were obtained by Kovalev in Refs. [68, 67], when analytical solutions to the light propagation equations were constructed making use of the renormalization group symmetry analysis. Subsequently, explicit analytical formulae for the self-focusing length were obtained.

Here we have to note that all exact analytical solutions obtained so far were

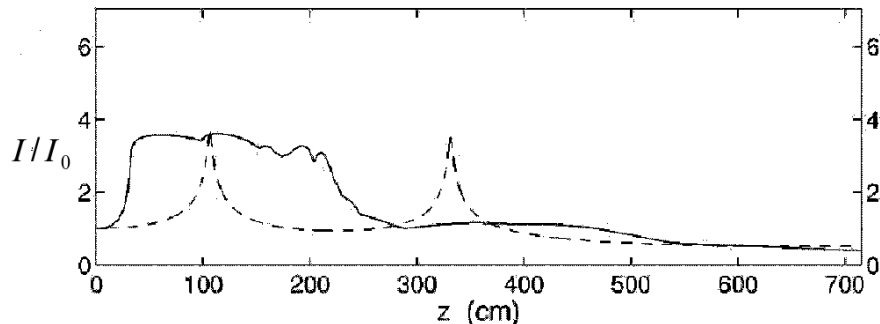


Figure 1.1: Normalized laser beam peak intensity versus the propagation distance from Ref. [12]. Solid curve is the result of a numerical solution of the light propagation equations; dashed curve represents a semi-analytical solution for this equations constructed on the basis of the variational approach.

constructed only for the Kerr's form of the refractive index. However, modern experimental pulse laser facilities allow one to achieve electric field intensities comparable with the intensity of the atomic field [21, 34, 30, 15] what allowed one to observe many new nonlinear optical phenomena. In particular, self-guiding versus collapse in air [11, 12], filament formation in fused silica [110, 116, 31], splitting of a filament into several ones [14], their stability and features of their interactions [119, 124] were investigated. The linear approximation to the function $n(I)$ turns out to be inadequate for a theoretical description of such experiments, and more complicated forms of the refraction index must be considered [56, 16, 20]. Unfortunately, up to now there were no solid analytical results obtained from exact or approximate analytical solutions of the light propagation equations with a highly nonlinear refractive index. All analytical deductions on the solutions behavior in case of a higher nonlinearity were made only on the basis of either some general estimates as in Refs. [66, 16], or an artificial assumption that the beam keeps its initial shape upon propagation and only the beam radius, phase and intensity amplitude are function of the propagation distance (so called variational approach). However, this assumption is too restrictive to provide a good accuracy what can be seen from a comparison between a numerical simulation and a solution obtained on the basis of the semi-analytical variational method from Ref. [12] presented in Fig. 1.1. Therefore, analytical expressions capable to accurately describe intensity distribution in case of the highly nonlinear media response are very desirable.

In the present dissertation we construct analytical solutions to the problem of light propagation in nonlinear media in case of arbitrary (higher order) nonlinear media response avoiding any artificial assumptions on the beam profile. In comparison to the semi-analytical methods used previously, the approach suggested in the dissertation allowed us to get explicit analytical expressions for the nonlinear self-focusing positions. These expressions are exact under the geometrical optics

approximation. Their accuracy can be easily controlled in contrast to the accuracy of the empirical Marburger formula and predictions of the variational approach.

The dissertation is organized as follows: In Chapter 2, mainly following Ref. [21, 15, 103], we discuss the derivation of model equations. A mathematical model commonly accepted nowadays for light intensities below 10^{14} W/cm² is considered. The obtained light propagation equation is usually referred to as a nonlinear Schrödinger equation (NLSE). We demonstrate the derivation of this equation starting from the wave equations and discuss possible approximations and ranges of their applicability. The basic model equation (2.51) still remains rather complicated from the mathematical point of view. Therefore, in the next Chapter 3, further possible simplifications of the model equations (2.51) are discussed. We demonstrate that in many physical situations the geometrical optics approximation is still capable of providing a good accuracy of the constructed solutions. The ranges of beam parameters for which the geometrical optics approximation remains valid are presented in Fig. 3.1.

In Chapter 4 the most widely known analytical results obtained so far in the field are collected. First, we present exact analytical solutions obtained by Akhmanov *et al.* in Refs. [3, 4] and Zakharov and Shabat in Ref. [125]. Another set of approximate analytical solutions constructed by Kovalev in Refs. [69, 68] on the basis of the renormalization group symmetries (RGS) analysis is also mentioned. We also discuss a case of boundary conditions of the special form, so called Townes profile, first found in Ref. [28]. This solution is very important due to the fact that before its collapse the beam reaches the intensity distribution given by the Townes formula (see e.g. Ref. [39]) and this solution also defines a critical power which is a minimum power necessary to provide the self-focusing of the beam. Unfortunately, all these accurate results were obtained for the Kerr form of refractive index only. For more complicated media response the situation changes dramatically: the majority of analytical results was obtained only making use of an artificial assumption about a fixed functional dependence of the intensity on the radius and phase of the beam. The crucial point of such an approach lies in the proper choice of a trial function (e.g. Eqs. (4.23, 4.30)). This problem is discussed in Chapter 4 as well.

In order to obtain exact analytical solutions for the light propagation equations with higher order nonlinear refractive index, a modern method of mathematical physics - the renormalization group symmetry (RGS) analysis was employed in the dissertation. This method was introduced into mathematical physics by Shirkov and Kovalev. Its outlines are presented in the Chapter 5 of the dissertation closely following the Ref. [102]. Making use of the RGS we construct an exact analytical solution to the light propagation equations with refractive index which is a saturating function of the electric field intensity. Properties of the obtained solution are discussed in details.

Unfortunately, the renormalization group symmetry analysis is not able to provide us with an exact solution for any physically interesting form of both the refractive index and the boundary conditions. Moreover, the RGS approach requires at least a basic knowledge of Lie symmetry analysis which usually does not constitute a part of university courses for physicists.

Therefore, in the present dissertation we formulated our own approach to the analytical investigation of the light propagation equations. It is outlined at the beginning of the Chapter 6. It does not require knowledge of any special mathematical technique or trial functions and is applicable to any nonlinear refractive index and boundary conditions. The basic result of this chapter is the solutions (6.5, 6.6) in (1+1) dimensions and solutions (6.71) in $(1+\nu)$ dimensions where $\nu \geq 2$. These solutions were obtained for initial Gaussian beam profile and arbitrary nonlinear refractive index whose contribution is via $\varphi \equiv \partial_I n(I)$. In Sec. 6.3, the solutions are constructed for an arbitrary initial beam profile in (1+1) dimensions and Kerr nonlinearity.

General analytical expressions obtained in this chapter enable us to study the light propagation in media described by various forms of refractive indices. In particular, the cases of power, saturating and polynomial nonlinearities are considered in detail. Based on our analytical solution we are able to deduce a general law Eq. (6.28) for intensity definition in a single light channel. This expression corrects the previous one (see e.g. reports [30, 15]) obtained from the fixed-shape semi-analytical methods and fitting results of numerical simulations; we demonstrated that the scaling law (functional dependence of the nonlinear self-focusing position on the beam intensity) is defined by the form of the nonlinear refractive index but not the beam shape (noise in the beam) at the boundary as it was assumed previously (e.g. in Refs. [48, 30]). Experimentally observable change of the scaling law for the high beam intensity was observed in Ref. [48] and is presented in Fig. 1.2. We provide an explanation of this result in the dissertation.

The Chapter 7 is devoted to a theoretical explanation of the fused silica ablation experiments from Refs. [35, 36]. The most unusual feature observed in these experiments is a presence of a small inner hole inside the ablation crater. The results of the experiment are presented in Fig. 1.3. We suppose that this result can be explained within the frame of the theory of Refs. [58, 51]. From the Fig. 7.4 one can conclude that such an explanation is in a good agreement with experimental results of Refs. [35, 36].

Finally, the results are summarized in the Conclusion.

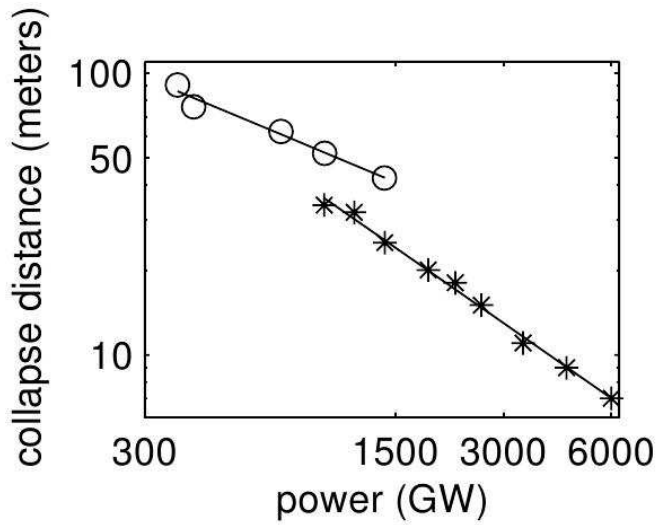


Figure 1.2: Change of the scaling law for high beam power. Nonlinear self-focusing position (collapse distance) versus the beam power. Experimental data from Ref. [48]. Different slope of the lines for moderate and high power exhibit a change of the scaling law.

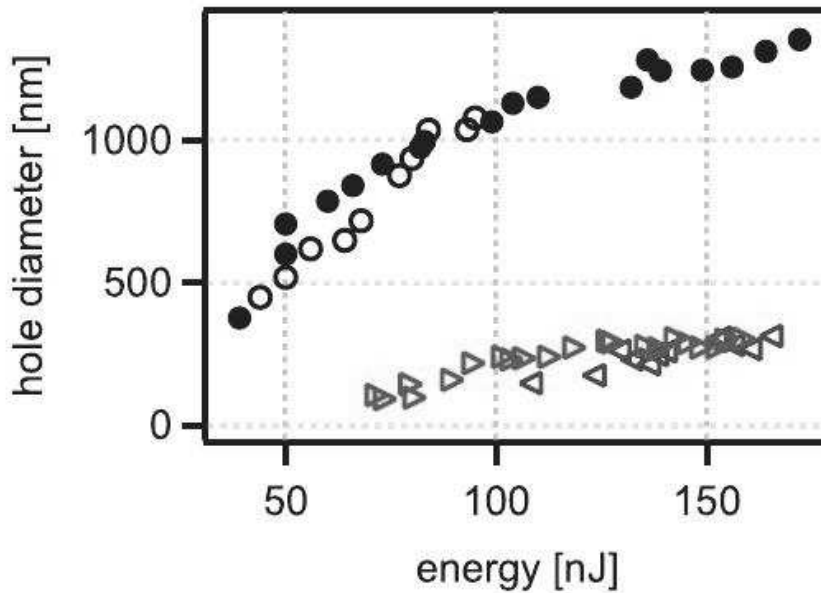


Figure 1.3: Diameter of the ablation crater: triangles and circles stand for the inner and outer hole diameters respectively. Experimental data from Ref. [35].

Chapter 2

Model equations

The present chapter of the dissertation is devoted to a derivation of the equations describing propagation of intense light radiation in nonlinear media. These equations will be based on some approximations and, as a result, will be applicable to particular physical situations, as a rule related to propagation of a laser beam in transparent dielectrics. All approximations and the range of their applicability will be discussed at every derivation step.

2.1 Propagation equations

Since we are going to study propagation of light, we have to start our consideration from the Maxwell equations:

$$\nabla \cdot \mathbf{E} = \epsilon_0^{-1}(-\nabla \mathbf{P} + \rho), \quad (2.1)$$

$$\nabla \cdot \mathbf{B} = 0, \quad (2.2)$$

$$\nabla \times \mathbf{E} = -\frac{\partial \mathbf{B}}{\partial t}, \quad (2.3)$$

$$\nabla \times \mathbf{H} = \mathbf{J} + \epsilon_0 \partial_t \mathbf{E} + \partial_t \mathbf{P}, \quad (2.4)$$

where, as usual, \mathbf{E} and \mathbf{H} are strengths of electric and magnetic fields, \mathbf{P} is a polarization, \mathbf{B} is an induced magnetization $\mathbf{B} \simeq \mu_0 \mathbf{H}$, ρ and \mathbf{J} are carrier and current densities respectively. ϵ_0 , μ_0 denote the electric permittivity and magnetic permeability respectively. ∂_t stands for a partial derivative with respect to time, ∇ , as usually, is a vector of first order spatial derivatives.

A simple combination of Maxwell equations (2.1-2.4) yields [2, 21]

$$\nabla^2 \mathbf{E} - \nabla(\nabla \cdot \mathbf{E}) - c^{-2} \partial_{tt} \mathbf{E} = \mu_0(\partial_{tt} \mathbf{P} + \partial_t \mathbf{J}), \quad (2.5)$$

$$\nabla \cdot \mathbf{E} = (\rho - \nabla \cdot \mathbf{P})/\epsilon_0, \quad (2.6)$$

where c is the speed of light in vacuum $c = 1/\sqrt{\epsilon_0 \mu_0}$.

For the sake of convenience we shall also list here the standard Fourier transformations for the fields

$$\tilde{\mathbf{E}}(\mathbf{r}, \omega) = \int_{-\infty}^{\infty} \mathbf{E}(\mathbf{r}, t) e^{-i\omega t} d\omega / 2\pi, \quad (2.7)$$

$$\tilde{\mathbf{J}}(\mathbf{r}, \omega) = \int_{-\infty}^{\infty} \mathbf{J}(\mathbf{r}, t) e^{-i\omega t} d\omega / 2\pi, \quad (2.8)$$

$$\tilde{\mathbf{P}}(\mathbf{r}, \omega) = \int_{-\infty}^{\infty} \mathbf{P}(\mathbf{r}, t) e^{-i\omega t} d\omega / 2\pi, \quad (2.9)$$

The current density \mathbf{J} describes the motion of free electrons created by the ionization of atoms. The dynamics of the ions is discarded. Polarization vector \mathbf{P} is responsible for the bound electron response driven by the laser radiation. It is usually decomposed into a linear part $\mathbf{P}_L \equiv \mathbf{P}^{(1)}$ related to the first-order susceptibility tensor $\hat{\chi}^{(1)}$ and a nonlinear one \mathbf{P}_{NL} satisfying $|\mathbf{P}^{(1)}| \gg |\mathbf{P}_{NL}|$. For isotropic, homogeneous, non magnetizable media and spectral ranges far from any material resonance, \mathbf{P} can be expressed as a power series in \mathbf{E} :

$$\tilde{\mathbf{P}} = \tilde{\mathbf{P}}^{(1)}(\mathbf{r}, \omega) + \tilde{\mathbf{P}}^{(3)}(\mathbf{r}, \omega) + \tilde{\mathbf{P}}^{(5)}(\mathbf{r}, \omega) + \dots \quad (2.10)$$

with scalar components given by

$$\begin{aligned} \tilde{P}_{\mu}^{(j)} &= \epsilon_0 \sum_{\alpha_1 \dots \alpha_j} \int \dots \int \chi_{\mu\alpha_1 \dots \alpha_j}^{(j)}(-\omega_{\sigma}; \omega_1, \dots, \omega_j) \\ &\times \hat{E}_{\alpha_1}(\mathbf{r}, \omega_1) \dots \hat{E}_{\alpha_j}(\mathbf{r}, \omega_j) \delta(\omega - \omega_{\sigma}) d\omega_1 \dots d\omega_j, \end{aligned} \quad (2.11)$$

where $\omega_{\sigma} = \omega_1 + \dots + \omega_j$. All susceptibility tensors $\hat{\chi}^{(j)}$ with even indices j vanish due to inversion symmetry. The subscript μ enumerates vector field components in Cartesian coordinates and the indices α_j have to be summed up over x , y and z . The tensor $\hat{\chi}^{(1)}$ is diagonal: $\chi_{\mu\alpha}^{(1)} = \chi^{(1)} \delta_{\mu\alpha}$, so that

$$\tilde{\mathbf{P}}^{(1)}(\mathbf{r}, \omega) = \epsilon_0 \chi^{(1)}(\omega) \tilde{\mathbf{E}}(\mathbf{r}, \omega), \quad (2.12)$$

and the scalar dielectric function, defined by

$$\epsilon(\omega) = 1 + \chi^{(1)}(\omega), \quad (2.13)$$

enters the wave number of the electromagnetic field $k(\omega) = \sqrt{\epsilon(\omega)}\omega/c$. Since $\chi^{(1)}(\omega)$ is complex-valued, the dielectric function $\epsilon(\omega)$ contains not only the information about material dispersion but also about linear losses specified by the imaginary part of $\chi^{(1)}(\omega)$. When these losses are negligible, $\epsilon(\omega)$ is approximately real and can be represented as $\epsilon(\omega) = n^2(\omega)$ where $n(\omega)$ denotes the linear refractive index of the medium, which can in certain frequency ranges (far from resonances) be described by e.g. a Sellmeier formula [99].

$$n^2(\lambda) = 1 + \sum_i \frac{B_i \lambda^2}{\lambda^2 - C_i}.$$

Here B_i and C_i are experimentally determined coefficients unique for every material.

By convention, $n_0 \equiv n(\omega_0)$ for the central frequency $\omega_0 = 2\pi c/\lambda_0$ of a laser operating at a wavelength λ_0 and $k_0 \equiv k(\omega_0)$. Without any specification $\omega = 2\pi c/\lambda$, $w_\perp = 2\pi/k_\perp$ is the waist of the optical wave packet in the plane (x, y) and k_\perp is the corresponding extent in the transverse Fourier space.

In what follows it will be convenient to use a complex version of the electric field

$$\mathbf{E} = \sqrt{c_1}(\mathcal{E} + \mathcal{E}^*), \quad \mathcal{E} = \frac{1}{\sqrt{c_1}} \int \Theta(\omega) \tilde{\mathbf{E}} e^{-i\omega t} d\omega, \quad (2.14)$$

where $*$ stands for the complex conjugate, $c_1 \equiv \omega_0 \mu_0 / 2k_0$ and $\Theta(x)$ denotes a Heaviside function.

Let us in the following section discuss the nature of variables \mathbf{P} , ρ and \mathbf{J} in equations (2.1–2.4). Here, the first one is related to the bound electron response, and ρ and \mathbf{J} describe the ionization of the medium by the applied laser field.

2.2 Bound electron response

For centrally symmetric materials, only one relevant component of the tensor χ remains in the cubic contribution $P^{(3)}$, e.g. $\chi^{(3)} = \chi_{xxxx}^{(3)}$ [2]. Let us first for simplicity assume $\chi^{(3)}$ being a constant in a spectral domain centered around ω_0 . Eq. (2.11) then simplifies with a single remaining component denoted $\chi_{\omega_0}^{(3)}$ and in time domain one finds $P^{(3)}(\mathbf{r}, t) = \epsilon_0 \chi_{\omega_0}^{(3)} E^3$. This expression remains valid, as long as an instantaneous response of the medium and the contribution of molecular vibrations and rotations to $\chi^{(3)}$ can be neglected. However, if the laser field interacts with anisotropic molecules, a phenomenon of Raman scattering comes into play.

This interaction can be schematized by a three-level system built upon rotational states of a molecule. Assume that the molecular scatterer has two rotational eigenstates, the ground state (level 1) with energy $\hbar\Omega_1$ and an excited one (level 2) with energy $\hbar\Omega_2$ where \hbar is the Planck constant and Ω_m stands for the frequency of the state $m = 1, 2, 3$. Far above these levels, there lies an electronic (or translational) state with energy $\hbar\Omega_3 \gg \hbar\Omega_2 - \hbar\Omega_1$. This molecule interacts with the laser field whose photon frequency ω_0 fulfills a following condition: $\Omega_{13}, \Omega_{23} \gg \omega_0 \gg \Omega_{21}$, [$\Omega_{nm} \equiv \Omega_n - \Omega_m$], so that the state $|3\rangle$ cannot be populated. Because of the defined parity of these molecular states the dipole matrix element μ_{12} associated with the transition $|1\rangle \rightarrow |2\rangle$ via a single photon vanishes, and the rotational state $|2\rangle$ can only be excited via transition through a virtual state $|3\rangle$ [$\mu_{13} \simeq \mu_{23} \equiv \mu \neq 0$]. Following this path, a Stokes photon with energy $\hbar\omega_s = \hbar\omega_0 - \hbar\Omega_{21}$ is emitted and the corresponding polarization vector involves the density matrix element associated with the states $|1\rangle$ and $|2\rangle$ as $\mathbf{P}_{\text{Raman}} = \chi^{(1)}[\rho_{12} e^{i\omega_R t} + c.c.] \mathbf{E}$. Here, $\omega_R = \Omega_{21}$ is the

fundamental rotational frequency and ρ_{12} is found to satisfy [93]

$$\partial_t \rho_{12} \simeq -\frac{\rho_{12}}{\tau_2} - i \frac{\mu^2 E^2}{\hbar^2 \Omega_{31}} e^{-it/\tau_1}, \quad (2.15)$$

where $\tau_1 = 1/\omega_R$ and τ_2 is the dipole dephasing time. From Eq. (2.15) the Raman response:

$$\mathbf{P}_{\text{Raman}} = \frac{2\chi^{(1)}\mu^2}{\Omega_{31}\hbar^2} E \int_{-\infty}^t e^{-\frac{t-t'}{\tau_2}} \sin\left(\frac{t-t'}{\tau_1}\right) E^2(t') dt' \quad (2.16)$$

can be derived, which originates from nonresonant nonlinear couplings.

With the latter expression rewritten in terms of the rescaled complex field \mathcal{E} (2.14) and appropriate normalizations [15], the full expression for cubic polarization reads

$$\mathbf{P}^{(3)} = 2n_0 n_2 \epsilon_0 \sqrt{c_1} \int_{-\infty}^{+\infty} \bar{R}(t-t') |\mathcal{E}(t')|^2 dt' \mathcal{E} + O(\mathcal{E}) + c.c., \quad (2.17)$$

where $\bar{R}(t) = (1 - x_K)\delta(t) + x_K\Theta(t)h(t)$, and

$$h(t) = \frac{2}{3} \frac{\tau_1^2 + \tau_2^2}{\tau_1 \tau_2} e^{-t/\tau_2} \sin(t/\tau_1), \quad (2.18)$$

with the definition of the nonlinear refractive index $n_2 = 3\chi_{\omega_0}^{(3)}/(4n_0^2 c \epsilon_0)$. In subsequent exposition the term $O(\mathcal{E}^3)$ in Eq. (2.17) is omitted, because it is responsible for the generation of third-harmonics, and this process is not taken into account in this dissertation. Expression (2.17) possesses both retarded and instantaneous components in the ratio x_K . The instantaneous part $\sim \delta(t)$ describes the response of bound electrons upon a few femtoseconds or less. The retarded part $\sim h(t)$ accounts for nuclear responses, namely the Raman contribution, in which fast oscillations in E^2 give negligible contributions as τ_1 and τ_2 by far exceed the optical period $\sim \omega_0^{-1}$.

Let us briefly discuss values of parameters contributing into Eq. (2.17). For example, for propagation of $\lambda = 800$ nm laser pulse in air, in Ref. [104] the authors suggested $\tau_1 \simeq 62$ fs, $\tau_2 \simeq 77$ fs and $x_K = 1/2$. This choice is consistent with the one proposed in experimental publications [89, 98]. When $\tau_1 \sim \tau_2$, the function $h(t) \simeq (1/\tau_1)e^{-t/\tau_1}$ can also be used in the ratio $x_K = 1/2$ Ref. [29]. In Refs. [127, 2] the parameter ranges $\tau_2/\tau_1 = 2 - 4$, $\tau_2 = 30 - 50$ fs with $x_K = 0.15 - 0.18$ have been suggested for condensed materials. Values of the nonlinear Kerr index n_2 normally lie in between 10^{-19} cm²/W for gases and 10^{-16} cm²/W in dense media (see e.g. Refs. [15, 30]). The exact value may vary by a factor of the order of unity depending on the procedure used for its evaluation (polarization spectroscopy, self- or cross-phase modulated spectra or time-resolved interferometry), as well as on the laser wavelength and pulse durations at which measurements are performed.

Besides, the susceptibility tensor has nonlinear components $\chi^{(j>3)}$ satisfying the ordering [21]

$$\frac{P^{(k+2)}}{P^{(k)}} = \frac{\chi^{(k+2)}}{\chi^{(k)}} \cdot \frac{E^{k+2}}{E^k} \approx \frac{|E|^2}{|E_{\text{at}}|^2}, \quad (2.19)$$

where $E_{\text{at}} \simeq 3 \times 10^{10}$ V/m is the characteristic atomic electric field strength with intensity $I_{\text{at}} > 10^{14}$ W/cm². Normally the estimate $\chi^{(5)}/\chi^{(3)} \sim 10^{-12}$ remains valid for nonresonant interactions in, e.g. gases. Despite the exact sign of $\chi^{(5)}$ is not yet known it is often assumed that the quintic susceptibility saturates Kerr focusing and should therefore have a negative sign Ref. [15]. Since the relation of Eq. (2.19) suggests that $\chi^{(j)}$ is rapidly decreasing with the order j , the Taylor series with respect to the electric field is usually truncated at the 5th order. Quintic polarization can then be derived following the same procedure as above with $\chi^{(5)}$ assumed constant in the frequency domain. Expressing E^5 in terms of $(\mathcal{E}, \mathcal{E}^*)$ Eq. (2.14), the quintic contribution of the polarization vector can be rewritten as (see Ref. [15])

$$\mathbf{P}^{(5)} = -2n_0n_4\epsilon_0\sqrt{c_1} \left(|\mathcal{E}|^4 + \frac{1}{2} |\mathcal{E}|^2 \mathcal{E}^2 + \frac{1}{10} \mathcal{E}^4 \right) \mathcal{E} + c.c. \quad (2.20)$$

where $n_4 = 5|\chi_{\omega_0}^{(5)}|/(4n_0^3c^2\epsilon_0^2)$.

2.3 Free electron response

As we see from Eq. (2.5), both bound and free electrons contribute to the light intensity distribution in media. The origin of free electrons lies in the ionization of media via intense light propagation. The free electrons, moving in a material, induce a current density $\mathbf{J} = q_e\rho\mathbf{v}_e$, where $q_e = -1.6 \times 10^{-19}$ C is the electron charge, ρ is the electron density and \mathbf{v}_e is the electron velocity. The free electron current \mathbf{J} can be computed from the fluid equations Ref. [128]:

$$\partial_t\rho + \nabla \cdot (\rho\mathbf{v}_e) = \mathcal{S}, \quad (2.21)$$

$$\partial_t\mathbf{v}_e + (\mathbf{v}_e \cdot \nabla)\mathbf{v}_e = \frac{q_e}{m_e} \left(\mathbf{E} + \frac{\mathbf{v}_e \times \mathbf{B}}{c} \right) - \nu_e\mathbf{v}_e - \mathcal{S}\mathbf{v}_e/\rho. \quad (2.22)$$

Here, \mathcal{S} represents external plasma sources and ν_e is the effective electron collision frequency. These equations can be combined to yield

$$\partial_t\mathbf{J} + \nu_e\mathbf{J} = \frac{q_e^2\rho}{m_e}\mathbf{E} + \mathbf{G}, \quad (2.23)$$

where

$$\mathbf{G} = \frac{q_e}{m_e c} \mathbf{J} \times \mathbf{B} - \frac{\mathbf{J}}{\rho q_e} (\nabla \cdot \mathbf{J}) - (\mathbf{J} \cdot \nabla) \mathbf{v}_e \quad (2.24)$$

represents ponderomotive forces acting on a slowly-varying time scale.

In case of linearly-polarized electromagnetic fields \mathbf{E} and \mathbf{B} oscillating at a high frequency ω_0 , the driving term \mathbf{G} admits envelope components containing gradients of the field intensity, radiation pressure due to electron collisions and changes in the electron density. Due to the low plasma currents induced by the ponderomotive forces, the electromagnetic pulses will be generated providing sources of coherent

sub-THz radiation Refs. [26, 27]. On the other hand, numerical simulations in Refs. [105, 93] have shown that for 100-fs pulses reaching intensities of 10^{14} W/cm² and free electron densities $\rho \sim 10^{16}$ cm⁻³ in the atmosphere, the efficiency conversion to electromagnetic pulse is of the order of 10^{-9} with local intensities attaining only 10 kW/cm². In dielectrics, the plasma generates electromagnetic pulse intensities remaining about \sim MW/cm² for peak laser intensities of $\sim 10^{13}$ W/cm². Thus the ponderomotive terms can be ignored, as long as peak intensities are below 10^{15} W/cm². Plasma density perturbations due to Langmuir wave oscillations and relativistic increase of the electron mass can also be neglected at these intensities.

Therefore, the equation for the current density reduces to Eq. (2.23) with $\mathbf{G} = 0$. Neglecting the higher orders in \mathbf{v}_e , the growth of the electron density reads

$$\partial_t \rho = \mathcal{S} = W(I)(\rho_{\text{nt}} - \rho) + \frac{\sigma}{U_i} \rho I - f(\rho), \quad (2.25)$$

i.e. it only depends on the source term \mathcal{S} involving photo-ionization processes with rate $W(I)$, collisional ionization with cross-section σ , and a function describing electron recombination or attachment with neighboring ions denoted by $f(\rho)$. ρ_{nt} and U_i in the above equations stand for the density of neutral species and the ionization potential respectively, while $\rho \ll \rho_{\text{nt}}$. The recombination function in gases is typically written as $f(\rho) = \beta_{\text{recomb}} \rho^2$ with $\beta_{\text{recomb}}[\text{cm}^3/\text{s}] \sim 2 \times 10^{-8}$ at electron temperatures $T_e = 1$ eV Ref. [104]. Typical recombination times in gases belong to the nanosecond scale. In solid dielectrics, the recombination function is linearly decreasing: $f(\rho) = \rho/\tau_{\text{recomb}}$ Ref. [15] and much shorter recombination times of the order 50 – 150 fs are expected.

The electron collisional rate is also depending on the electron energy distribution function and temperature versus the ionization potential U_i . Making an assumption of Maxwell distribution for the electron velocity, one arrives at a linear expression for the rate variation $\sigma |\mathcal{E}|^2 / U_i$ which remains valid as long as the electron thermal energy is small compared to U_i . Here σ is the inverse bremsstrahlung cross-section Refs. [30, 15]. Neglecting the Ohmic heating the solution of the current density Eq. (2.23) in terms of Fourier transforms reads:

$$\tilde{\mathbf{J}} = \frac{q_e^2}{m_e(\nu_e^2 + \omega^2)} (\nu_e + i\omega) (\rho \tilde{\mathbf{E}}). \quad (2.26)$$

The current density term in Eq. (2.5) transforms as

$$\mu_0 \partial_t \mathbf{J} \rightarrow \left[-i \frac{\omega n_0 \sigma(\omega)}{c} + \frac{\omega_0^2}{c^2 \rho_c (1 + \nu_e^2 / \omega^2)} \right] (\rho \tilde{\mathbf{E}}), \quad (2.27)$$

after introducing the critical plasma density

$$\rho_c \equiv \frac{\omega_0^2 m_e \epsilon_0}{q_e^2} \simeq \frac{1.11 \times 10^{21}}{\lambda_0^2 [\mu\text{m}]} \text{cm}^{-3}, \quad (2.28)$$

at which the laser wave number vanishes. Then, for the cross-section one gets

$$\sigma(\omega) = \frac{q_e^2}{m_e \epsilon_0 n_0 c \nu_e (1 + \omega^2 / \nu_e^2)} \quad (2.29)$$

This expression is usually referred to as a "Drude" model. It determines the energy losses via plasma (cascade) ionization.

In Eq. (2.25) $W(I)$ denotes the photo-ionization rate. Generally speaking, this function must be found from the solution of the Schrödinger equation describing ionization of an atom (molecule) in a strong electromagnetic field. This problem is quite difficult and is mostly approached numerically (Refs. [65, 96]). However, an analytical solution can sometimes also be found, e.g. in two limiting cases depending on the value of the Keldysh parameter of "adiabaticity" Refs. [63]:

$$\gamma = \omega_0 \frac{\sqrt{2m_e U_i}}{|q_e| E_p}. \quad (2.30)$$

The limit $\gamma \gg 1$ corresponds to the case of the multiphoton ionization (MPI), while the limit $\gamma \ll 1$ is related to the tunnel ionization when, for high intensities, the Coulomb barrier becomes low enough to allow an electron to tunnel out. Here, E_p denotes the peak optical amplitude $E_p = \sqrt{2c_1 I}$.

For laser intensities $I = |E|^2 < 10^{13}$ W/cm², the MPI dominates and gives the following ionization rate:

$$W_{\text{MPI}} = \sigma_K I^K, \quad (2.31)$$

where $K = \text{mod}(U_i / \hbar \omega_0) + 1$ is the number of photons necessary to liberate one electron.

For higher intensities the tunnel ionization starts to contribute as well, because of electrons tunneling out within one optical cycle. The first formula for tunnel ionization was obtained by Keldysh in Ref. [63]:

$$W_{\text{tunnel}} = \frac{4\sqrt{3}}{\sqrt{\pi} E_p} \exp\left(\frac{-2}{3E_p}\right),$$

where E is the stress of electric field taken in atomic system of units ($q_e = m_e = \hbar = 1$).

This result was further improved by Perelomov, Popov and Terent'ev in Ref. [94], and Ammosov, Delone and Krainov in Ref. [6]. Since both of these formulae are rather complicated and not relevant for intensities below 10^{13} W/cm² considered in this dissertation, we do not present these expressions here.

In order to take energy losses related to ionization processes into account in Eq. (2.5), Kandidov *et al.* in Ref. [59] suggested a following scheme: the temporal evolution of the energy density w should be determined by a local version of the Poynting theorem, i.e.

$$\frac{d}{dt} w(\mathbf{r}, t) = \mathbf{J}(\mathbf{r}, t) \cdot \mathbf{E}(\mathbf{r}, t), \quad (2.32)$$

from which one can compute the energy lost by the pulse to extract electrons via single ionization process. The amount of energy per time and volume units is then given by $\mathbf{J} \cdot \mathbf{E} = U_i \partial_t \rho_{\text{PI}}$ where $\partial_t \rho_{\text{PI}} \equiv W(I)(\rho_{\text{nt}} - \rho)$. Using complex-valued fields, the current associated with photo-ionization losses is easily found to be

$$\mathbf{J}_{\text{loss}} = \sqrt{\frac{k_0}{2\omega_0\mu_0}} U_i \frac{W(I)}{I} (\rho_{\text{nt}} - \rho) (\mathcal{E} + \mathcal{E}^*), \quad (2.33)$$

After the above discussion on \mathbf{J} and \mathbf{P} dependence on the electric field, let us now turn back to the derivation of pulse propagation equations.

2.4 Back to the propagation equations. Nonlinear Schrödinger equation (NLSE)

The direct substitution of all the expressions derived above into Eq. (2.5), yields an equation which is extremely difficult to solve. That is why, a following sequence of steps Refs. [21, 30, 15] can be performed in order to bring the nonlinear wave equation (2.5) to a tractable form.

First, performing a Fourier transformation of Eqs. (2.5) we get

$$(\partial_z^2 + k^2(\omega) + \nabla_{\perp}^2) \tilde{\mathbf{E}} = -\mu_0 \omega^2 \tilde{\mathcal{F}}_{\text{NL}} + \nabla(\nabla \cdot \tilde{\mathbf{E}}), \quad (2.34)$$

which should be supplemented by the gauge fixing condition (2.6):

$$\nabla \cdot \tilde{\mathbf{E}} = (\epsilon_0 \epsilon)^{-1} (\tilde{\rho} - \nabla \cdot \tilde{\mathbf{P}}_{\text{NL}}), \quad (2.35)$$

where $\nabla_{\perp}^2 \equiv \partial_x^2 + \partial_y^2$ and

$$\tilde{\mathcal{F}}_{\text{NL}} \equiv \tilde{\mathbf{P}}_{\text{NL}} + i\tilde{\mathbf{J}}/\omega. \quad (2.36)$$

Now the most fundamental assumption allowing us to simplify the Eq. (2.34) is that for $k(\omega)$ located around ω_0 the transverse waist of the beam always fulfills

$$k_{\perp}^2/k^2(\omega) \ll 1, \quad (2.37)$$

The second assumption is on small nonlinearities, i.e.

$$\frac{\tilde{F}}{\epsilon_0 \epsilon(\omega)} \ll 1. \quad (2.38)$$

These conditions make vectorial effects negligible. Then, from Eqs. (2.34) combined with the continuity equation $\partial_t \rho + \nabla \cdot \mathbf{J} = 0$ expressed in Fourier variables one gets

$$(\partial_z^2 + k^2(\omega) + \nabla_{\perp}^2) \tilde{\mathbf{E}} = -\mu_0 \omega^2 \left(\tilde{\mathcal{F}}_{\text{NL}} + \frac{\nabla(\nabla \cdot \tilde{\mathcal{F}}_{\text{NL}})}{k^2(\omega)} \right). \quad (2.39)$$

If we project the vectors $\mathbf{E} = (E_\perp, E_z)$, $\mathbf{P}_{\text{NL}} = (P_{\text{NL},\perp}, P_{\text{NL},z})$, $\mathbf{J} = (J_\perp, J_z)$, $\nabla = (\nabla_\perp, \partial_z)$ onto the transverse and longitudinal axes with unit vectors \vec{e}_\perp and \vec{e}_z respectively, \tilde{E}_z can be found to scale as $O(k_\perp/k)$. This follows from a direct Fourier transformation of Eq. (2.35) for weak nonlinearities Eq. (2.38). The vector \vec{e}_\perp embraces x - and y -components: $\vec{e}_\perp = (\vec{e}_x, \vec{e}_y)$.

Expressed in Fourier space, the nonlinear coupling of transversal/longitudinal components described by the last term in Eq. (2.39) behaves as $O(k_\perp^2/k^2)$ [15, 21], thus only becoming important in the limit $k_\perp \rightarrow k(\omega)$. As it was demonstrated in Ref. [15], the compression processes are stopped before k_\perp becomes comparable with k (by e.g. chromatic dispersion or plasma generation) and, that is why the last term in the right-hand side of Eq. (2.39) is close to zero, implying thereby $E_z \simeq 0$. As a result, the field remains transversally polarized along the propagation axis, making the influence of $\nabla(\nabla \cdot \mathcal{F}_{\text{NL}})/k^2$ negligible. Hence, as long as the nonlinear polarization and current density preserve the conditions (2.37) and (2.38), vectorial effects can be ignored for purely optical or weakly-ionized materials as well. This result allows us to confine ourselves to a scalar description for linearly-polarized beams having, e.g. $E_y = 0$.

Let us now represent the electric field as a superposition of forward and backward propagating waves

$$\tilde{E} = \tilde{U}_+ e^{ik(\omega)z} + \tilde{U}_- e^{-ik(\omega)z}, \quad (2.40)$$

where \tilde{U}_+ and \tilde{U}_- stand for the Fourier components of the forward and backward running waves correspondingly. In case we study the wave reflection from a media interface (e.g. fused silica - air) or remote sensing experiments [60], which spectrally analyze the photons returning towards the laser source, backscattering process should be taken into account. For all these cases one normally assumes $|\partial_z U_\pm| \ll |k(\omega)U_\pm|$ and $U_+ \gg U_-$.

Substituting the Eq. (2.40) into Eq. (2.39) and keeping the conditions above in mind, we get

$$\begin{aligned} e^{2ik(\omega)z} [\partial_z^2 + 2ik(\omega)\partial_z + \nabla_\perp^2 + \mu_0\omega^2\tilde{F}]\tilde{U}_+ \\ + [\partial_z^2 - 2ik(\omega)\partial_z + \nabla_\perp^2 + \mu_0\omega^2\tilde{F}]\tilde{U}_- = 0. \end{aligned} \quad (2.41)$$

Following [43] we shall also assume that $\tilde{F} = F\delta(\omega)$. The Eq. (2.41) can then be integrated in an interval $z - \pi/2k \leq z \leq z + \pi/2k$ (one fast oscillation). Let us also Taylorize $\hat{U}_\pm(z)$ in order to evaluate:

$$2ik(\omega)\partial_z\tilde{U}_- \sim -\frac{e^{2ik(\omega)z}}{2ik(\omega)}\partial_z[\nabla_\perp^2 + \mu_0\omega^2F]\tilde{U}_+. \quad (2.42)$$

Since $\nabla_\perp^2 \sim -k_\perp^2$ in Fourier space, the backscattered component has a weak influence on the beam dynamics provided that $k_\perp^2 \ll k^2(\omega)$ and as long as the longitudinal variations of the nonlinearities remain small.

The limit Eq. (2.37) moreover implies that the wave components, forming the angle $\theta = \arcsin(k_{\perp}/k)$ between the transverse and longitudinal directions, mostly propagate forwards since $\theta \ll \pi/2$ [15]. Because the propagation physics is mainly described by the forward component, one has $\tilde{U}_{-} \rightarrow 0$ and $\tilde{E} \simeq \tilde{U}_{+} e^{ik(\omega)z}$. As a result we obtain a unidirectional pulse propagation equation [21, 15]:

$$\partial_z \tilde{E} = \frac{i}{2k(\omega)} \nabla_{\perp}^2 \tilde{E} + ik(\omega) \tilde{E} + \frac{i\mu_0 \omega^2}{2k(\omega)} \tilde{\mathcal{F}}_{\text{NL}} \quad (2.43)$$

Validity of this model explicitly requires that the second-order derivative in z of the envelope function \tilde{U}_{+} is small as compared with $|k(\omega) \partial_z \tilde{U}_{+}|$. This inequality, more often expressed in the form $|\partial_z \tilde{U}_{+}| \ll |k(\omega) \tilde{U}_{+}|$, is usually referred to as the "paraxiality" assumption. If the field envelope U_{+} does not change considerably over the propagation distances of the order of λ for all wavelengths, this condition is valid.

Let us now use again the notation of Eq. (2.14). Since \mathcal{E} satisfies the condition $\tilde{\mathcal{E}}^*(\omega) = \tilde{\mathcal{E}}(-\omega)^*$ it is sufficient to consider the Eq. (2.43) in the frequency domain $\omega > 0$ only. The field intensity can be defined by \mathcal{E}^2 averaged over at least one optical period for a given central frequency ω_0 . This quantity usually follows from the modulus of the time averaged Poynting vector.

In such a way, the propagation equation (2.43) in Fourier space reads

$$\begin{aligned} \partial_z \tilde{\mathcal{E}} &= \left[\frac{i}{2k(\omega)} \nabla_{\perp}^2 + ik(\omega) \right] \tilde{\mathcal{E}} + \frac{i\mu_0 \omega^2}{2k(\omega) \sqrt{c_1}} \Theta(\omega) \tilde{P}_{\text{NL}} \\ &- \frac{ik_0^2 \Theta(\omega)}{2\epsilon(\omega_0) k(\omega) (1 + \frac{\nu_e^2}{\omega^2})} \left(\frac{\rho \tilde{\mathcal{E}}}{\rho_c} \right) - \frac{\Theta(\omega)}{2} \sqrt{\frac{\epsilon(\omega_0)}{\epsilon(\omega)}} \mathcal{L}(\omega), \end{aligned} \quad (2.44)$$

where

$$\mathcal{L}(\omega) = \frac{U_i}{2\pi} \int \mathcal{E} \left[\frac{W(I)}{I} (\rho_{\text{nt}} - \rho) + \frac{\sigma(\omega)}{U_i} \rho \right] e^{i\omega t} dt. \quad (2.45)$$

The next step in the derivation of the pulse propagation equation is the so-called *slowly varied envelope approximation*

When a central frequency ω_0 is imposed, the nonlinear envelope equation earlier derived by Brabec and Krausz in Ref. [22] is restored from Eq. (2.43). Making use of the Taylor expansion

$$k(\omega) = k_0 + k' \bar{\omega} + \tilde{\mathcal{D}}, \quad \tilde{\mathcal{D}} \equiv \sum_{n \geq 2}^{+\infty} \frac{k^{(n)}}{n!} \bar{\omega}^n, \quad (2.46)$$

where $\bar{\omega} = \omega - \omega_0$, $k' = \partial k / \partial \omega|_{\omega=\omega_0}$, $k^{(n)} = \partial^n k / \partial \omega^n|_{\omega=\omega_0}$ and substituting Eq. (2.46) into Eq. (2.43), one gets

$$\begin{aligned} \partial_z E &= \int \left[\frac{i \nabla_{\perp}^2}{2k(\omega)} + i(k_0 + k' \bar{\omega} + \tilde{\mathcal{D}}) \right] \hat{E}(\omega) e^{-i\omega t} d\omega \\ &+ i \frac{\mu_0}{2} \int \frac{\omega^2}{k(\omega)} \tilde{\mathcal{F}}_{\text{NL}}(\omega) e^{-i\omega t} d\omega. \end{aligned} \quad (2.47)$$

Here the property that $\tilde{E}(\omega)$ is the Fourier transform of $E(t)e^{i\omega_0 t}$ in $\bar{\omega}$ was used, and terms containing $k(\omega)$ in their denominator are expanded up to the first order in $\bar{\omega}$.

Let us now introduce a complex valued representation

$$\mathcal{E} = Ue^{ik_0 z - i\omega_0 t}, \quad (2.48)$$

involving a novel envelope function U . As a next step, the new time variable $t \rightarrow t - z/v_g$ can be utilized in order to place the pulse into a frame moving with the group velocity $v_g = k'^{-1}$. Thus, from Eq. (2.47) we arrive at

$$(i\partial_z + \mathcal{D})U \simeq -\frac{T^{-1}}{2k_0}(\nabla_{\perp}^2 U) - \frac{\mu_0\omega_0^2}{2k_0\sqrt{c_1}}T\mathcal{F}_{\text{NL}}^{\text{env}}(U), \quad (2.49)$$

where

$$\mathcal{D} \equiv \sum_{n \geq 2}^{+\infty} (k^{(n)}/n!)(i\partial_t)^n, \quad T = \left(1 + \frac{i}{\omega_0}\partial_t\right), \quad (2.50)$$

whenever $|k_0 - \omega_0 k'|/k_0 \ll 1$. This condition is met if the relative deviation between group and phase velocities is small, which is fulfilled in a wide range of propagation phenomena. The operator T^{-1} introduces a space-time focusing in front of the diffraction term. The nonlinearities of the envelope function $\mathcal{F}_{\text{NL}}^{\text{env}}(U)$ are also affected by the operator T corresponding physically to a self-steepening.

For dispersion relations truncated at some finite order $n < +\infty$ the derived model equation (2.49) is applied to optical fields with sufficiently narrow spectral bandwidths.

If the dispersion relation admits a Taylor expansion around ω_0 and retaining only waveforms oscillating at ω_0 the nonlinear envelope equation for the forward component U can be directly obtained from Eqs. (2.49, 2.17, 2.20, 2.33):

$$\begin{aligned} \partial_z U &= \frac{i}{2k_0}T^{-1}\nabla_{\perp}^2 U + i\frac{\omega_0}{c}n_2 T \left[(1 - x_K)|U|^2 + x_K \int_{-\infty}^t h(t-t')|U(t')|^2 dt' \right] U \\ &+ i\mathcal{D}U - i\frac{\omega_0}{c}n_4 T|U|^4 U - i\frac{k_0}{2n_0^2\rho_c}T^{-1}\rho U - \frac{\sigma}{2}\rho U - \frac{\beta_{\text{MPA}}(|U|)}{2}U, \end{aligned} \quad (2.51)$$

$$\partial_t \rho = W(I)(\rho_{\text{nt}} - \rho) + \frac{\sigma(\omega_0)}{U_i}\rho|U|^2 - f(\rho), \quad (2.52)$$

where t stands for the retarded time variable $t - z/v_g$. The function $\beta_{\text{MPA}}(|U|) = (\rho_{\text{nt}} - \rho)U_i W(I)/|U|^2$ takes the losses caused by photo-ionization into account. In the MPI limit (2.31) this dissipative function takes the form $\beta_{\text{MPA}}(|U|) \rightarrow \beta^{(K)}|U|^{2K-2}$ where $\beta^{(K)} \equiv K\hbar\omega_0\sigma_K\rho_{\text{nt}}$ is the coefficient of multiphoton absorption (MPA). The first term of the operator \mathcal{D} corresponds to a group-velocity dispersion (GVD) with a coefficient $k'' = \partial^2 k/\partial\omega^2|_{\omega=\omega_0}$. Equations (2.51) describe wave diffraction, Kerr focusing response, plasma generation, chromatic dispersion with a self-consistent action of deviations from the classical slowly-varying envelope approximation through

space-time focusing and self-steepening operators ($T^{-1}\nabla_{\perp}^2\mathcal{E}$) and ($T|\mathcal{E}|^2\mathcal{E}$) respectively.

Evidently, equations (2.51, 2.52) must be supplemented with initial and boundary conditions. For Eq. (2.52) it is usually chosen in the form $\rho(0) = 0$ what physically corresponds to the absence of free charges in the media before the laser pulse propagation.

Usually the intensity distribution at the boundary is given by either Gaussian or super-Gaussian beam shapes

$$U(x, y, z = 0, t) = U_0 \exp\left(-\frac{r^{2N}}{w_0^{2N}} - ik_0\frac{r^2}{2f} - \frac{t^2}{t_p^2} - iC\frac{t^2}{t_p^2}\right), \quad (2.53)$$

which may be focused through a lens of focal length f and be temporally chirped if $C \neq 0$. Here, $r = \sqrt{x^2 + y^2}$, w_0 is the beam waist and t_p (the $1/e^2$ pulse half-width) is such that its full-width-at-half-maximum (FWHM) equals $\Delta t = \sqrt{2 \ln 2} t_p$. For Gaussian beams ($N = 1$), $U_0 = \sqrt{2P_{\text{in}}/\pi w_0^2}$ including the input power P_{in} . In the next sections we shall discuss some most important properties of the obtained model equation (2.51).

2.5 Properties of the nonlinear pulse propagation equation

Let us now briefly describe basic properties of Eq. (2.51, 2.52). For the sake of simplicity, following Bergé *et al.* Ref. [15], first of all it is convenient to convert the Eqs. (2.51, 2.52) into dimensionless form.

As it has been discussed above, the main contribution into the ionization processes under moderate intensity ($I < 10^{13}\text{W}/\text{cm}^2$) comes from MPI, therefore, the plasma kinetic equation (2.52) can be approximately written as $\partial_t \rho = \Gamma|\psi|^{2K}$, where the rescaled MPI coefficient reads $\Gamma = (2z_0 k_0/n_0^2 \rho_c)\sigma_K \rho_{\text{nt}} t_p c_2^K$ and $c_2 \equiv \lambda_0^2/8\pi^2 n_0 n_2 w_0^2$. Then, assuming an instantaneous response ($x_K = 0$), the nonlinear Schrödinger equation in dimensionless form reads

$$i\partial_z \psi + \nabla_{\perp}^2 \psi + |\psi|^2 \psi + \mathcal{F}(\psi) = 0, \quad (2.54)$$

All processes whose influence on the beam propagation is small in comparison to the Kerr nonlinearity are included in the so-called "perturbation function":

$$\mathcal{F} = -\delta\partial_t^2 \psi - \rho\psi - \epsilon|\psi|^4 \psi + i\nu|\psi|^{2K-2} \psi + \frac{i(|\psi|^2 \psi - \nabla_{\perp}^2 \psi)_t}{t_p \omega_0},$$

Here we used the approximation $T^{-1} \simeq 1 - (i/\omega_0)\partial_t$ supposing $\omega_0 t_p \gg 1$, neglected the recombination and only treated the plasma coupling term driven by MPI and

subject to the limit $T^{-1} \rightarrow 1$. Equations (2.51) are then rescaled in dimensionless form by using the substitutions $r \rightarrow w_0 r$, $t \rightarrow t_p t$, $z \rightarrow 4z_0 z$ ($z_0 = \pi n - 0w_0^2/\lambda_0$ is the diffraction length of the collimated beam), $U \rightarrow \sqrt{c_2} \psi$, $\rho \rightarrow (n_0^2 \rho_c / 2z_0 k_0) \rho$, $\delta \equiv 2z_0 k'' / t_p^2$ and $\nu = 2z_0 \beta^{(K)} c_2^{K-1}$ respectively. Quintic saturation is taken into account through $\epsilon = n_4 c_2 / n_2$. For Gaussian beams, the incident amplitude (2.53) reduces to

$$|\psi(z=0)| = \sqrt{\frac{16\pi n_0 n_2 P_{\text{in}}}{\lambda_0^2}} e^{-r^2 - t^2}. \quad (2.55)$$

Wave collapse in nonlinear media: $\mathcal{F} = 0$. In this case Eq. (2.54) describes wave self-focusing at a certain point z_{sf} . This causes a compression of the beam in the diffraction plane, which leads to "wave collapse" when the Kerr nonlinearity is not saturated. A necessary condition for the collapse is that the input power $P_{\text{in}} = \int |\mathcal{E}|^2 d\vec{r}$ exceeds some critical value,

$$P_{\text{cr}} \simeq \frac{3.72 \lambda_0^2}{8\pi n_0 n_2}, \quad (2.56)$$

computed on the Townes mode¹. The beam waist decreases more and more as the field amplitude $|U|$ diverges. The distance, also termed as nonlinear self-focusing position locates the point at which the beam amplitude diverges along the optical path. One of the first results defining the position of the nonlinear self-focusing as a function of the beam power was obtained by Marburger in Ref. [86]. The obtained empirical formula (also referred to as the Marburger formula) reads

$$z_{\text{sf}} = 0.367 z_0 \left((\sqrt{P_{\text{in}}/P_{\text{cr}}} - 0.852)^2 - 0.0219 \right)^{-1/2}. \quad (2.57)$$

We have to note that taking a delayed Kerr response $x_K \neq 0$ into account leads to a shift of the self-focusing position. In other words in that case P_{cr} in the Marburger formula should be replaced by an effective critical power $P_{\text{cr}}^{\text{eff}} = P_{\text{cr}} x_K$ Ref. [116].

However, in real physical systems a whole beam collapse is never observed: for low intensity, the nonlinear beam compression is arrested by diffraction; for high light intensity, additional nonlinear effects, leading to the collapse arrest, appear in the system.

Collapse arrest by higher order material polarization: $\mathcal{F} = -\epsilon |\psi|^4 \psi$. As it has been demonstrated in many papers (e.g. Refs. [30, 15] and references therein) an introduction of additional defocusing quintic nonlinearities produce stable solitons in continuous-wave (cw) media. This property follows from a balance between diffraction, Kerr focusing and nonlinear saturation.

¹More closely we consider this case in Chapter 4.

At sufficiently high values of n_4 the high-order saturation can prevail over ionization and induces a soliton-like dynamics before the occurrence of an electron plasma Ref. [15]. Whether the higher-order optical nonlinearities are relevant is governed by the ionization rate: e.g. in air, if the laser intensity saturates above 10^{14} W/cm² by plasma generation alone, then even weak values of n_4 can noticeably soften this peak intensity. At lower intensities the quintic saturation has a more limited role.

Collapse arrest by plasma defocusing: $\mathcal{F} = -\rho\psi$. Because of MPI the pulse temporal profile gets depleted through the sudden emergence of an ionization front near the focus point z_{sf} . In the absence of time dispersion and nonlinear losses, the plasma equation $\partial_t \rho = \Gamma|\psi|^{2K}$ can be integrated as $\rho \simeq \Gamma|\psi|^{2K}t_p$. This term in equation (2.51), similar to the case considered previously, leads to the beam collapse arrest.

The fact that the beam collapse can be prevented by the media ionization was demonstrated in many papers, like Refs. [56, 11, 5, 12] to mention only first ones. In all of them this result was obtained on the basis of the variational approach (see. Chapter 4) and numerical simulations. Instead of the beam collapse the authors observed intensity saturation: upon propagation the beam radius decreased and achieved a certain nonzero magnitude. On-axial beam intensity I_{sat} which corresponds to this beam radius was suggested to be found from a rule (see Refs. [30, 15]):

$$n(I_{sat}) = 0, \quad (2.58)$$

where $n(I)$ is as usual the refractive index of the model.

Collapse arrest by group velocity dispersion: $\mathcal{F} = -\delta\partial_t^2\psi$. Besides wave focusing in the transverse direction the Kerr nonlinearity also causes defocusing in time for $k'' > 0$ (normal dispersion) and temporal compression for $k'' < 0$ (anomalous dispersion) by mixing GVD and spatial diffraction in case $T \simeq 1$. In case of normal GVD the interplay of these processes leads to symmetric splitting of the pulse along the time axis. In contrast, an anomalous GVD yields a spatiotemporal collapse. In addition, when ultrashort pulses develop sharp temporal gradients, the operator T in front of the Kerr term (self-steepening) induces a shock dynamics: the field develops a singular profile with $|\psi_t| \rightarrow +\infty$ in the trail ($t > 0$) of the pulse [7]. This dynamics is reinforced by space-time focusing [15].

To understand it, one can consider ultrashort pulses as being stacked along the temporal direction into different time slices having each their own power, e.g., $P(t) = P_{in}e^{-2t^2}$ for Gaussian profiles. Slices located at times $t < 0$ correspond to the front (or leading) pulse; those at $t > 0$ constitute the back (trailing) pulse. Each time

a slice self-focuses at its respective singularity point, $z_{\text{sf}}(t)$, according to Eq. (2.57) in which the ratio $P_{\text{in}}/P_{\text{cr}}$ must be replaced by $P_{\text{in}}e^{-2t^2}/P_{\text{cr}}$. This scenario is known as the "moving-focus" model [85] and yields simple comprehension elements to figure out the pulse distortions. Here, the central time slice focuses at the shortest distance $z_{\text{sf}}(t=0)$. Furthermore, $\dot{z}_{\text{sf}}(t)$ is positive for $t > 0$ and negative for $t < 0$ [$\dot{z}_{\text{sf}}(0) = 0$], whereas $\ddot{z}_{\text{sf}}(t)$ always remains positive. Normal GVD transfers power towards non-zero instants, symmetrically located with respect to $t = 0$. Self-steepening and space-time focusing moreover produce a transfer of power from the leading ($\dot{z}_{\text{sf}} < 0$) to the trailing portion of the pulse ($\dot{z}_{\text{sf}} > 0$). Normal GVD alone "splits" a focusing pulse into two regular, symmetric spikes at powers $< 2P_c$. For higher powers, the peak edges develop shock profiles and disintegrate into ripplelike cells [47].

At powers moderately above critical the normal GVD ($k'' > 0$) and plasma formation constitute two competing processes to halt the wave collapse. Generally, the stronger the GVD coefficient is, the larger is the power interval required for collapse arrest by pulse splitting. By solving the cubic NLS equation with normal GVD, a boundary $\delta_{\text{crit}}(\bar{p})$ being a function of the ratio of input power over critical, $\bar{p} = P_{\text{in}}/P_{\text{cr}}$, it can be shown that initial conditions fulfilling $\delta > \delta_{\text{crit}}(\bar{p})$ will limit the Kerr self-focusing through GVD splitting not giving rise to solutions describing divergences into a singular state. Involving higher order dispersion together with steepening effects (T, T^{-1}) into consideration modifies this curve by "delaying" the self-focusing threshold to higher powers. In particular, third-order dispersion tends to delocalize the pulse by pushing the temporal centroid to the back [41].

In contrast, for anomalous GVD ($k'' < 0$) power is transferred to center. Ultra-short pulses thus collapse both in space and time. A mapping $|\delta| > \delta_{\text{crit}}(\bar{p})$ can again be constructed on the basis of virial-type arguments [13]. As the result one obtains that the pulse spreading will take place when the dispersion length $\sim t_p^2/|k''|$ is short enough to prevail over diffraction and Kerr nonlinearity. Again as in the previous paragraph the theoretical boundaries are to some extent influenced by higher-order dispersion and steepening terms in the equation.

Chapter 3

Model equations. The geometrical optics approximation.

As we demonstrated in Chapter 2, the basic mathematical model for intense light propagation in the media is the nonlinear Schrödinger equation (2.51). Taking into account the simplification discussed in the end of the previous chapter, the Eq. (2.51) can be rewritten as follows:

$$i\partial_z\mathcal{E} + \frac{1}{2k_0}\nabla_{\perp}^2\mathcal{E} + \frac{k''}{2}\partial_{tt}\mathcal{E} + k_0n(|\mathcal{E}|^2)\mathcal{E} = 0. \quad (3.1)$$

Here \mathcal{E} is the slowly-varying envelope of the electric field, z is the propagation length, k_0 is the wave number $k_0 = n_0\omega_0/c$, ω_0 is the carrier frequency of the laser irradiation and c is the velocity of light, k'' is the dispersion coefficient, $k'' \equiv \frac{\partial^2 k}{\partial \omega^2}|_{\omega=\omega_0}$. If $k'' > 0$, the dispersion is assumed to be normal, and anomalous in opposite case. $n = n(|\mathcal{E}|^2)$ is a nonlinear refractive index in a general form.

Equation (3.1) is a basic mathematical model for many physical situations. For example in case of (1+1) dimensions, Eq. (3.1) describes propagation of a laser pulse in the fiber, where radial intensity variation is small in comparison to the fiber radius, and the second term in Eq. (3.1) can be neglected. Further, we shall refer to this case as a dispersive one. Another situation is a continuous wave laser beam propagation in a planar geometry in a media where dispersion, i.e. the third term in Eq. (3.1), is negligible. If we consider the propagation of a laser beam in a cylindrical geometry, which is more typical for experimental conditions, the Laplace operator ∇_{\perp}^2 will describe diffraction in two dimensions, and we arrive at (1+2) dimensional problem. Both these cases, with the Laplace operator taking diffraction into account, will be referred to as diffractive cases.

Let us now represent electric field \mathcal{E} in the eikonal form: $\mathcal{E} = \sqrt{I}\exp(ik_0S)$ in diffractive and $\mathcal{E} = \sqrt{I}\exp(i\omega_0S)$ in dispersive cases, respectively. Then, starting

from Eq. (3.1), after some algebraic manipulations we obtain

$$\partial_z S = -\frac{\kappa_1}{2}(\partial_x S)^2 + \kappa_2 n(I) + \kappa_3 \left(\frac{x^{1-\nu}}{\sqrt{I}} \partial_x (x^{\nu-1} \partial_x \sqrt{I}) \right), \quad (3.2)$$

$$\partial_z I = -\kappa_4 \partial_x (I \partial_x S) - (\nu - 1) \frac{I \partial_x S}{x}, \quad (3.3)$$

where $\nu = 1$ and $\nu = 2$ correspond to the (1+1) and (1+2) dimensional cases respectively.

For the diffractive case x corresponds to the spatial variable and $\kappa_1 = 1$, $\kappa_2 = 1$, $\kappa_3 = 1/2k_0^2$ and $\kappa_4 = 1$; for the dispersive case x denotes time t , and $\kappa_1 = k''\omega_0$, $\kappa_2 = k_0 n_2 / \omega_0$, $\kappa_3 = k'' / \omega_0$, and $\kappa_4 = k'' \omega_0$.

Let us differentiate the first equation with respect to x and introduce a new variable $v \equiv \partial_x S$. For the sake of convenience, we introduce dimensionless variables $\tilde{I} \equiv I/I_0$, $\tilde{x} \equiv x/w_{\text{in}}$, $\tilde{t} \equiv t/t_p$, where I_0 is an initial peak intensity of the beam, w_{in} is an initial beam radius, and t_p is an initial pulse duration ($t_{FWHM} = \sqrt{2 \ln 2} t_p$). For the propagation distance we use the following normalization: $\tilde{z} \equiv z|k''|\omega_0/t_p$ in dispersive and $\tilde{z} \equiv z/w_{\text{in}}$ in diffractive cases, correspondingly. Further we shall always use dimensionless variables, omitting tilde for the sake of simplicity. Moreover, let us introduce new dimensionless variables α and θ as being $\alpha = k_0 n_2 I_0 / |k''| \omega_0^2$, $\theta = (2\omega_0^2 t_p^2)^{-1}$ in dispersive case and $\alpha = n_2 I_0$, $\theta = (2k_0^2 w_{\text{in}}^2)^{-1}$ in diffractive case. Thus, finally we get the following equations:

$$\partial_z v + v \partial_x v - \alpha \varphi \partial_x I - \theta \partial_x \left(\frac{x^{1-\nu}}{\sqrt{I}} \partial_x (x^{\nu-1} \partial_x \sqrt{I}) \right) = 0, \quad (3.4)$$

$$\partial_z I + v \partial_x I + I \partial_x v + (\nu - 1) \frac{v I}{x} = 0. \quad (3.5)$$

Evidently, Eqs. (3.4, 3.5) must be supplemented with a boundary conditions. In case of collimated Gaussian beam these read

$$v(0, x) = 0, \quad I(0, x) = \exp(-x^2). \quad (3.6)$$

Let us now make some estimates. For example, in the case of (1+2) dimensions, the last term in Eq. (3.2) describes diffraction. Typical values of the parameters in modern experiments are: $\lambda = 800\text{nm}$, initial beam radius $\omega_0 = 3\text{mm}$ Ref [14]. Using these values, we get $\theta_2 \simeq 2 \times 10^{-9}$. For pulse propagation in air $n_2 = 3.19 \times 10^{-19} \text{cm}^2/\text{W}$, $I_0 = 10^{12} \text{W}/\text{cm}^2$ $\alpha = 3 \times 10^{-7}$. This means that the diffraction term in (1+2) dimensions can be neglected and that the geometrical optics approximation should give a reasonable description of the problem of intense laser beam propagation in gases. Typically, solid media have refractive indices of the order $n_2 \sim 10^{-16} \text{cm}^2/\text{W}$, and, consequently the geometrical optics approximation will provide a good accuracy in this case as well. In (1+1) dimensions, when this term is responsible for the dispersion, a validity of the semi-classical approximation is discussed in detail in Ref. [123].

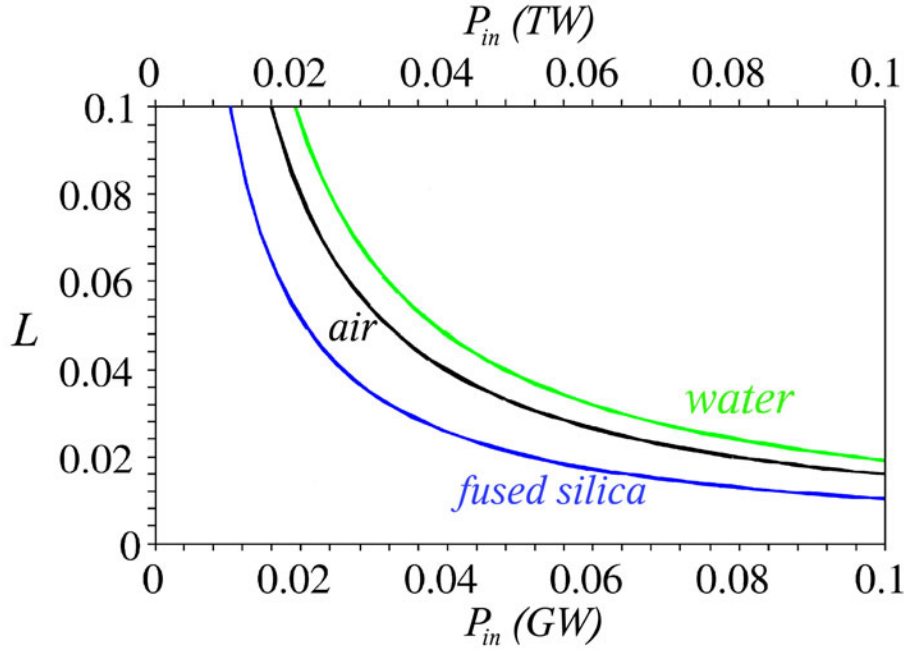


Figure 3.1: (Color online.) Accuracy $L \equiv L_{\text{nl}}/L_{\text{diff}}$ of the geometrical optics approximation for different media as a function of the laser pulse power P_{in} . The green, black and blue curves refer to water, air and fused silica, respectively. The pulse wavelength is assumed to be 800nm. P_{in} is given in units of TW for air, and of GW for water and fused silica.

Another argument in favor of geometrical optics approximation can be deduced via comparison of the magnitudes of diffraction contributions and the nonlinear effects to the beam propagation. They can be estimated through the comparison of the characteristic distances: the diffractive length L_{diff} , and the nonlinear length L_{nl} , at which the beam suffers considerable changes [30]. Then, $L \equiv L_{\text{nl}}/L_{\text{diff}}$ can serve as a measure of the accuracy of the geometrical optics approximation: if $L \ll 1$, diffraction can be neglected.

The main contribution to $n(|\mathcal{E}|^2)$ is usually given by the Kerr cubic term $n_2|\mathcal{E}|^2$. Therefore it is natural to define a nonlinear length $L_{\text{nl}} = 1/(k_0 n_2 I_0)$, where I_0 is the intensity of the beam at the entry plane of the nonlinear medium. The diffraction length is defined as $L_{\text{diff}} = n_0 k_0 w_0^2/2$, where w_0 is the initial beam radius [30]. In Fig.3.1 we plot L as a function of the initial beam power P_{in} ($P_{\text{in}} = I_0 w_0^2 \pi/2$) for different media and $\lambda = 800$ nm. In many recent experiments $L \sim 0.05$ or smaller (see [30] and Refs. therein), thus making the geometrical optics approximation valid.

For propagation of X-ray laser radiation in future experiments Ref. [37], the geometrical optics approximation will provide an even better accuracy. This fact enables us to omit the last higher order derivative term in Eq. (3.7), and search for the solution under the geometrical optics approximation.

In such a way, in case when diffraction (dispersion) can be neglected, we have

the following equations:

$$\partial_z v + v \partial_x v - \varphi \partial_x I = 0, \quad (3.7)$$

$$\partial_z I + v \partial_x I + I \partial_x v + (\nu - 1) \frac{Iv}{x} = 0. \quad (3.8)$$

Further simplification of these equations can be achieved in (1+1) dimensions if we notice that in this case the system (3.7-3.8) is linear with respect to the first order derivatives. Therefore, it is convenient to use the hodograph transformation [17] in order to transform it into a linear system of partial differential equations.

The key point of the hodograph transformation is exchange of dependent and independent variables. In order to perform this trick, let us first write down the total derivatives:

$$dv = v_x dx + v_z dz, \quad dI = I_x dx + I_z dz. \quad (3.9)$$

Dividing both of the Eqs. (3.9) by dv and dI , we obtain a system of four equations

$$1 = v_x \frac{\partial x}{\partial v} + v_z \frac{\partial z}{\partial v}, \quad 1 = I_x \frac{\partial x}{\partial I} + I_z \frac{\partial z}{\partial I}, \quad (3.10)$$

$$0 = v_x \frac{\partial x}{\partial I} + v_z \frac{\partial z}{\partial I}, \quad 0 = I_x \frac{\partial x}{\partial v} + I_z \frac{\partial z}{\partial v}. \quad (3.11)$$

Resolving system of algebraic Eqs. (3.10-3.11) with respect to v_x , v_z , I_x and I_z , we get

$$v_x = \frac{1}{J} \frac{\partial t}{\partial I}, \quad v_z = -\frac{1}{J} \frac{\partial x}{\partial I} \quad (3.12)$$

$$I_x = -\frac{1}{J} \frac{\partial t}{\partial v}, \quad I_z = \frac{1}{J} \frac{\partial x}{\partial v}, \quad (3.13)$$

where J is the Jacobian of the transition

$$J = \frac{\partial x}{\partial v} \frac{\partial z}{\partial I} - \frac{\partial x}{\partial I} \frac{\partial z}{\partial v} \quad (3.14)$$

Let us now introduce the new variables $\tau \equiv I_z$, $\chi \equiv x - v_z$, $w \equiv v/\alpha$. Then, we get

$$J = \frac{\partial_w \chi \partial_I \tau}{\alpha I} - \frac{\partial_w \tau \partial_I \chi}{\alpha I} - \frac{\tau \partial_w \chi}{\alpha I^2} + \frac{\tau \partial_I \tau}{I^2} - \frac{\tau^3}{I^3}, \quad (3.15)$$

$$\frac{\partial t}{\partial I} = \frac{\partial_I \tau}{I} - \frac{\tau}{I^2} \quad \frac{\partial x}{\partial v} = \frac{1}{\alpha} \partial_w \chi + \frac{\tau}{I} + \frac{w}{I} \partial_w \tau \quad \text{etc.} \quad (3.16)$$

Substituting Eqs. (3.13, 3.15, 3.16) into Eqs. (3.7, 3.8), in (1+1) dimensions we arrive at

$$\partial_w \tau - \frac{I}{\varphi(I)} \partial_I \chi = 0, \quad (3.17)$$

$$\partial_w \chi + \alpha \partial_I \tau = 0. \quad (3.18)$$

In $(1+\nu)$ dimensions the Eqs. (3.7-3.8) read

$$\partial_w \tau - \frac{I}{\varphi(I)} \partial_I \chi = 0, \quad (3.19)$$

$$\begin{aligned} & \partial_w \chi + \alpha \partial_I \tau + \\ & \frac{(\nu - 1)\alpha w}{\chi I + \alpha \tau w} \left[\partial_w \chi \partial_I \tau - \partial_w \tau \partial_I \chi - \frac{\tau \partial_w \chi}{I} + \frac{\alpha \tau \partial_I \tau}{I} - \frac{\alpha \tau^3}{I^2} \right] = 0, \end{aligned} \quad (3.20)$$

The boundary conditions are transformed as follows: for $w = 0$

$$\tau = 0, \quad \chi = H(I). \quad (3.21)$$

Evidently, for example in case of the Gaussian beam we have $\chi = \sqrt{\ln(1/I)}$.

Chapter 4

Review of Analytical Results

Let us now present a short review of analytical results and approaches in the problem of light propagation in nonlinear media. Because of the immense number of papers devoted to this issue, we can only mention some here which are more often cited in the literature and/or important for our further exposition.

4.1 Exact analytical solutions

4.1.1 Geometrical optics approximation

One of the first reviews devoted to analytical studies of the nonlinear optics equation, was published by Akhmanov *et al.* Ref. [4]. In this paper, the authors presented the solutions constructed by them under the geometrical optics approximation for Kerr nonlinear refractive index. For this situation Eqs. (3.7-3.8) read

$$\partial_z v = -v \partial_x v + \alpha \partial_x I, \quad (4.1)$$

$$\partial_z I = -\partial_x(Iv) - (\nu - 1) \frac{Iv}{x}, \quad (4.2)$$

where ν is equal to dimensionality of the problem: $\nu = 1$ in (1+1) dimensions, $\nu = 2$ in (1+2) etc.

In Ref. [3] it was shown that in (1+1) dimensions, equations (4.1,4.2) allow an exact solution:

$$v = -2\alpha I z \tanh(x - vz), \quad \alpha I^2 z^2 = I \cosh^2(x - vz) - 1, \quad (4.3)$$

which, evidently, corresponds to the boundary conditions: $I(0, x) = \cosh^2(x)$, $v(0, x) = 0$.

The solution Eq. (4.3) exhibits a singularity at the point $z_{\text{sf}} = 1/2\sqrt{\alpha}$. At this point the derivative $\partial_z I(z)|_{z_{\text{sf}}}$ goes to infinity, but on-axial intensity magnitude remains finite and equal to $I_{\text{ext}} = 2$.

In (1+2) dimensions, Eqs. (4.1, 4.2) admit the solution

$$v = \frac{-2\alpha z}{1 - 2\alpha z^2}, \quad I = \frac{1}{1 - 2\alpha z^2} \left(1 - \frac{x^2}{1 - 2\alpha z^2} \right), \quad (4.4)$$

which describes the propagation of an initially parabolic laser beam, $I(0, x) = 1 - x^2$. The solution becomes singular at the point $z_{sf} = 1/\sqrt{2\alpha}$.

4.1.2 Exact solutions beyond the geometrical optic approximation

At the moment, there are only two known exact analytical solutions for the nonlinear Schrödinger equation (3.1) with physically interesting boundary conditions. Both of them were constructed for Kerr nonlinearity in (1+1) and (1+2) dimensions.

Exact solution in (1+1) dimensions. Inverse scattering method

In (1+1) dimensions for Kerr refractive index, the Eq. (3.1) in dimensionless form reads

$$i\partial_t\psi(x, t) + \partial_{xx}\psi(x, t) + \kappa|\psi(x, t)|^2\psi(x, t) = 0. \quad (4.5)$$

In order to find a solution to Eq. (4.5), one takes $\psi(x, t)$ in the form Ref. [1]:

$$\psi(x, t) = A(x - vt) \exp(i\phi\xi + ivx). \quad (4.6)$$

Substituting Eq. (4.6) into Eq. (4.5), we get

$$-\phi A + \frac{1}{2}A_{xx} - \frac{1}{2}v^2A + A^3 = 0. \quad (4.7)$$

Introducing $B \equiv \phi + v^2/2$, and substituting this expression into Eq. (4.7) one obtains

$$\frac{1}{2}A_{xx} - BA + A^3 = 0,$$

which, after multiplication by A_x and subsequent integration reads

$$(A_x)^2 = 2AB - A^4, \quad (4.8)$$

where we took into account that both function A and its derivative A_x must vanish for $|x| \rightarrow \infty$. Equation (4.8) admits a solution:

$$A(x) = \sqrt{2B} \cosh^{-1}[\sqrt{2B}(x - x_0)]. \quad (4.9)$$

Then, returning to the original variables, we get a result:

$$\psi(x, t) = \eta\sqrt{2\kappa} \frac{\exp(-4i(\xi^2 - \eta^2)t - 2i\xi x + i\varphi)}{\cosh(2\eta(x - x_0) + 8\eta\xi t)}. \quad (4.10)$$

This formula is referred to as a soliton solution. It describes evolution of a localized symmetric intensity distribution and is characterized by four constants: η , ξ , x_0 and φ which can be independent and arbitrary. However, we see that initial radius, amplitude of the soliton and the nonlinearity parameter κ are related to each other. In its turn, the velocity of the soliton can be arbitrary.

A generalization of this solution for multiple soliton case has been performed in Ref. [125]. Zakharov and Shabat found the solution to Eq. (4.5) making use of the inverse scattering method. They demonstrated that Eq. (3.1) can be rewritten in the form of a so-called Lax equation:

$$\partial_t \widehat{L} = \widehat{L}\widehat{A} - \widehat{A}\widehat{L}, \quad (4.11)$$

where \widehat{L}, \widehat{A} is the Lax pair.

$$\begin{aligned} \widehat{L} &= i \begin{pmatrix} 1+p & 0 \\ 0 & 1-p \end{pmatrix} \partial_x + \begin{pmatrix} 0 & \psi^* \\ \psi & 0 \end{pmatrix} \\ \widehat{A} &= -p \begin{pmatrix} 1 & 0 \\ 0 & 1 \end{pmatrix} \partial_{xx} + \begin{pmatrix} |\psi|^2/(1+p) & i\psi_x^* \\ -i\psi_x & -|\psi|^2/(1-p) \end{pmatrix} \end{aligned}$$

and p related to κ as $\kappa = 2/(1-p^2)$.

The method requires the eigenvalues and the continuous spectrum of \widehat{L} to be independent of t . Then, as a first step, named a direct scattering problem, one needs to find the time evolution of eigenfunctions of the operator \widehat{L} . The eigenvalue equation, $\widehat{L}\psi = \lambda\psi$, turns into a system of ordinary differential equations containing a solution ψ_0 at the boundary which can be described as a potential:

$$\phi_x^1 + i\zeta\phi^1 = i\frac{\psi_0}{\sqrt{1-p^2}}\phi^2, \quad (4.12)$$

$$\phi_x^2 - i\zeta\phi^2 = -i\frac{\psi_0^*}{\sqrt{1-p^2}}\phi^1. \quad (4.13)$$

Now we have to do some a priori assumptions about the spectrum of the problem. If $\zeta \equiv \lambda p/(1-p^2)$ is real (in this case we denote it as ξ), then a solution can be represented as a superposition $\varphi = a(\xi)\overline{\psi} + b(\xi)\psi$, where the overline denotes Hermitian conjugation, and condition $|a(\xi)|^2 + |b(\xi)|^2 = 1$ has to be satisfied. If ζ is a complex number, ζ_j , $j = 1, \dots, N$ should be determined as the points on the upper half complex plane $\Im\zeta > 0$ where $a(\zeta) = 0$. The solution then can be written as $\varphi(x, \zeta_j) = c_j\psi(x, \zeta_j)$ (for details see Ref. [125]).

From Eq. (4.11) it follows that eigenfunctions of the operator \widehat{L} are governed by equation:

$$i\partial_t\psi = \widehat{A}\psi,$$

which defines the temporal evolution of the coefficients:

$$b(\xi, t) = b(\xi, 0)e^{4i\xi^2 t}, \quad c_j(t) = c_j(0)e^{4i\zeta_j^2 t}, \quad (4.14)$$

and $a(\xi)$ does not depend on time.

The next step is referred to as the inverse scattering problem, when we have to reconstruct the solution $\psi(x, t)$ on the basis of obtained coefficients $a(\xi)$, $b(\xi, t)$, $-\infty < \xi < +\infty$; $c_j(t)$, $j = 1, \dots, N$. As we have seen, the values of these functions at $t = 0$ were defined by the initial conditions $\psi(x, 0)$; their subsequent evolution is defined by Eq. (4.14). Therefore, it is sufficient to define $\psi(x)$ as a function of $a(\xi)$, $b(\xi)$, and c_j . Calculation of this function can be done via integration of so-called Gelfand-Levitan-Marchenko integral equation. Let

$$F(x) = \frac{1}{2\pi} \int_{-\infty}^{+\infty} \frac{b(\xi)}{a(\xi)} e^{i\xi x} d\xi + \sum_{k=1}^N c_k e^{i\zeta_k x},$$

then the solution to Eq. (4.5) is $\psi(x) = iq(x)\sqrt{2/\kappa}$, where $q(x) = -2K_1(x, x)$, $\int_{-x}^{\infty} |q(s)|^2 ds = -2K_2(x, x)$ and $K_1(x, x)$, $K_2(x, x)$ are defined from the equations:

$$\begin{aligned} K_1(x, y) &= F^*(x+y) + \int_x^{\infty} K_2^*(x, s)F^*(s+y)ds, \\ K_2^*(x, y) &= - \int_x^{\infty} K_1(x, s)F(s+y)ds. \end{aligned}$$

In general, exact solution is a superposition of a number N of solitons (4.10) with $4N$ arbitrary constants η_i , ξ_i , x_{0i} and φ_i . Mathematically, an evolution of the system (3.1) can be modeled as a process of N soliton scattering.

As it was demonstrated in Ref. [125], under the semi-classical limit all eigenvalues ζ lie at the imaginary axis, and the initial multisoliton solution is unstable.

The solution obtained by Zakharov and Shabat is exact. However, for a majority of actual cases the mathematical models corresponding to real physical situations belong to the class of the so-called unintegrable systems for which stable soliton solutions do not exist and the method of inverse scattering turns out to be no longer applicable [66]. For example, the method does not yield results already in the case of light propagation in (1+2) dimensions, typical for all experiments with nonlinear self-focusing and filamentation.

In their seminal paper [125], Zakharov and Shabat studied the stability of soliton solutions. They demonstrated that a single soliton solution is stable. However, this result was obtained under the assumption that the so-called nonsolitonian part (deviation on the solution from the single soliton profile) is negligible, and it hardly can be expanded to the case when the amplitude of the solution considerably exceeds the value $\eta\sqrt{2\kappa}$.

Townes profile and beam collapse

In case of (1+2) dimensions, Eq. (3.1) has solutions of the form $\psi = e^{i\lambda z} R_\lambda(r)$, where $R_\lambda(r) = \lambda R(\lambda r)$, and R is the solution of equation

$$R''(r) + \frac{1}{r}R' - R + R^3 = 0, \quad R'(0) = 0, \quad R(\infty) = 0. \quad (4.15)$$

Equation (4.15) has an infinite number of solutions. Of most interest, however, is the ground-state solution, known as the Townes profile, which is positive, symmetric and monotonically decreasing to zero under $|x| \rightarrow \infty$.

The Townes-profile solution was firstly introduced in Ref. [28]. Further, it was demonstrated that this solution is unstable: if the initial condition is perturbed, $\psi_0 = (1 + \epsilon)R(r)$, where $0 < \epsilon \ll 1$, then the corresponding solution will collapse after a finite propagation distance. The Townes solution is very important for the NLSE theory, since it provide the magnitude of the critical power for the beam collapse, and since it is universal, self-similar profile of collapsing beam in case of Kerr nonlinear refractive index.

In Ref. [121], the author proved that a necessity condition for the beam collapse is that the input power exceed the power of the Townes profile, i.e. that $P \geq P_{cr}$, where

$$P_{crT} = \int R^2 dx dy \approx 11.70. \quad (4.16)$$

Later, Merle in Refs. [87, 88] proved that for other beam profiles the critical power for the beam collapse should be strictly above the critical one calculated for the Townes profile Eq. (4.16). For example, for the Gaussian beam, the critical power is 2 % above P_{crT} , and for super-Gaussian - 9% P_{crT} . For the elliptic input profile $\psi_0 = cF(\sqrt{(x/a)^2 + (y/b)^2})$, the critical power defined as $P_{cr} \approx (0.2(g + 1/g) + 0.6)P_{cr0}$, where a, b, c are constants, $g = b/c$, and P_{cr0} is the critical power for the input profile $\psi_0 = cF(\sqrt{x^2 + y^2})$ [39].

Thus, the stronger is deviation of the input beam from the Townes profile, the bigger is the power of the beam required for the beam collapse.

In Ref. [39] Fibich emphasized that the amount of power that collapses into the singularity is independent on the initial conditions and always is given by P_{crT} Eq. (4.16). This means that part of the power equal to P_{crT} absorbed by the media at the collapse point whiles other part $P_{in} - P_{crT}$ continues to propagate forward.

The lens transformation

Concluding the part devoted to the exact solution we want to mention the lens transformation. It is based on the symmetry properties of the cubique Schrödinger equation (3.1) in (1+2) dimensions, which allow to transform results obtained for a

collimated beam to a beam focused by the lens with a focal length, f . In Ref. [111] it is demonstrated that, if at the boundary, the solution to the nonlinear Schrödinger equation (3.1) is given by function

$$\psi(0, x, y) = \psi_0 \exp\left(\frac{-i(x^2 + y^2)}{4f}\right),$$

where x and y are radial variables, then at a certain point z the solution reads

$$\psi(z, x, y) = \frac{1}{L(z)}\psi(\zeta, \xi, \eta) \exp\left(\frac{iL(z)_z(x^2 + y^2)}{L(z)4}\right), \quad (4.17)$$

where

$$L(z) = 1 - \frac{z}{f}, \quad \zeta = \int_0^z L^{-2}(s)ds, \quad \xi = \frac{x}{L(z)}, \quad \eta = \frac{y}{L(z)}. \quad (4.18)$$

As a consequence of this transformation, we get the lens rule

$$\frac{1}{z_{\text{sf}}} + \frac{1}{f} = \frac{1}{z_{\text{sf},f}} \quad (4.19)$$

where $z_{\text{sf},f}$ is a self-focusing position which is a sum of the nonlinear self-focusing and focusing by the lens at the boundary.

4.2 Approximate Results. Quasi self-similar methods

Existence of exact solutions for Kerr nonlinear refractive index motivated many authors for searching approximate solutions in a quasi self-similar form.

4.2.1 Variational approach

For the first time, variational approach was applied to the Nonlinear Schrödinger equation with Kerr nonlinearity by Anderson in Ref. [7]. Later, in great number of papers (see e.g. [30, 8, 5, 103, 12]) this ideology was applied to NLSE with a more complicated form of the refractive index. In many interesting situations, the model equation has form (see Chapter 2):

$$\begin{aligned} \frac{\partial E}{\partial z} &= \frac{i}{2k} \left(\frac{\partial^2}{\partial r^2} + \frac{1}{r} \frac{\partial}{\partial r} \right) E + ik_0 n_2 T |E|^2 E \\ &- \left(\frac{\sigma_n}{2} + \frac{ik_0}{2\rho_c} \right) \rho_{at} \tau_r \sigma_K |E|^{2K} E - \frac{\beta_K}{2} |E|^{2K-2} E, \end{aligned} \quad (4.20)$$

where K is a number of photons required for a simultaneous ionization, and all other notations are similar to Chapter 2.

It is easy to verify that equation (4.20) is the Euler-Lagrange equation of motion

$$\frac{\partial}{\partial z} \frac{\partial L}{\partial \left(\frac{\partial E^*}{\partial z}\right)} + \frac{\partial}{\partial r} \frac{\partial L}{\partial \left(\frac{\partial E^*}{\partial r}\right)} - \frac{\partial L}{\partial E^*} = Q,$$

with Lagrangian

$$L = \frac{i}{2} \left(E \frac{\partial E^*}{\partial z} - E^* \frac{\partial E}{\partial z} \right) r + \frac{r}{4k} \left| \frac{\partial E}{\partial r} \right|^2 - \frac{k_0 n_2 r}{2} |E|^4 + \frac{\alpha_K r}{2(K+1)} |E|^{2K+2}, \quad (4.21)$$

and dissipative right hand side

$$Q = -i \frac{\beta_K r}{2} |E|^{2K-2} E - i \frac{\gamma_K r}{2} |E|^{2K} E, \quad (4.22)$$

where asterisk means the complex conjugation. We introduced notations: $\alpha_K = \sigma \tau_r \sigma_K \rho_{at}$, $\gamma_K = k_0 \tau_r \sigma_n \rho_{at} / \rho_c$.

Let at the boundary intensity distribution is given by the Gaussian profile:

$$E(0, r, t) = W_0 \exp \frac{-r^2}{2a_0^2}.$$

Then, at the next step one assumes that upon propagation, the beam profile will keeps its Gaussian shape, but the average radius, intensity and phase of the beam will be functions of the propagation distance z . Thus, one search for the solution in the form:

$$E(z, r) = W \exp(-r^2/2a^2 + ibr^2 + i\phi), \quad (4.23)$$

where $W = W(z)$, $a = a(z)$, $b = b(z)$, and $\phi = \phi(z)$ are variational parameters.

Substituting the trial solution (4.23) into (4.21,4.22) and integrating over the transverse coordinate, we obtain the reduced Lagrangian

$$L_R = \frac{1}{2} \frac{\partial b}{\partial z} W^2 a^4 + \frac{1}{2} \frac{\partial \phi}{\partial z} W^2 a^2 + \frac{W^2}{8k} + \frac{b^2 a^4 W^2}{2k} - \frac{k_0 n_2 W^4 a^2}{8} - \frac{\alpha W^{2K+2} a^2}{4(K+1)^2}. \quad (4.24)$$

Equation of motion for the variational parameters could be obtained from Ref. [25] and read

$$\frac{\partial}{\partial z} \frac{\partial L_R}{\partial \left(\frac{\partial \mu_j}{\partial z}\right)} - \frac{\partial L_R}{\partial \mu_j} = 2Re \int Q \frac{\partial E^*}{\partial \mu_j} dr,$$

where μ_j has meaning W , a , b , and ϕ for $j = 1..4$, correspondingly. Then, after some algebra, we get the final analytical result in form of a set of ordinal differential equations:

$$\begin{aligned} \frac{\partial a}{\partial z} &= ab + \frac{P^{K-1}}{a^{2K-3}} \left(\frac{\beta_K P_{cr}^{K-1}}{2K a_0^{2K-4}} \right) \left(1 - \frac{1}{K} \right) + \frac{P^K}{a^{2K-1}} \left(\frac{\gamma_K P_{cr}^K K}{2(K+1)^2 a_0^{2K-2}} \right), \\ \frac{\partial b}{\partial z} &= -b^2 + \frac{1}{4a^4} - \frac{P}{2a^4} - \frac{P^K}{a^{2K+2}} \left(\frac{\alpha_K K k}{2(K+1)^2 a_0^{2K-2} \pi^K} \right), \\ \frac{\partial P}{\partial z} &= -\frac{P^K}{a^{2K-2}} \left(\frac{\beta_K k P_{cr}^{K-1}}{K a_0^{2K-4} \pi^K} \right) - \frac{P^{K-1}}{a^{2K}} \left(\frac{\gamma_K P_{cr}^K}{(K+1) a_0^{2K-2} \pi^{K+1}} \right). \end{aligned} \quad (4.25)$$

Where we introduce dimensionless variables $P = 2\pi \int |E|^2 r dr / P_{cr}$, $a = a/a_0$, $b = ba_0^2$ and z in units of ka_0^2 ; $P_{cr} = \lambda_0^2 / 2\pi n_0 n_2$ is the critical power for self focusing for laser beam.

Finally, the used approach allowed to reduce initial partial differential equations (4.20) into a system of nonlinear ordinal differential equations (4.25). From the mathematical point of view, the new problem is evidently rather simple in comparison to the original one. However, Eqs. (4.25) must still to be solve numerically and give no explicit/implicit expressions for the self-focusing position and value of intensity along the propagation.

The most important shortcoming of the method is the fact that it is based on an assumption of a fixed (Gaussian) shape of the beam upon the propagation, that is normally not the case as was demonstrated in many papers, e.g. in Refs. [67, 52]. Consequently, the approach is not able to provide a sufficient accuracy of theoretical results.

In spite of this problem, up to now, the variational approach with its numerous corrections are extremely popular. The reason for this is a flexibility of this method. It is applicable to NLSE with any nonlinear response and any dimensionality of the problem. This method allows to predict a qualitative behavior of the solutions. In particular, based on this method in Refs. [56, 11], the authors demonstrated that multiphoton ionization leads to the self-focusing collapse arrest in a media with original Kerr response.

4.2.2 Berge's variational approach

Disadvantage of the variational approach described above is as following: this formalism does not take care about conservation laws. In order to improve this, Berge *et at.* [12, 103] suggested the following modification of the method: They considered dimensionless nonlinear Schrödinger equation in (1+3) dimensions [103]:

$$i\partial_z \psi + r^{-1} \partial_r (r \partial_r \psi) - \delta \partial_{tt} \psi + |\psi|^4 = 0, \quad (4.26)$$

and the boundary conditions

$$\psi_0 = \sqrt{8p} \exp(-r^2 - t^2) \quad (4.27)$$

Here p is related to the beam perimeters as $8p = 2P_{in} / \pi w_0$, r is normalized into the initial beam radius w_0 , t is normalized into the pulse duration t_p , $\delta \equiv 2z_0 k'' / t_p$, and z_0 is the Rayleigh distance $z_0 = \pi n_0 w_0^2 / \lambda_0$.

Integration of Eq. (4.26) gives the moment equations:

$$d_z^2 \int r^2 |\psi|^2 dr dt = 8 \int |\partial_r \psi|^2 dr dt - 4 \int |\psi|^4 dr dt, \quad (4.28)$$

$$d_z^2 \int t^2 |\psi|^2 dr dt = 4\delta \left(2\delta \int |\partial_t \psi|^2 dr dt + \frac{1}{2} \int |\psi|^4 dr dt \right). \quad (4.29)$$

As a next step, the authors made assumption about a fixed Gaussian form of the solution in both space and time. They suggested the following trial substitution:

$$\psi = \frac{\sqrt{T(z)}}{R(z)\sqrt{T(z)}} \exp\left(\frac{-r^2}{2R^2(z)} - \frac{t^2}{2T^2(z)} + \frac{iR_z(z)r^2}{4R(z)} - \frac{iT_z(z)t^2}{4\delta T(z)}\right). \quad (4.30)$$

One can see that it is different from Eq. (4.23), in spite on the bigger dimensionality, it contains a smaller number of variational parameters. Reduction of number of parameters was achieved by taking into account conservation laws Ref. [12].

Substitution of Eq. (4.30) into Eqs. (4.28-4.29) gives a system of ordinal differential equations:

$$\frac{1}{4}R^3R_{zz} = 1 - \frac{p}{2T}, \quad \frac{1}{4}T^3T_{zz} = \delta \left(\delta + \frac{Tp}{2R^2} \right). \quad (4.31)$$

These equations, generally speaking, must be again solved numerically. However, using the empirical Margurger formula Eq. (2.57), and a fact that for realistic physical system $pT/2R^2\delta \simeq const.$ the authors managed to get a critical value of δ

$$\delta = \frac{\sqrt{p^2 - 1}\sqrt{(\sqrt{2} - 0.852)^2 - 0.0219}}{1.835} \quad (4.32)$$

above which the self-focusing would be arrested by the normal group velocity dispersion, $\delta > 0$.

If the plasma response is taken into account in Eq. (2.51), then the reduced equations read Ref. [12]

$$\begin{aligned} \frac{1}{4}R^3R_{zz} &= 1 - \frac{P}{2T} + \chi(K, p)\frac{p^K}{R^{2K-2}T^{K-1}}, \\ \frac{1}{4}T^3T_{zz} &= \delta \left(\delta + \frac{Tp}{2R^2} \right), \end{aligned} \quad (4.33)$$

where $\chi(K) = \frac{\gamma_0\omega_0\tau}{2^{K+1}\sqrt{2^K}\beta_0^{2K}} \frac{\sqrt{\pi K}}{(K+1)^2} \frac{1+\omega_0^2\tau^2}{\omega_0^2\tau^2}$, as usually, K is a number of photons required for a simultaneous ionization, and all other parameters are discussed in Chapter 2.

Based on this approach (supplemented with numerical simulations) the authors shown that the electron density produced by photo-ionization defocuses the beam and arrests the self-focusing promoted by the Kerr response of the gas. Such a description of the self-guided beams emphasize the distortions caused by multiphoton sources in the temporal pulse profiles.

4.2.3 Fibich's quasi self-similar method

All previously mentioned semi-analytical methods were based on assumption about a self-similarity of the initial beam profile. In their papers Fibich and Papanicolaou see

Ref. [39] used an opposite assumption: It is proven that in vicinity of the collapsing point, the solution achieves the Townes profile. Therefore, these authors used the trial function in the form:

$$\begin{aligned}\psi_R &= \frac{1}{L(z)} R(\rho) \exp(iS), \quad \rho = \frac{r}{L}, \\ S &= \tau(z) + \frac{L_z r^4}{L 4}, \quad \partial_z \tau = 1/L^2,\end{aligned}$$

and $R(r)$ is the Townes solution Eq. (4.16).

Since deviation from the Townes profile assumed to be small, the key parameter of the problem

$$\beta(z) \equiv -L^3 L_{zz} \tag{4.34}$$

is small.

They considered NLSE with a small perturbation $|\epsilon| \ll 1$

$$i\partial_t \psi + \Delta \psi + |\psi(x, t)|^2 \psi(x, t) + \epsilon F(\psi, \psi_z, \nabla \psi, \dots) = 0, \tag{4.35}$$

and $|\epsilon F| \ll |\Delta \psi|$, $|\epsilon F| \ll |\psi|^3$.

Then, to the leading order, one can arrive at the following system:

$$\begin{aligned}\partial_z \beta + \frac{\nu(\beta)}{L^2} &= \frac{\epsilon \partial_z f_1}{2M} - \frac{2\epsilon f_2}{M}, \\ \partial_{zz} &= -\frac{\beta}{L^3},\end{aligned}$$

where

$$\begin{aligned}f_1(z) &= 2L \Re \int F(\psi_R) e^{-iS} [R(\rho) + \rho R'(\rho)] dx dy, \\ f_2 &= \Im \int F(\psi_R) \psi_R^* dx dy,\end{aligned} \tag{4.36}$$

$\nu(\beta) \sim 4\pi A_R^2 \exp(-\pi/\sqrt{\beta})$ if $\beta > 0$, and $\nu(\beta) = 0$ if $\beta \leq 0$, and $M = \|rR\|_2^2/4 \cong 3.46$, $A_R = \lim_{r \rightarrow \infty} R(r) \sqrt{r} \exp(r) \cong 3.52$.

This approach allowed the authors to get expression for the intensity distribution in neighbourhood of singularity, $2(z_{\text{sf}} - z) \sqrt{\beta(z)} = L^2(z)$, and expression for the nonlinear self-focusing position [39]:

$$z_{\text{sf}} \sim \sqrt{\frac{M P_{crT}}{P_{in} - 1}} \left(\int_0^\infty |\nabla_\perp \psi_0|^2 r dr \right)^{-1}. \tag{4.37}$$

Details of application of this method to modifications of Eq. (4.35) are given in Refs. [40, 42, 44, 45, 46].

4.3 Renormalization group symmetry analysis

A special chapter of the present dissertation is devoted to construction of the solution for the light propagation equations make in use the renormalization group symmetry (RGS) analysis. Therefore, in this part, we only briefly review main results in nonlinear optics achieved with RGS method.

The key point in construction of the solution is to construct the RGS. For that purpose, following the general RGS theory Refs. [102] one uses the Lie-Bäcklund symmetries admitted by both original differential equations and boundary conditions. This symmetry is determined by the group operator X . This operator serves as a tool for finding solution of the boundary value problem.

Usually the constructed symmetry operator has form: $X = \xi_i(x_1, x_2, \dots, x_n)\partial_{x_i}$, where x_i denote both independent and depend variables, $i = 1, \dots, n$, then one can obtain the solution via integration of the Lie equations Ref. [57]:

$$\frac{dx_1}{\xi_1} = \dots = \frac{dx_n}{\xi_n}.$$

Advantage of the method is an exitance of the formal step-by-step schema (see Chapter 5) which can be apply to any equations (which, of course, does not guaranty exitance of the appropriate symmetry group). If such group of symmetry can be constructed exactly (approximately) the boundary value problem can be solved exactly (approximately) without any artificial assumptions such as e.g. fixed beam form upon propagation.

4.3.1 RGS results in (1+1) dimensions

Application of the RGS method to the LNSE with Kerr nonlinearity and in (1+1) dimensions was done in Ref. [69]. In this case, Eq. (3.1) turns into a linear system of partial differential equations (see Chapter 2):

$$\begin{aligned} \tau_w - I\chi_I &= 0, & \chi_w + \alpha\tau_I &= 0, \\ \tau_s(0, I) &= 0, & \chi(0, I) &= \chi_0(I), \end{aligned} \quad (4.38)$$

where index s denotes derivative of arbitrary order with respect to I .

For a Gaussian beam, $\chi_0 = \sqrt{\ln(1/I)}$, Eqs. (4.38) admit an approximate symmetry group with generator:

$$X = -2\chi\partial_w + 2\alpha\tau\partial_I + (1 + \alpha\tau^2/I)\partial_\tau. \quad (4.39)$$

this symmetry operator gives an approximate analytical solution to Eq. (4.38) [69]

$$x^2 = (\alpha I z^2 - \ln I)[1 - P(\sqrt{\alpha I z^2})]^2, \quad v = -\frac{x}{z} \frac{P(\sqrt{\alpha I z^2})}{[1 - P(\sqrt{\alpha I z^2})]},$$

where $P(h) = 2he^{-h^2/2} \int_0^h e^{t^2/2} dt$.

If parameter α is involved into the symmetry transformation as an independent variable, the symmetry operator reads

$$X = 2\tau\partial_w + 2I\chi\partial_I + 2\alpha\chi\partial_\alpha - \partial_x \quad (4.40)$$

and provides the solution:

$$\begin{aligned} \frac{-x^2}{(1-2\alpha z^2 I)^2} &= \ln(I[1-\alpha z^2 I]), \\ v &= -\frac{2\alpha z x I}{1-2\alpha z^2 I}. \end{aligned} \quad (4.41)$$

For the boundary condition $I_0 = \cosh^{-2}(x)$, Eqs. (4.38) admit an approximate symmetry

$$X = \left(1 + \frac{\alpha\tau^2}{I \cosh^2(\chi)}\right) [\partial_\tau - 2 \tanh(\chi)\partial_w] + \frac{2\alpha\tau}{\cosh^2(\chi)\partial_I} \quad (4.42)$$

with the solution

$$v = -2\alpha I z \tanh(x - vz), \quad \alpha I^2 z^2 = I \cosh^2(x - vz) \ln(I \cosh^2(x - vz)), \quad (4.43)$$

An exact symmetry group

$$\begin{aligned} X &= \left(2I(1-I)\tau_2 - I\tau_1 - 2Iw(\chi_1 + I\chi_2) + \frac{\alpha I w^2 \tau_2}{2}\right) \partial_\tau \\ &+ \left(2I(1-I)\chi_2 + (2-3I)\chi_1 + \alpha w(2I\tau_2 + \tau_1) + \frac{\alpha w(I\chi_2 + \chi_1)}{2}\right) \partial_\chi, \end{aligned}$$

provides the exact solution Eq. (4.3).

Both solutions Eq. (4.43) and Eq. (4.3) are singular at the points $z_{\text{sf,approx}} = 1/\sqrt{e\alpha}$, and $z_{\text{sf,exact}} = 1/2\sqrt{\alpha}$, respectively.

4.3.2 RGS results in (1+2) dimensions

For a parabolic laser beam at the boundary $\chi_0 = \sqrt{1-I}$, Eq. (4.1,4.2) are invariant with respect to the action of infinitesimal symmetry operator

$$X = -2\chi\partial_w + 4\alpha\tau\partial_I + I(1+2\alpha\tau^2/I^2)\partial_\tau - \alpha w\partial_\chi \quad (4.44)$$

which gives exact solution (4.4).

Approximate solution for Kerr nonlinearity and arbitrary initial beam profile was obtained in Refs. [68, 67]. The infinitesimal RGS operator for this case reads:

$$\begin{aligned} X &= \left(\left(1 - \frac{z}{R}\right)^2 + z^2 S_{xx}\right) \partial_z + \left(\frac{r}{R^2} + \frac{v}{R} \left(1 - \frac{z}{R}\right) + S_x\right) \partial_v \\ &+ \left(-\frac{r}{R} \left(1 - \frac{z}{R}\right) + z S_x + v z^2 S_{xx}\right) \partial_r \\ &+ \left(\frac{2I}{R} \left(1 - \frac{z}{R}\right) - Iz \left(1 + \frac{vz}{r}\right) S_{xx} - \frac{Iz}{r} S_x\right) \partial_I. \end{aligned} \quad (4.45)$$

where

$$S(\chi) = \alpha N(\chi) + \frac{\theta}{\chi\sqrt{N(\chi)}}\partial_\chi \left(\chi\partial_\chi\sqrt{N(\chi)} \right) \quad (4.46)$$

Integration of the Lie equation determined by operator (4.45) provides the solution Ref. [67]:

$$v(z, r) = \frac{r - \chi}{z}, \quad I(z, r) = N(\mu) \left(1 - \frac{z}{R} \right)^{-1} \frac{\chi}{r} \frac{\partial_{\chi^2} S}{\partial_{\mu^2} S}, \quad (4.47)$$

where the dependence of two functions χ and μ on z and r is defined by the following relations:

$$r = \chi \left(1 - \frac{z}{R} \right) \left(1 + \frac{2z^2\partial_{\chi^2} S}{(1 - z/R)^2} \right), \quad S(\mu) - S(\chi) = \frac{z^2(\partial_{\chi^2} S)^2}{2(1 - z/R)^2} \quad (4.48)$$

The solution Eq. (4.47) allowed to study important features of the beam propagation. In the model equations (4.1,4.2) there are two parameters $\alpha = n_2 I_0$ and $\theta = 1/(2k_0^2 w_0^2)$ which are represents magnitude of the nonlinearity and the diffraction, respectively.

If $\alpha < \theta$, the diffraction is dominating, and the position of nonlinear focal plane is defined as

$$z_{nl} = R/(1 + 2(\theta - \alpha)R^2). \quad (4.49)$$

Under the limit $\alpha = 0$, expression (4.49) turns into $z_l = R/(1 + 2\theta R^2)$ which define position of the linear focal plane where the rays become parallel to the beam axis, and the beam radius achieves its minimum equals to $w_{min} = 1/\sqrt{1 + 1/2\theta R^2}$. In the focal plane, $v = 0$, is a turning plane for the rays.

In case of Kerr nonlinearity, points where $v = 0$ can be found from equation:

$$r_{v=0}^2 = \ln \left(\frac{\alpha z}{\theta z - (1 - z/R)/2R} \right). \quad (4.50)$$

This formula defines the curve on which the beam rays turn. The positivity conditions $r_{v=0} > 0$ provides a constraint on the interval z , where curve (4.50) is defined

$$\frac{R}{1 + 2\theta R^2} < z < \frac{R}{1 + 2(\theta - \alpha)R^2} \quad (4.51)$$

for $\alpha > \theta$, there are no upper restriction for the value of z .

If $\alpha > \theta$, the nonlinearity dominates the diffraction. In this case in Ref. [67] was demonstrated that there was a minimal value of the wave front radius at the boundary $R_{min} = 1/\sqrt{2(\alpha - \theta)}$. If $R > R_{min}$, there was one nonlinear self-focusing point, its position was defined as $z_{sf} = R/(1 + R\sqrt{2(\alpha - \theta)})$. Otherwise, a second nonlinear self-focusing point appeared at $z_{sf,2} = R/(1 - R\sqrt{2(\alpha - \theta)})$.

In such a way, application of RGS to the problem provided a quantitative description of the beam electric field everywhere in a nonlinear media and allowed to defined the global self-focusing characteristics in a more accurate way. Constructed solution indicated also that the singularity at the beam intensity shown up at low powers, before the whole beam started to converge, and the asymptotic behavior of the light intensity near the singularity depended on the incident beam profile. The RGS solution allowed to derive a parametric scaling for self-focusing. It predicted the dependence of the trapped power and the length of self-focusing on the nonlinearity α , diffraction θ , and the initial wave-front curvature R .

Chapter 5

Renormalization group symmetry analysis. Exact solutions

5.1 Introduction

In Chapters 2, 4 we discussed that for many situations typical for modern experiments, the refractive index has a rather complicated dependence on the electric field. Nevertheless, all exact analytical solutions were up to now obtained only for the Kerr-type refractive index $n = n_0 + n_2 I$. In the present chapter we shall for the first time construct an exact analytical solution for the light propagation equations in case of a more complicated dependence of the refractive index on intensity. Generally speaking, exact analytical solutions have already been constructed in several papers (See e.g. Refs. [49, 50]), however these solutions do not correspond to any physically based boundary value problem. Indeed, for physical reasons the solution must provide a positive (symmetric) bell-like intensity distribution upon propagation distance. Moreover, the refractive index must be a nonsingular saturating function of intensity. In order to find an exact solution fulfilling both of these (from the technical point of view rather difficult) requirements, we shall use a special mathematical formalism called a renormalization group symmetry analysis.

The renormalization group symmetry (RGS) analysis was introduced in mathematical physics in the beginning of the 1990s as a result of combining the quantum field theory Stueckelberg-Bogoliubov [109, 19, 18] renormalization group (RG) generalized in a form of functional self-similarity [100] with the Sophus Lie group formalism. Here, the central idea is tightly connected with Bogoliubov RG method [19] of improving an approximate solution of a QFT problem in the vicinity of a solution singularity.

The RG concept was transferred to mathematical physics having the same pragmatic goal in mind: to improve the solution behavior in the vicinity of a singularity. For the boundary value problems (BVPs) based on differential equations

(DEs), a RG algorithm was developed (see, e.g., [74, 102]) that unites the RG ideology of the quantum field theory with a regular symmetry construction procedure for BVP solutions. This algorithm gave rise to the concept of the RGS for BVP solutions: these symmetries result from a calculation procedure similar to the one used in modern group analysis. The algorithm of construction of renormalization-group symmetries can also be applied to problems involving differential and integral equations (see, e.g. Refs. [78, 79]).

Before proceeding any further, let us make a short review of results already obtained on the basis of the formulated scheme. The first application of RG-approach to a particular problem of laser plasma was announced in [72]. The problem, namely a nonlinear interaction of a powerful laser radiation with inhomogeneous plasma, has been detailed in subsequent publications [71, 76, 77]. A mathematical model was given by a system of nonlinear DEs for components of electron velocity, electron density and the electric and magnetic fields. The presence of small parameters (such as weak inhomogeneity of the ion density, low electron thermal pressure and small incident angles of a laser beam on plasma surface) in the initial system of equations provided a way to construct a RG-manifold, based on approximate group methods.

Application of the method to an initial value problem was done for the modified Burgers equation in Ref. [75]. This example yielded a detailed illustration of the method of constructing RG-symmetries when a basic RG-manifold is given by an original DE with parameters included in the list of independent variables. It was argued that the exact solution can be reconstructed from the perturbative solution with the help of any of the admitted RG-symmetry operators which form an eight-dimensional algebra. Two illustrative examples were given, dealing with perturbation theory in time and in nonlinearity parameter.

To demonstrate the method of constructing Lie-Bäcklund RG-symmetries, the initial value problem for a linear parabolic equation was considered in Ref. [73]. It was shown that appending Lie-Bäcklund RG-symmetries to point RG-symmetries extends the algebra of RG-symmetries up to an arbitrary order.

In Refs. [69, 68, 67] the RGS algorithm was applied in nonlinear optics to the problem of propagation and self-focusing of a wave beam in a medium with Kerr nonlinearity. It was revealed that RG-symmetries are related to formal symmetries that are constructed in the form of infinite series in medium nonlinearity parameter. For a specific form of boundary data infinite series are truncated with RG-symmetries presented by finite sums. Generally, this is not the case for arbitrary boundary data and in that event a finite sum describes approximate RG-symmetry for small nonlinearity parameter.

5.2 Renormgroup analysis: General scheme

The general idea of the algorithm is to find a specific renormgroup manifold \mathcal{RM} that contains the desired solution of BVP. The subsequent construction of a RGS, leaving this solution unaltered, is performed by standard methods of a group analysis of DEs.

Let us now following Ref. [102] present here the regular algorithm of constructing RGS as a step-by-step procedure. First of all, we emphasize that the desired regular approach to constructing RG-symmetries turns out to be possible for those mathematical models of physical systems that are based on differential or, in some particular cases, integro-differential equations. The key idea uses the fact [73, 101] that such models can be investigated by algorithms of modern group analysis.

A formal scheme can be presented as a sequence of steps:

First. A specific renormgroup manifold \mathcal{RM} for the given BVP should be constructed. This manifold is identified with a system of the k th-order differential equations

$$F_\sigma(x, u, u_{(1)}, \dots, u_{(k)}) = 0, \quad \sigma = 1, \dots, s. \quad (5.1)$$

which define surfaces in the space of independent, x^i , $i = 1, \dots, n$ and dependent u^α , $\alpha = 1, \dots, m$ variables and their derivatives, $u_i^\alpha(x) \equiv \partial u^\alpha / \partial x^i$, $u_{ij}^\alpha(x) \equiv \partial^2 u^\alpha / \partial x^i \partial x^j$, \dots .

Following Refs.[102] and notations of differential algebra, we shall treat all u^α , u_i^α , u_{ij}^α , \dots as variables as well. Thus we shall be dealing with an infinite number of variables

$$x = \{x^i\}, \quad u = \{u^\alpha\}, \quad u_{(1)} = \{u_i^\alpha\}, \quad u_{(2)} = \{u_{i_1 i_2}^\alpha\}, \dots; \quad (i, i_1, \dots = 1, \dots, n). \quad (5.2)$$

A locally analytic function $f(x, u, u_{(1)}, \dots, u_{(k)})$ of variables (5.2), with the highest k th-order derivative involved, is called a *differential function* of order k . The set of all differential functions of a given order form a space of differential functions \mathcal{A}_k , the universal space of the approach [90, 57].

Second. The next step of the scheme consists in calculation of a most general symmetry group \mathcal{G} leaving the manifold \mathcal{RM} intact. The term ‘‘symmetry group’’, along the similar lines with the classical group analysis, means the property of the system (5.1) to admit a local Lie group of point transformations in the space \mathcal{A}_k .

The Lie algorithm of finding such symmetries is based on a construction of tangent vector fields defined by operators

$$X = \xi^i \partial_{x^i} + \eta^\alpha \partial_{u^\alpha}, \quad \xi^i, \eta^\alpha \in \mathcal{A}_k, \quad (5.3)$$

with the coordinates, ξ^i , η^α being functions of group variables that have to be determined by a system of equations

$$X F_\sigma \Big|_{F_\sigma(x,u,u_{(1)},\dots,u_{(k)})=0} = 0, \quad \sigma = 1, \dots, s, \quad (5.4)$$

following from the invariance of \mathcal{RM} .

Here the symbol $|_{(5.1)}$ means calculated on the frame (5.1) and X is extended to all derivatives involved in F_σ : $X = \xi^i \partial_{x^i} + \eta^\alpha \partial_{u^\alpha} + \zeta_i^\alpha \partial_{u_i^\alpha} + \zeta_{i_1 i_2}^\alpha \partial_{u_{i_1 i_2}^\alpha} + \dots$, where the first, second etc prolongations defined as $\zeta_i^\alpha = D_i(\eta^\alpha - \xi^j u_j^\alpha) + \xi^j u_{ij}^\alpha$, $\zeta_{i_1 i_2}^\alpha = D_{i_1} D_{i_2}(\eta^\alpha - \xi^j u_j^\alpha) + \xi^j u_{j i_1 i_2}^\alpha$, Ref. [57].

The system of linear homogeneous PDEs (5.4) for coordinates ξ^i , η^α known as determining equations is, as a rule, overdetermined. Its solution defines a set of infinitesimal operators (5.3) (also known as group generators), which correspond to the admitted vector field and form a Lie algebra.

In case when the general element of this algebra

$$X = \sum_j A^j X_j, \quad (5.5)$$

where A^j are arbitrary constants, contains a finite number of operators, $1 \leq j \leq l$, the group is called finite-dimensional (or simply finite) with the dimension l . Otherwise, for unlimited j the group is called infinite.

The use of the infinitesimal criterion (5.4) for calculating the symmetry group makes the whole procedure algorithmic and can be carried out not only “by hand” but using modern symbolic packages of computer algebra (see, e.g., Vol.3 in [57]) as well.

The generator (5.3) of the group \mathcal{G} is equivalent to the canonical Lie–Bäcklund operator

$$Y = \kappa^\alpha \partial_{u^\alpha}, \quad \kappa^\alpha \equiv \eta^\alpha - \xi^i u_i^\alpha, \quad (5.6)$$

known as a canonical representation of X . It will play an essential role in subsequent RGS construction.

However, the group defined by the generators (5.3) and (5.6) cannot yet be referred to as a renormgroup, as it is not related to a partial BVP solution of interest.

Third. To arrive at a RGS, the restriction of the group \mathcal{G} on particular BVP solution is to be made. Mathematically, this procedure means imposing a vanishing condition on a linear combination of coordinates κ_j^α of the canonical operator equivalent to (5.5) on a particular approximate (or exact) BVP solution $U^\alpha(z)$

$$\left\{ \sum_j A^j \kappa_j^\alpha \equiv \sum_j A^j (\eta_j^\alpha - \xi_j^i u_i^\alpha) \right\} \Big|_{u^\alpha = U^\alpha(z)} = 0. \quad (5.7)$$

Evaluating (5.7) on a particular BVP solution $U^\alpha(z)$ transforms the system of DEs for group invariants into algebraic relations.

Firstly, it gives relations between A^j thus “combining” different coordinates of group generators X_j admitted by the \mathcal{RM} (5.1). Secondly, it eliminates (partially or entirely) the arbitrariness that may appear in coordinates ξ^i, η^α in the case of an infinite group \mathcal{G} .

Generally, the restriction procedure reduces the dimension of \mathcal{G} . It also “fits” boundary conditions into the operator (5.5) by a special choice of coefficients A_j . In case of infinite group, the restriction procedure can be done by choosing a particular form of arbitrary functions in coordinates ξ^i, η^α . Hence, the general element (5.5) of the group \mathcal{G} after the fulfillment of a restriction procedure can be expressed as a linear combination of new generators R_i with the coordinates $\tilde{\xi}^i, \tilde{\eta}^\alpha$,

$$X \Rightarrow R = \sum_j B^j R_j, \quad R_j = \tilde{\xi}_j^i \partial_{x^i} + \tilde{\eta}_j^\alpha \partial_{u^\alpha}, \quad (5.8)$$

where B^j are arbitrary constants.

The set of RGS generators R_i each containing the desired BVP solution in its invariant manifold, define a group of transformations that we also refer to as renormgroup.

In a particular case, when RG is constructed from a Lie group admitted by the original system of DEs, it turns out to be a subgroup of this group and a solution of the BVP appears as an invariant solution with respect to the point RG obtained (compare with [91]). Generally, not only the Lie point group, but also Lie-Bäcklund groups, approximate groups, nonlocal transformation groups, etc. (see, e.g. [57]), are employed as basic groups which are then to be restricted on the solution of a BVP.

Fourth. On this step the RGS generators are used to find analytical expressions for the solution of BVP. Mathematically, this is achieved by solving a combined system of (5.1) and the vanishing condition for the linear combination of coordinates $\tilde{\kappa}_j^\alpha$ of the canonical operator to (5.8),

$$\sum_j R^j \tilde{\kappa}_j^\alpha \equiv \sum_j B^j \left(\tilde{\eta}_j^\alpha - \tilde{\xi}_j^i u_i^\alpha \right) = 0. \quad (5.9)$$

One can see that conditions (5.9) are similar to (5.7). However, in contrast to the previous step, the differential variables u in (5.9) should not be replaced by an approximate expression for the BVP solution $U(z)$, but be treated as usual dependent variables.

For the one-parameter Lie point renormgroup, RG invariance conditions lead to the a first order PDE that gives rise to so-called group invariants arising as

solutions of associated characteristic equations. A general solution of the BVP can then be expressed in terms of these invariants (see below).

However, as we shall see later, in a general case of arbitrary RGS the group invariance conditions obtained for BVP do not necessarily coincide with characteristic equations for the Lie point group operator. They may appear in a more complicated form, e.g. as a combination of PDE and higher order ODE. Nevertheless, the general idea of finding solution of the BVP as RG invariant solutions remains valid.

Finally, let us consider in more details a case of approximate RGS. In the case when BVP contains a small parameter α , the desired \mathcal{RM} can be obtained by simplification of these equations and making use of ‘‘perturbation methods of group analysis’’ (see Vol.3, Chapter 2, in Ref. [57]). The main idea here is to consider a simplified ($\alpha = 0$) model, admitting a wider symmetry group in comparison with the case $\alpha \neq 0$. This symmetry is inherited by boundary equations and after the contributions from small α are taken into account additional power corrections with respect to α appear in the RGS generator.

5.3 Renormalization group solutions for the eikonal equations with a saturating nonlinearity

Let us now apply the developed formalism to the problem of light propagation in (1+1) dimensions. In this case, as we discussed in Chapter 3, the equations of motion read

$$\tau_v - \psi(I)\chi_I = 0, \quad \chi_v + \tau_I = 0, \quad (5.10)$$

where $\psi = I/(\alpha\varphi)$, ($\varphi = \partial_I n$). As a boundary condition, we take a collimated continuous wave beam with a localized symmetric intensity distribution at the entry plane

$$\tau(I, 0) = 0, \quad \chi(I, 0) = \chi_0(I). \quad (5.11)$$

Our goal is now to construct an exact analytical solution to the system of equations (5.10) with a nonlinear function $\psi(I)$ that corresponds to a saturating dependence of the refractive index on the intensity. For this goal, we take $\psi = e^{bI/I_0}/n_2 I_0$. The refractive index corresponding to this form of ψ is presented in Fig. 5.1.

Let us first sketch the broad outlines of our solution: first, we construct a Lie symmetry group admitted by Eqs. (5.10). Second, following a formal scheme discussed above, the obtained group shall be restricted to the surface of boundary conditions: $v = 0$, $\tau = 0$. All derivatives of τ with respect to I have to vanish too. Third, based on the requirement of vanishing of group coordinates on the boundary,

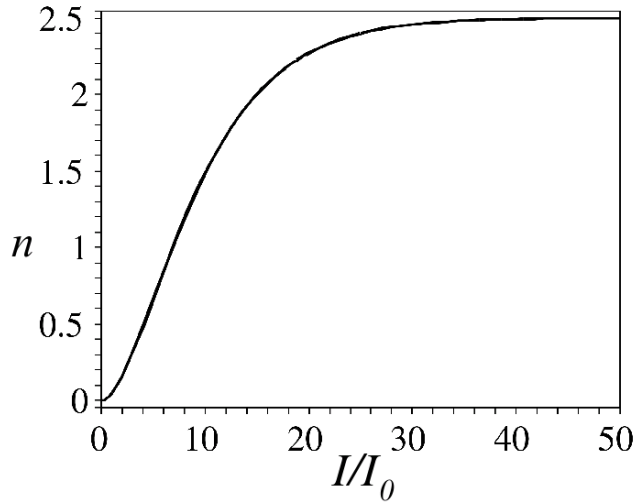


Figure 5.1: Nonlinear refractive index corresponding to $\psi = e^{bI/I_0}/n_2I_0$ as a function of the normalized intensity I/I_0 .

we shall construct such a linear superposition of them, which provides a localized intensity distribution. Finally, the integration of the constructed superposition shall yield a desired solution to Eqs. (5.10).

5.3.1 Recursion operators and Lie-Bäcklund symmetries of the second order

We start from the search for the Lie-Bäcklund symmetry group admissible by Eqs. (5.10). It is generated by the canonical infinitesimal operators [57]

$$X_i = f_i^s \partial_\tau + g_i^s \partial_\chi, \quad (5.12)$$

with coordinates f^s and g^s . For the Lie-Bäcklund symmetry of arbitrary order $s > 1$ the coordinates f^s and g^s depend on v , I , τ , χ and corresponding derivatives of τ and χ up to the s -th order with respect to I

$$f^s = f^s(v, I, \tau, \chi, \dots, \tau_I^s, \chi_I^s), \quad g^s = g^s(v, I, \tau, \chi, \dots, \tau_I^s, \chi_I^s),$$

Here, the index s stands for the order of the derivatives: $\tau_I^s \equiv \partial^s \tau / \partial I^s$ etc. The coordinates f^s and g^s must be found from the determining equation which in the case of Eqs. (5.10) reads [70]:

$$\begin{aligned} D_v(f^s) - \psi D_I(g^s) &= 0, \\ D_v(g^s) + D_I(f^s) &= 0, \end{aligned} \quad (5.13)$$

where D_I and D_v are operators of the total differentiation with respect to I and v :

$$D_I \equiv \partial_I + \sum_{s=0}^{\infty} (\tau_{I^{s+1}} \partial_{\tau_I^s} + \chi_{I^{s+1}} \partial_{\chi_I^s}), \quad (5.14)$$

$$D_v \equiv \partial_v + \sum_{s=0}^{\infty} (\tau_{v^{s+1}} \partial_{\tau_v^s} + \chi_{v^{s+1}} \partial_{\chi_v^s}). \quad (5.15)$$

Derivatives with respect to v in Eq. (5.15) in brackets should be excluded in accordance with Eqs. (5.10): $\tau_v = \psi \chi_I$, $\tau_{vv} = \psi \chi_{Iv} = -\psi \tau_{II}$ and so on.

In order to solve the Eqs. (5.13), it appears more convenient to use a recursion operator [70]. The latter is defined as 2×2 matrix operator transforming any linear solution of the determining equation (5.13) of the order s to the solution of these equations of higher order ($s+1$)

$$L \begin{pmatrix} f^s \\ g^s \end{pmatrix} = \begin{pmatrix} f^{s+1} \\ g^{s+1} \end{pmatrix}, \quad L = \begin{pmatrix} L^{11} & L^{12} \\ L^{21} & L^{22} \end{pmatrix}, \quad (5.16)$$

Substitution of Eq. (5.16) into the determining equation (5.13) yields the following system of equations for the elements of L

$$\begin{aligned} (D_v L^{11} - \psi D_I L^{21}) f^s + (D_v L^{12} - \psi D_I L^{22}) g^s &= 0 \\ (D_I L^{11} + D_v L^{21}) f^s + (D_I L^{12} + D_v L^{22}) g^s &= 0, \end{aligned} \quad (5.17)$$

which should be valid for any solutions f^s and g^s .

Explicit formulae for the recursion operators (5.16) obtained from Eqs. (5.17) were found in Ref. [70] and read

$$L_1 = \begin{pmatrix} 0 & -\psi D_I / \alpha \\ D_I & 0 \end{pmatrix}, \quad L_2 = \begin{pmatrix} 2\sigma D_I - 1 & -\psi(1 - 2\sigma_I)v D_I \\ (1 - 2\sigma_I)v D_I & 2\sigma D_I \end{pmatrix}, \quad (5.18)$$

$$L_3 = \begin{pmatrix} 2\sigma v D_I - (1 - \sigma_I)v & -\psi q D_I - \sigma \\ q D_I + \psi_I^{-1} & 2\sigma v D_I + v \sigma_I \end{pmatrix}, \quad (5.19)$$

where $\sigma \equiv \psi / \psi_I$ and $q \equiv (1 - 2\sigma_I)v^2/2 + 2 \int \psi_I^{-1} dI$. The formula for the recursion operator L_1 is valid for arbitrary nonlinearity function $\psi(I)$, while operators L_2 and L_3 arise for those functions $\psi(I)$ that fulfill the condition [70]:

$$\left(\frac{\psi}{\psi_I} \right)_{II} = 0. \quad (5.20)$$

The last requirement defined our choice of the function $\psi(I)$ in initial Eqs. (5.10). For this form of ψ we have:

$$\varphi = I e^{-bI}, \quad \sigma = b^{-1}, \quad q = v^2/2 - 2\alpha e^{-bI}/b^2.$$

In this particular case, the recursion operators read:

$$\begin{aligned} L_1 &= \begin{pmatrix} 0 & -e^{bI} D_I / \alpha \\ D_I & 0 \end{pmatrix}, \quad L_2 = \begin{pmatrix} 2D_I/b - 1 & -e^{bI} v D_I / \alpha \\ v D_I & 2D_I/b \end{pmatrix}, \\ L_3 &= \begin{pmatrix} 2v D_I/b - v & -e^{bI} (v^2/2 - 2\alpha e^{-bI}/b^2) D_I / \alpha - 1/b \\ (v^2/2 - 2\alpha e^{-bI}/b^2) D_I + e^{-bI} \alpha / b & 2v D_I/b \end{pmatrix}, \end{aligned}$$

Let us proceed with constructing the Lie-point symmetry group admitted by Eqs. (5.10) on the basis of these operators.

An evident solution of the determining equation (5.13) is

$$f_0^0 = \tau, \quad g_0^0 = \chi. \quad (5.21)$$

The action of three recursion operators L_i , $i = 1, 2, 3$ on the vector with coordinates given by Eq. (5.21) in accordance with Eq. (5.16) generates the symmetry group given by

$$f_1^1 = -e^{bI} \chi_I / \alpha, \quad (5.22)$$

$$f_2^1 = \frac{2\tau_I}{b} - \tau - \frac{e^{bI} v \chi_I}{\alpha}, \quad (5.23)$$

$$f_3^1 = \frac{2v\tau_I}{b} - v\tau - \frac{e^{bI}}{\alpha} \left(\frac{v^2}{2} - \frac{2\alpha e^{-bI}}{b^2} \right) \chi_I - \frac{\chi}{b}, \quad (5.24)$$

$$g_1^1 = \tau_I, \quad (5.25)$$

$$g_2^1 = v\tau_I + 2\chi_I/b, \quad (5.26)$$

$$g_3^1 = \left(\frac{v^2}{2} - \frac{2\alpha e^{-bI}}{b^2} \right) \tau_I + \frac{\alpha e^{-bI} \tau}{b} + \frac{2v\chi_I}{b}, \quad (5.27)$$

Admissible for arbitrary nonlinearity $\psi(I)$, the symmetries f_0^0 , g_0^0 describe the dilatation of τ and χ ; f_1^1 and g_1^1 generate translations along v -axis.

As it was formulated in Refs. [70, 102], an invariant solution to the boundary value problem, in particular the one, given by Eqs. (5.10), must be found from the constructed Lie-Bäcklund symmetries under the invariance conditions

$$f = 0, \quad g = 0. \quad (5.28)$$

In Eqs. (5.28) the functions f and g being arbitrary linear combinations of coordinates f_i and g_i of the group generators Eqs. (5.27) and must be chosen to satisfy the boundary conditions what in the actual case provide a localized intensity distributions.

Unfortunately, the point group Eqs. (5.27) are not sufficient in order to choose a linear superposition able to satisfy a localized intensity distribution at the boundary. Therefore, we shall continue using the discussed approach with operators L_i given by Eqs.(5.16) and vectors with coordinates of Eq. (5.27) in order to find the Lie-Bäcklund symmetries of the higher order. However, since the further calculations are quite cumbersome, for the sake of simplicity we shall first find the symmetry coordinates at the boundary where they have the simplest form. Afterwards, we completely reconstruct only such of them that will be included into the chosen linear superposition.

Table 5.1: Coordinates of the symmetry operators on the boundary.

	f_i	g_i
$i = 0$	0	χ
$i = 1$	$-e^{bI}\chi_I/\alpha$	0
$i = 2$	0	$2\chi_I/b$
$i = 3$	$2\chi_I/b^2 - \chi/b$	0
$i = 4$	$-2e^{bI}\chi_{II}/\alpha b$	0
$i = 5$	0	$-be^{bI}\chi_I/\alpha - e^{bI}\chi_{II}/\alpha$
$i = 6$	0	$2\chi_{II}/b^2 - \chi_I/b$
$i = 7$	0	$4\chi_{II}/b^2$
$i = 8$	$-2e^{bI}\chi_{II}/\alpha b - e^{bI}\chi_I/\alpha$	0
$i = 9$	$4\chi_{II}/b^3 - 4\chi_I/b^2 + \chi/b$	0
$i = 10$	$4\chi_{II}/b^3 - 2\chi_I/b^2$	0
$i = 11$	0	$2\chi_{II}/b^2 + \chi_I/b$
$i = 12$	0	$-4\alpha e^{-bI}\chi_{II}/b^4 + 4\alpha e^{-bI}\chi_I/b^3 - \alpha\chi e^{-bI}/b^2$

Thus, at the boundary $\tau = 0$, $v = 0$ the recursion operators read

$$L_1 = \begin{pmatrix} 0 & -e^{bI}D_I/\alpha \\ D_I & 0 \end{pmatrix}, \quad L_2 = \begin{pmatrix} 2D_I/b - 1 & 0 \\ 0 & 2D_I/b \end{pmatrix}, \quad (5.29)$$

$$L_3 = \begin{pmatrix} 0 & 2/b^2D_I - 1/b \\ -2\alpha e^{-bI}/b^2D_I + e^{-bI}\alpha/b & 0 \end{pmatrix}, \quad (5.30)$$

Action of these operators on Eqs. (5.21) gives 9 symmetry operators x_i which coordinates f_i g_i are listed in the Table 5.1.

Based on the operators presented in the Table 5.1, one can construct a linear superposition providing a localized intensity distribution. For instance, the equation

$$(2 - e^{bI-1})\chi_{II} + b(1 - e^{bI-1})\chi_I = 0 \quad (5.31)$$

has a particular solution $\chi = \sqrt{2e^{-bI+1} - 1}$. Resolving I as a function of χ , we get a convex symmetric on x intensity distribution

$$I = \frac{1}{b} \left(1 - \ln \left(\frac{\chi^2 + 1}{2} \right) \right), \quad (5.32)$$

which is presented by the black curve in Fig. 5.2.

From the Table 5.1 one can see that Eq. (5.31) corresponds to the following symmetry operators' superposition

$$\frac{\alpha}{e}g_5^2 + \frac{b^2}{2}g_7^2 + \frac{b^2}{2}g_2^1 = 0, \quad (5.33)$$

which, evidently, shall be supplemented by the equation:

$$\frac{\alpha}{e}f_5^2 + \frac{b^2}{2}f_7^2 + \frac{b^2}{2}f_2^1 = 0. \quad (5.34)$$

It is easy to see that in order to find an invariant solution satisfying Eqs. (5.10) and the boundary conditions of Eq. (5.32), we have to reconstruct a complete form of the symmetry coordinates f_5^2 , g_5^2 and f_7^2 , g_7^2 . Acting by the operator L_1 on the couple f_1^1 , g_1^1 , we get

$$\begin{pmatrix} f_5^2 \\ g_5^2 \end{pmatrix} \equiv \begin{pmatrix} -e^{bI}\tau_{II}/\alpha \\ -be^{bI}(\chi_{II} + b\chi_I)/\alpha \end{pmatrix}. \quad (5.35)$$

The similar procedure applied to the operator L_2 and coordinates f_2^1 , g_2^1 yields:

$$\begin{pmatrix} f_7^2 \\ g_7^2 \end{pmatrix} \equiv \begin{pmatrix} (4\alpha - e^{bI}v^2b^2)\tau_{II}/\alpha b^2 - 4\tau_I/b - e^{bI}v\chi_I/\alpha - 4e^{bI}v\chi_{II}/\alpha b + \tau \\ 4v\tau_{II}/b - v\tau_I - e^{bI}bv^2\chi_I/\alpha + (4\alpha - e^{bI}v^2b^2)\chi_{II}/\alpha b^2 \end{pmatrix}. \quad (5.36)$$

These equations together with Eq. (5.27) represent the list of symmetry operators required for construction of analytical solutions.

5.3.2 Invariant solutions

Equations (5.33-5.34) with expressions substituted from Eq. (5.35,5.36) represent a system of partial differential equations

$$2bv\tau_{II} + \left(2 - e^{bI-1} - \frac{v^2b^2e^{bI}}{2\alpha}\right)\chi_{II} + b\left(1 - e^{bI-1} - \frac{v^2b^2e^{bI}}{2\alpha}\right)\chi_I = 0, \quad (5.37)$$

$$-\frac{2vbe^{bI}}{\alpha}\chi_{II} - \frac{vb^2e^{bI}}{\alpha}\chi_I + \left(2 - e^{bI-1} - \frac{v^2b^2e^{bI}}{2\alpha}\right)\tau_{II} - b\tau_I = 0. \quad (5.38)$$

The first integral to the equation (5.37) can be easily found:

$$2bv\tau_I + \left(2 - e^{bI-1} - \frac{v^2b^2e^{bI}}{2\alpha}\right)\chi_I + b\chi = J(v). \quad (5.39)$$

$J(v)$ in the above formula should be found from the comparison with Eq. (5.38). Differentiating Eq. (5.39) with respect to v , taking Eqs. (5.10) into account and comparing obtained expression with Eq. (5.38), one can see that $J(v)$ should be a constant. In view of a symmetric initial intensity distribution with respect to $x \rightarrow -x$ reflections we are bound to choose $J = 0$. Then, substituting $\tau_I = -\chi_v$ into Eq. (5.39), we arrive at the following first order partial differential equation

$$-2bv\chi_v + \left(2 - e^{bI-1} - \frac{v^2b^2e^{bI}}{2\alpha}\right)\chi_I + b\chi = 0, \quad (5.40)$$

which can be integrated with a standart technique.

Integration of Eq. (5.40) gives two first integrals,

$$J^1 = \frac{\chi^2}{\sqrt{p}}, \quad J^2 = \frac{1}{\sqrt{p}} \left(2e^{1-bI} - 1 + \frac{b^2 e}{2\alpha} p \right) \quad (5.41)$$

where we introduced a new variable $\sqrt{p} = -v$ in order to keep in mind that negative value of v corresponds to the focusing beam for the positive values of x .

Now we are finally in a position to find a particular solution $\chi(v, I)$ for the Eqs. (5.10) satisfying the boundary conditions Eq. (5.32). Let us first notice that from the system of equations (5.10) it follows the linear second order partial differential equation

$$\alpha\chi_{vv} + (e^{bI}\chi_I)_I = 0,$$

which in new variables $\sqrt{p} = -v$ (consequently, $\partial p/\partial v = -2\sqrt{p}$) can be rewritten as:

$$\alpha 2\chi_p + 4p\chi_{pp} + (e^{bI}\chi_I)_I = 0. \quad (5.42)$$

Based on the result obtained in Eqs. (5.41), one can search for the solution to Eq. (5.42) based on the following Ansatz

$$\chi^2 = \sqrt{p}H^2(J^2), \quad (5.43)$$

Substituting Eq. (5.43) into Eq. (5.42) we get

$$\begin{aligned} \chi_p &= \frac{1}{4}p^{-3/4}H + p^{1/4}H_{J^2}J_p^2, \\ \chi_{pp} &= -\frac{3}{16}p^{-7/4}H + \frac{1}{2}p^{-3/4}H_{J^2}J_p^2 + p^{1/4}H_{J^2J^2}(J_p^2)^2 + p^{1/4}H_{J^2}J_{pp}^2, \\ \chi_I &= p^{1/4}H_{J^2}J_I^2, \\ \chi_{II} &= p^{1/4}H_{J^2J^2}(J_I^2)^2 + p^{1/4}H_{J^2}J_{II}^2. \end{aligned}$$

After some calculations the following linear equation on H can be obtained

$$(1 + s^2)H_{ss} + sH_s - H/4 = 0, \quad s = J^2/\sqrt{2b^2e/\alpha}. \quad (5.44)$$

Eq. (5.44) can be easily solved using the substitution $s = \sinh \mu$. Indeed, $H_s = H_{\mu\mu s} = H_{\mu}/\sqrt{1+s^2}$, $H_{ss} = H_{\mu\mu}/(1+s^2) - H_{\mu}s/(1+s^2)^{3/2}$, and after the substitution one gets

$$H_{\mu\mu} - H/4 = 0. \quad (5.45)$$

Eq. (5.45) has an evident general solution

$$H = C_1e^{-\mu/2} + C_2e^{\mu/2},$$

where C_1 and C_2 are constants which should be found from the boundary conditions.

Taking the Eq. (5.43) into account we get the expression for χ :

$$\chi = p^{1/4}[C_1 e^{-\mu/2} + C_2 e^{\mu/2}], \quad (5.46)$$

where $e^{\mu/2}$ should be found from the equation:

$$\sinh \mu = \sqrt{\frac{\alpha}{2b^2 e}} \frac{1}{\sqrt{p}} \left(2e^{1-bI} - 1 + \frac{b^2 e}{2\alpha} p \right). \quad (5.47)$$

Now we can now express e^μ from Eq. (5.47)

$$e^\mu = K/2 \pm \sqrt{K^2/4 + 1}, \quad (5.48)$$

where

$$K \equiv \sqrt{\frac{2\alpha}{b^2 e}} \frac{1}{\sqrt{p}} \left(2e^{1-bI} - 1 + \frac{b^2 e}{2\alpha} p \right).$$

Summarizing, we get the following formula

$$\chi = \frac{C_1 \sqrt{p}}{(\alpha/b^2 e)^{1/4} \sqrt{\Theta}} + C_2 (\alpha/b^2 e)^{1/4} \sqrt{\Theta} = \frac{\tilde{C}_1 \sqrt{p}}{\sqrt{\Theta}} + \tilde{C}_2 \sqrt{\Theta}, \quad (5.49)$$

where

$$\Theta \equiv \left\{ \left(2e^{1-bI} - 1 + \frac{b^2 e p}{2\alpha} \right) + \sqrt{\left(2e^{1-bI} - 1 + \frac{b^2 e p}{2\alpha} \right)^2 + \frac{2b^2 e p}{\alpha}} \right\}. \quad (5.50)$$

From the boundary conditions Eq. (5.32) and $v(z, 0) = 0$ it is easy to see that \tilde{C}_1 should be zero, and $\tilde{C}_2 = 1/\sqrt{2}$. In such a way, one of the solutions to the system of equations (5.10) is:

$$\chi = \frac{1}{\sqrt{2}} \sqrt{\left(2e^{1-bI} - 1 + \frac{b^2 e p}{2\alpha} \right) + \sqrt{\left(2e^{1-bI} - 1 + \frac{b^2 e p}{2\alpha} \right)^2 + \frac{2b^2 e p}{\alpha}}}. \quad (5.51)$$

In order to find the second function $\tau(I, v)$, we shall integrate the original equation (5.10) keeping the result (5.51) in mind. From Eqs. (5.10) we have

$$\tau = \frac{1}{\alpha} \int_0^v dv e^{bI} \chi_I. \quad (5.52)$$

For the sake of convenience, let us introduce a new variable ξ :

$$\cosh(\xi) \equiv \frac{2e^{1-bI} + \frac{b^2 e p}{2\alpha} + 1}{\sqrt{8e^{1-bI}}}. \quad (5.53)$$

Then

$$p = \frac{2\alpha}{b^2 e} \left[2\sqrt{2} e^{\frac{1-bI}{2}} \cosh(\xi) - 2e^{1-bI} - 1 \right], \quad (5.54)$$

$$\Theta = 2\sqrt{2} \exp\left(\xi + \frac{1-bI}{2}\right) - 2,$$

$$dv = \left(\frac{\partial v}{\partial p}\right) \left(\frac{\partial p}{\partial \xi}\right) d\xi = \frac{-1}{\sqrt{p}} \frac{2\sqrt{2}\alpha}{b^2 e} e^{\frac{1-bI}{2}} \sinh(\xi) d\xi. \quad (5.55)$$

Differentiating Eq. (5.51) with respect to I , in new variables we get

$$\chi_I = \frac{b}{4\sqrt{\Theta}} \frac{e^{\frac{1-bI}{2}} - \sqrt{2}e^{\xi+1-bI}}{\sinh(\xi)}.$$

The expression for τ becomes:

$$\tau = \frac{1}{b} \int_{\xi_0}^{\xi} \frac{(ae^{\xi} - 1)^{1/2}}{\sqrt{p}} d\xi = \sqrt{\frac{e}{2\alpha}} \ln \left(\frac{2e^{\xi}}{a} - 1 + \sqrt{\left(\frac{2e^{\xi}}{a} - 1\right)^2 - 1} \right) \Big|_{\xi_0}^{\xi},$$

where $a \equiv \sqrt{2} \exp(\frac{1-bI}{2})$. Considering the boundary conditions, the final solution reads:

$$\tau = \sqrt{\frac{e}{2\alpha}} \ln \left(e^{bI-1}(\chi^2 + 1) - 1 + \sqrt{(e^{bI-1}(\chi^2 + 1) - 1)^2 - 1} \right). \quad (5.56)$$

After direct substitution of Eqs. (5.51,5.56) into Eqs. (5.10) and a tedious calculation it is possible to verify that the obtained functions $\chi(I, v)$ and $\tau(I, v)$ are indeed exact analytical solutions for the formulated boundary value problem. In Fig. 5.2 we plot intensity beam distribution at different propagation distances calculated on the basis of the found solutions Eqs. (5.51, 5.56).

Let us now examine the obtained result a little more closely. Firstly let us find the total radius of the beam as a function of the propagation distance z . For this goal, we find where the intensity, which is implicitly given by Eqs. (5.51,5.56), intersects the surface $x = 0$. Putting $I = 0$ in Eq. (5.56), we find $\chi|_{I=0} = \pm\sqrt{2e-1}$. Substituting this number into Eq. (5.51) one can find that $v = 0$ and, consequently, $x = \pm\sqrt{2e-1}$. Thus, the phase gradient at the beam edge is equal to zero, the total radius of the beam is a constant and does not depend on the propagation length. By the numerical integration of the solutions Eqs. (5.51, 5.56) one can verify their consistence with the energy conservation: $\int I(x, z) dx$ from $x = \sqrt{2e-1}$ to $x = -\sqrt{2e-1}$ is a constant.

The fact that, for the considered case, the total radius of the beam is a constant and does not depend on z is a new one and completely different from all exact analytical results obtained so far. It was demonstrated earlier [4, 69] that for the Kerr nonlinearity the total beam radius decreases upon beam propagation. In the present

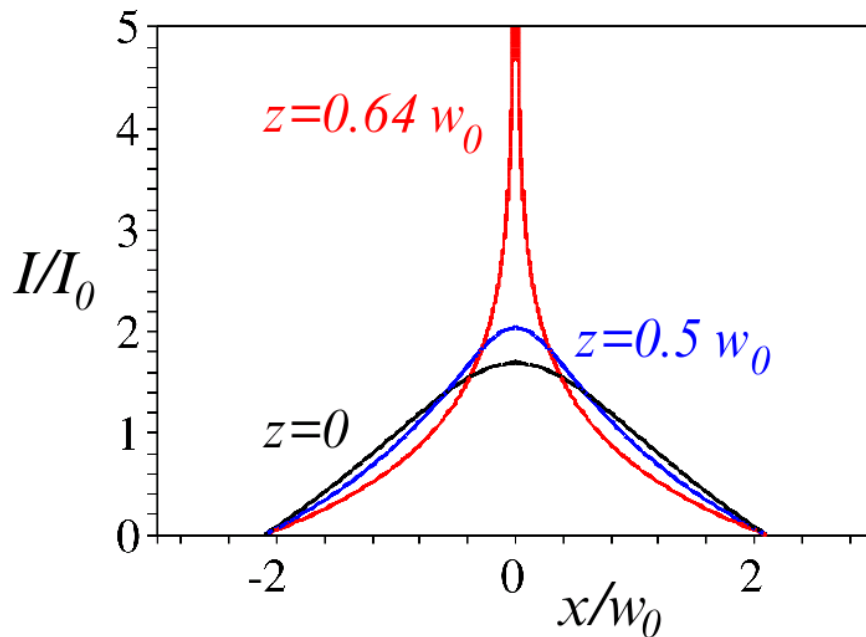


Figure 5.2: (Color online.) Beam profile at different propagation distances. $\alpha = 3$, $b = 1$ Black curve - $z = 0$, blue curve - $z = 0.5 w_0$, green curve - $z = 0.64 w_0$.

case, the beam shape and peak intensity are thus the only parameters depending on the propagation distance.

Evolution of the beam peak intensity, which for the symmetry reasons is situated at the beam axis, can be easily found from Eq. (5.56). Putting $x = 0$, $v = 0$ we have

$$z = \frac{1}{I} \sqrt{\frac{e}{2\alpha}} \ln \left(e^{bI-1} - 1 + \sqrt{(e^{bI-1} - 1)^2 - 1} \right). \quad (5.57)$$

On-axis intensity distribution versus the propagation distance is presented in Fig. 5.3. We see that the intensity monotonically increases and tends to infinity for z approaching a critical value denoted as a self-focusing position z_{sf} . Its exact value can be found from direct analysis of the Eq. (5.57). Considering Eq. (5.57) in the limit $I \rightarrow \infty$, we obtain

$$z_{\text{sf}} = b \sqrt{\frac{e}{2\alpha}}. \quad (5.58)$$

We notice that this result is different from all cases considered previously in Refs. [69, 113]. Previously one saw only such cases when the nonlinear self-focusing manifests itself by the fact that the derivative of the function $I(z)$ goes to infinity at the point z_{sf} . We see that in the present case the point z_{sf} is achieved only asymptotically.

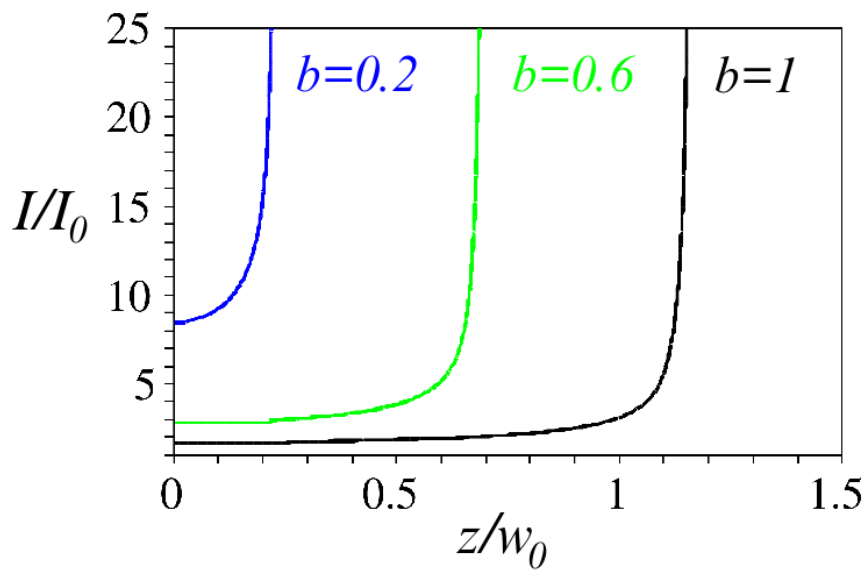


Figure 5.3: (Color online.) Onaxial intensity distribution as a function of the propagation length. $\alpha = 1$ Black curve - $b = 1$, green curve - $b = 0.6$ blue curve $b = 0.2$.

Chapter 6

Approximate analytical results

In the previous Chapter we succeeded in construction of exact analytical solutions for Eqs. (3.19-3.20) for a special form of refractive index and initial conditions. For this goal a special mathematical technique known as RGS analysis was used. Unfortunately an exact solution cannot be found for every problem under investigation, and often the problems allowing an exact solution do not correspond to interesting physical situations.

Therefore, it is very desirable to suggest a rather simple analytical approach in order to be able to construct an approximate analytical solution to a bigger set of physical situations. A review of existing approaches was given in Chapter 4. We see that only one of these methods RGS is able to provide a solution without the artificial assumption on a fixed beam shape Eq. (4.23,4.30) in the media. In presence of small parameters, analytical solution can be found based on RGS via construction of an approximate symmetry group. However, making use of this method requires an experience in Lie symmetry technique such as e.g. solution of the determining equation (5.4) which normally goes far beyond the university courses.

In the present chapter of the dissertation, we suggest our own approach to construction of approximate analytical solutions to the light propagation equations (4.2,4.1). Our approach, on one hand, is free from any assumption on the functional form of the solution in media, and on another hand it does not require knowledge of any special techniques. It is based on the following assumption: consider a dynamical system of the form

$$\partial_t f_1 = J_1(f_1, f_2), \quad (6.1)$$

$$\partial_t f_2 = \alpha J_2(f_1, f_2), \quad (6.2)$$

where α is a small parameter. Then the dynamics of variable f_2 is significantly "slower" in comparison with dynamics of f_1 , and one can assume that f_2 in Eq. (6.1) does not depend on t explicitly. Then, the Eq. (6.1) can be integrated yielding a functional dependence $f_1 = f_1(f_2)$. Substituting this result into Eq. (6.2), we

get a closed differential equation, which can be finally integrated analytically or numerically. Such an approach is well-known in problems of physical and chemical kinetics (see e.g. Refs. [80, 55]).

6.1 Analytical solutions in case of (1+1) dimensions

First, let us construct solutions for the case of (1+1) dimensions. Then the Eqs. (3.19-3.20) take a simple linear form Eqs. (3.17-3.18)

$$\begin{aligned}\partial_w \tau - \frac{I}{\varphi(I)} \partial_I \chi &= 0, \\ \partial_w \chi + \alpha \partial_I \tau &= 0,\end{aligned}$$

with boundary conditions

$$\tau(0, I) = 0, \quad \chi(0, I) = H(I).$$

Taking into account that, e.g. for $I_0 = 10^{10}$ W/cm² and the light propagation in air ($n_2 = 3.2 \times 10^{-19}$ cm²/W) α can be considered as a small parameter. Due to its smallness we can construct an approximate solution to the system (3.17-3.18) step-by-step distinguishing between two stages in the dynamics of the system [80, 55]. At the first stage we assume that $\partial_w \chi = 0$ and find $\tau = \tau(\chi, I, w)$ via integration of Eq. (3.17). The result reads

$$\tau = \frac{-w}{2\chi\varphi}. \quad (6.3)$$

As a second step, we substitute Eq. (6.3) into Eq. (3.18) and arrive at a first order partial differential equation

$$\partial_w \chi + \frac{\alpha w}{2\chi^2 \varphi} \partial_I \chi + \frac{\alpha w}{2\chi \varphi^2} \partial_I \varphi = 0, \quad (6.4)$$

the integration of which gives two integration invariants

$$\chi \varphi = \Psi_1 \quad (6.5)$$

$$\frac{\alpha w^2}{4} - \chi^2 \varphi^2 \int \frac{dI}{\varphi} = \Phi_2, \quad (6.6)$$

Accounting for Eq. (6.3), we rewrite this result as

$$\chi \varphi = \Psi_1, \quad \int \frac{dI}{\varphi} - \alpha \tau^2 = \Psi_2. \quad (6.7)$$

Now the desired solution for the boundary value problem Eqs. (3.7-3.8) (in case when $\varphi(I) \neq I$) can be found in a standard way: i) we express I and χ as functions of integration invariants $I = I(\Psi_1, \Psi_2)$ and $\chi = \chi(\Psi_1, \Psi_2)$ at the boundary $\tau = 0$, and construct the following relation between the integration invariants $I(\Psi_1, \Psi_2) = \exp(-\chi(\Psi_1, \Psi_2)^2)$; ii) substituting expressions (6.7) into this relation, we arrive at the desired solution to the boundary value problem.

6.1.1 An exact solution

First of all, we test approach suggested by us on the well-known analytical solution for the problem. In case of the semi-classical approximation, the Kerr nonlinearity and in (1+1) dimensions, the exact analytical solution exists for the initial intensity distribution given by the expression $I(x, 0) = \cosh^2(x)$. Applying suggested formalism, we get

$$\tau = -\frac{w}{2} \cosh(\chi), \quad (6.8)$$

consequently, $\tau_I = w \partial_I \chi \sinh^{-2}(\chi)/2$. From Eq. (3.18) we have

$$\partial_w + \frac{\alpha w}{2} \frac{\partial_I \chi}{\sinh^2(\chi)} = 0.$$

Integrating this equation and returning to the original variables, we get $\alpha I^2 z^2 = I \cosh^2(x - vz) - 1$, that coincides with the the exact solutions Eqs. (4.3). The first one, evidently, follows from Eq. (6.8) after transition to the original variables.

In such a way, we conclude that approach suggested by us allows find approximate solution with a good accuracy, and even reconstruct the known exact solution.

6.1.2 Accuracy of the approximate solutions

Let us consider parabolic intensity distribution at the boundary $I = 1 - \chi^2$. Differentiating the initial distribution with respect to time, we get $\chi_I = -1/2\chi$. Substituting this expression into Eq. (3.19), we get $\partial_w \tau = -I/2\chi$ and integrating

$$\tau = -\frac{Iw}{2\chi}.$$

This expression gives us $v = -2\alpha xz/(1 - 2\alpha z^2)$, and

$$I = \frac{1}{\sqrt{1 - 2\alpha z^2}} \left(1 - \frac{x^2}{1 - 2\alpha z^2} \right). \quad (6.9)$$

Substitution of these solutions into Eq. (3.8) gives zero, substitution of these solutions into Eq. (3.7) leads to the rest term

$$2\alpha x(1 - \sqrt{1 - 2\alpha z^2})/(1 - 2\alpha z^2)^2, \quad (6.10)$$

which accuracy can be estimated. Since $\alpha \equiv I_0 n_2$ is a small parameter, and x is normalized into the radius of the beam w_0 , we see that the error of the approximation is of order $w_0 I_0 n_2$. We see that at the beam axis the solution is exact, at the distance equals to the beam radius from the axis (e.g. for air $n_2 = 3 \times 10^{-19} \text{W/cm}^2$, $I_0 = 10^{10} \text{W/cm}^2$) the error of the solution is 3×10^{-9} . At the distance of $10w_0$ from

the beam axis, evidently, the error is 3×10^{-9} , we notice that for the Gaussian distribution magnitude of the intensity at this distance is 4×10^{-42} from its magnitude at $x = 0$.

However, the fact that in Eq.(6.10) the denominator turns to zero under z doing to z_{sf} excites some apprehension. We do an estimate: for the same magnitudes of n_2 and I_0 and $z = 0.99z_{\text{sf}}$, the error is $1.6 \times 10^{-4}x$. In such a way, we conclude that the used approach provides the result with a good accuracy.

6.1.3 Kerr nonlinearity

For the case of cubic Kerr nonlinearity, $\varphi = 1$, we get

$$\tau = \frac{-w}{2\chi}. \quad (6.11)$$

Substituting this result into Eq. (3.18), we obtain a first order partial differential equation $\partial_w \chi + (\alpha w/2\chi^2)\partial_I \chi = 0$. Its' solution reads $(\alpha w^2/4\chi^2) - I = F(\chi)$, where $F(\chi)$ is an arbitrary function which should be constructed in a way to fulfill the boundary condition (3.21). We have

$$\ln(I - \alpha\tau^2) = -\chi^2 \quad (6.12)$$

Returning to the original variables in Eq. (6.11) and Eq. (6.12), we obtain

$$\begin{aligned} \frac{-x^2}{(1 - 2\alpha z^2 I)^2} &= \ln(I[1 - \alpha z^2 I]), \\ v &= -\frac{2\alpha z x I}{1 - 2\alpha z^2 I}. \end{aligned} \quad (6.13)$$

This result was previously obtained by Kovalev on the basis of the Lie and renormalization group symmetries analysis [69, 102]. Differentiating these expressions by x and z , resolving the obtained system of four algebraic equations with respect to $\partial_x I$, $\partial_z v$ etc. and substituting the resulting expressions into (3.7-3.8), one can verify that the solutions (6.13) are exact on the beam axis ($x = 0$, $v|_{x=0} = 0$). All the solutions studied further have been probed in a similar way as well.

One can see that the solution (6.13) becomes singular at the point $z_{\text{sf}} = 1/(2\sqrt{\alpha})$ that provides the self-focusing distance of a Gaussian beam. The expressions for z_{sf} for Kerr nonlinearity and another initial intensity distribution are presented in Ref. [69]. We notice that all of them scale as $1/\sqrt{\alpha}$, ($\alpha = I_0 n_2$) as functions of the initial beam intensity. In such a way, a particular form of the initial intensity distribution changes only prefactor for $1/\sqrt{I_0}$. The functional dependence on the I_0 reminds.

Let us now start an investigation of the higher order nonlinearities.

6.1.4 Power nonlinearity

We consider the refractive index which in the original (dimensional) form reads $n(I) = n_{2k}I^k$, k being arbitrary integer positive number ($k \neq 2$, as we will see later, the present approach is not applicable to the case $k = 2$, and solution must be found with an another method). Then $\varphi = kI^{k-1}$, and $\alpha = n_{2k}I_0^k$. On the basis of Eq. (6.7) we obtain

$$\Psi_1 = kI^{k-1}\chi, \quad \Psi_2 = \frac{I^{2-k}}{k(2-k)} - \alpha\tau^2. \quad (6.14)$$

At the entry plane of nonlinear medium $\tau = 0$ we express n and χ as functions of these integration invariants:

$$n = \Psi_2(2k - k^2)^{1/(2-k)}, \quad \chi = \frac{\Psi_1}{(\Psi_2(2k - k^2))^{\frac{k-1}{2-k}}k} \quad (6.15)$$

Taking the boundary conditions into account, one gets

$$\Psi_2(2k - k^2)^{1/(2-k)} = \exp\left(\frac{-\Psi_1^2}{(\Psi_2(2k - k^2))^{\frac{k-1}{2-k}}k^2}\right),$$

that together with (6.14), gives

$$\begin{aligned} [I^{2-k} + (k^2 - 2k)\alpha I^2 z^2]^{\frac{1}{2-k}} &= \exp\left(\frac{-X^2 I^{2k-2}}{[I^{2-k} + (k^2 - 2k)\alpha I^2 z^2]^{\frac{2k-2}{2-k}}}\right), \\ v &= -2\alpha z X k I^k, \end{aligned} \quad (6.16)$$

where $X = x(1 - 2\alpha z^2 k I^k)^{-1}$. Similarly to the previous case, it is possible to verify that this solution is exact at the beam axis.

The on-axial intensity distribution is given by the expressions:

$$I^2[I^{-k} + k(k-2)\alpha z^2] = 1, \quad (6.17)$$

and presented in Fig. 6.1 for $\alpha = 1$ and various values of k .

For a negative α , Eq. (6.17) describes nonlinear defocusing with monotonic decrease of the on-axial intensity. For a positive α the expression (6.17) exhibits a singularity at a certain point z_{sf} : for each k derivative $\partial_z I$ goes to infinity, for a finite value of $I(z)$. This point corresponds to the beam collapse, or nonlinear self-focusing. Beyond this point the beam no longer propagates. We find z_{sf} in the following way: first, express $z(I)$ explicitly

$$z = \pm \sqrt{\frac{I^{-2} - I^{-k}}{\alpha k(k-2)}}. \quad (6.18)$$

Differentiate Eq. (6.18) with respect to I and using condition $\partial z(I)|_{I_{\text{ext}}} = 0$, we determine the magnitude of intensity captured in the beam collapse $I_{\text{ext}} = (2/k)^{1/(2-k)}$.

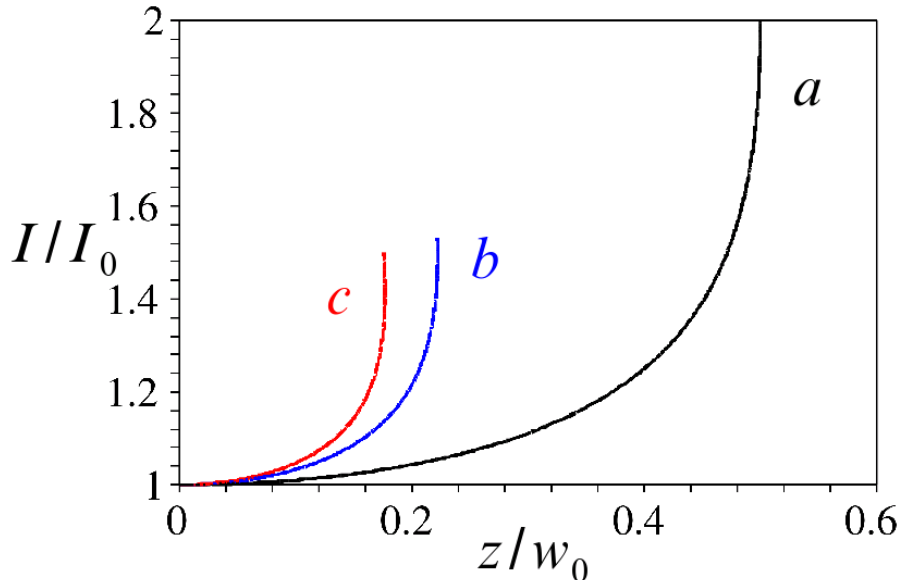


Figure 6.1: (Color online.) On-axial intensity distribution I/I_0 as a function of the propagation distance z/w_0 for the refractive index of the form $n(I) = n_{2k}I^k$ and various k . $\alpha = n_{2k}I^k = 1$: black curve (a) $k = 1$; blue curve (b) $k = 3$; red curve (c) $k = 4$. For each k , the beam propagates only up to certain point, both its coordinate z_{sf}/w_0 and the value of intensity I_{ext}/I_0 at this point are discussed in the text.

Substituting this value into Eq. (6.18), we obtain the self-focusing position for the given form of the refractive index:

$$z_{\text{sf}} = \left[\frac{(2/k)^{\frac{2}{k-2}} - (2/k)^{\frac{k}{k-2}}}{\alpha k(k-2)} \right]^{1/2}.$$

An increase of the power k leads to a decrease of the self-focusing distance. As expected, an increase of the incident intensity of the beam ($\alpha = n_{2k}I_0^k$) leads to a decrease of the self-focusing distance.

In several publications (see e.g. [30, 69]) it has been demonstrated both numerically and analytically that for the Kerr nonlinearity the self-focusing position scales as $\sim 1/\sqrt{I}$. From the presented result one can see that this scaling law is valid only for this particular nonlinearity. For an arbitrary k , z_{sf} , however scales as $z_{\text{sf}} \sim I_0^{-k+1/2}$ for power nonlinearities. We demonstrate in the following, that for other forms of nonlinearity the scaling law becomes even more complicated.

6.1.5 Saturating nonlinearities

From the physical point of view, the latter form of refractive index does not have many applications. It is mostly considered in papers devoted to the general problem of the wave collapse [95, 66]. A more physical form of the nonlinearity has to manifest

a saturating behavior: for example, refraction indices of the form $n = n_2 I / (1 + n_s I)$ or $n = n_2 / (1 + n_s I)$ appear in problems of the laser beam propagation in vapors of metals and dielectrics [16, 10]

Let us consider the first case. Then $\varphi = 1/(1 + \beta I)^2$, $\beta = n_s I_0$, $\alpha = n_2 I_0$ and from Eqs. (6.5,6.6) we have

$$\Psi_2 = (1 + \beta I)^3 / 3\beta - \alpha \tau^2, \quad \Psi_1 = \frac{\chi}{(1 + \beta I)^2}.$$

The boundary conditions provide us with the following relation:

$$(3\beta\Psi_2)^{1/3} - 1 = \beta \exp(-\Psi_1^2 (3\beta\Psi_2)^{4/3}),$$

the solution being

$$\begin{aligned} & [(1 + \beta I)^3 - \alpha 3\beta I^2 z^2]^{1/3} - 1 = \\ & \beta \exp\left(\frac{-x^2((1 + \beta I)^3 - 3\alpha\beta z^2 I^2)^{4/3}}{[(1 + \beta I)^2 - 2\alpha I z^2]^2}\right), \\ & v = \frac{-2\alpha I z x}{(1 + \beta I)^2 - 2\alpha I z^2}. \end{aligned} \quad (6.19)$$

As it was expected, these expressions turn into Eq. (6.13) under the limit $\beta \rightarrow 0$.

At the beam axis we have an expression for the intensity distribution

$$[(1 + \beta I)^3 - \alpha 3\beta I^2 z^2]^{1/3} - 1 = \beta. \quad (6.20)$$

The expression (6.20) can be analyzed similarly to the case considered above. Resolving z as a function of I we obtain

$$z = \pm \sqrt{\frac{(1 + \beta I)^3 - (1 + \beta)^3}{\alpha\beta 3I^2}}. \quad (6.21)$$

In contrast to the case considered above, the equation $\partial_I z(I) = 0$ gives us now three complex values of I_{ext} , (except for the case $\beta = -1$ when only one complex root exists). Obtained values of I_{ext} do not depend on α . Substitution of each value I_{ext} into (6.21) yields, generally speaking, a complex quantity. Obviously, if the obtained value of z_{sf} is not purely real, no beam collapse takes place for the chosen set of parameters. However, if the value of z_{sf} is real, a singularity at this point will be observed. In case of two positive real roots z_1 and z_2 , the intensity monotonically increases from $z = 0$ to the point z_2 and at $z_2 = z_{\text{sf}}$ the self-focusing will be observed. The intensity distribution in between the points z_1 to z_2 is not unique. This uncertainty corresponds to the developing beam instabilities before the self-focusing at the point z_2 . Due to this uncertainty, under the same experimental conditions, one can either observe appearance of several light channels before z_{sf} with their subsequent merging into a single filament, or only beam self-focusing at the point z_2 [30].

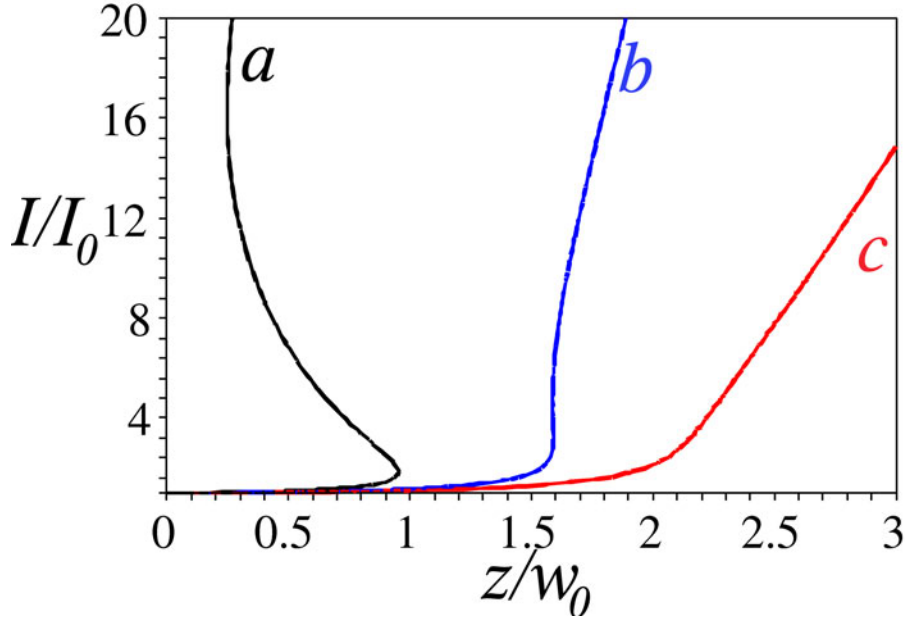


Figure 6.2: (Color online.) On-axial intensity distribution versus the propagation distance for nonlinear refractive index of the form $n = n_2 I / (1 + n_s I)$, $\alpha = n_2 I_0 = 0.2$, $\beta = n_s I_0$: black curve (a) $\beta = -0.1$; blue curve (b) $\beta = 0.25$; red curve (c) $\beta = 0.5$. The behavior of the intensity under the limit $z \rightarrow \infty$ is discussed in the text.

In Fig. 6.2 we present all these cases. The curve *c* corresponds to the absence of the self-focusing: there are no points where $\partial_I z(I)$ vanishes. The curve *b* is constructed for a single positive value $z_{\text{sf}} \sim 1.6$. Curve *a* represents a case of two critical values $z_1 \sim 0.3$, and $z_2 \sim 1$. The segment $[z_1, z_2]$ corresponds to the region of the beam instability before the self-focusing point $z_2 \sim 1$.

The fact that the on-axial intensity goes to infinity and, consequently, the diameter of the beam approaches zero under $z \rightarrow \infty$ originates from the semiclassical approximation. In reality, infinite beam compression will be arrested by the diffraction.

Position where intensity increase is arrested could be estimated from the assumption that this happens when the beam radius to be comparable to the wave length λ . The rough estimate give us that for laser beam with waste $w_0 = 1$ mm and $\lambda = 800$ nm the arrest occurs at the point where intensity increases about 100 times with respect to its initial value.

6.1.6 Two-terms nonlinearity

Now let us apply obtained results to the case of refractive index consisting of two terms; usually the first one is related to the Kerr nonlinearity and reads as $n_2 I$ whilst the second one is a higher order power function of intensity. Physically this term can be attributed to the fifth order nonlinear susceptibility $n_4 I^2$ or the material

ionization $\sigma_K I^K$, where K is the number of photons required for the simultaneous absorption.

Consider the case $n(I) = n_2 I - n_4 I^2$ first. Then dimensionless $\varphi = 1 - \beta I$, where $\beta \equiv 2n_4 I_0/n_2$. Substituting φ into (6.7) one gets

$$\Psi_2 = -\frac{1}{\beta} \ln(1 - \beta I) - \alpha \tau^2, \quad \Psi_1 = \chi(1 - \beta I). \quad (6.22)$$

From the boundary conditions it follows

$$1 - \exp(-\beta \Psi_2) = \beta \exp(-\Psi_1^2 e^{2\beta \Psi_2}) \quad (6.23)$$

$$1 - (1 - \beta I) e^{\alpha I^2 z^2 \beta} = \beta \exp\left(-\chi^2 e^{-2\alpha \beta I^2 z^2}\right),$$

$$v = -2\alpha I z X(1 - \beta I),$$

where $X = x(1 - 2\alpha I z^2(1 - \beta I))^{-1}$.

On-axial intensity distribution is given by the implicit expression:

$$\alpha I^2 z^2 = \frac{1}{\beta} \ln \left[\frac{1 - \beta}{1 - \beta I} \right], \quad (6.24)$$

and is presented in Fig. 6.3 for a positive α and several positive values of β .

Let α be positive, then for the self-focusing we obtain

$$z_{\text{sf}} = \sqrt{\frac{\beta(-4L(h) - 2)}{\alpha}} \frac{L(h)}{2L(h) + 1} \quad (6.25)$$

where $h \equiv e^{-1/2}/(2\beta - 2)$, and $L(h)$ denotes the Lambert function.

Looking on Eq. (6.25) and keeping in mind that the dimensionless coefficients $\alpha = n_2 I_0$ and $\beta = 2n_4 I_0/n_2$ are function of the initial beam intensity, we see that functional dependence of the self-focusing position on the beam intensity is again rather complicated and differs from the scaling law $1/\sqrt{I_0}$.

Similar to the case of saturating nonlinearity, the following three subcases can be distinguished depending on the magnitude of β : i) there is no beam collapse: intensity monotonically achieves a saturated value (curve *a* at the Fig. 6.3); ii) one critical point (curve *b* at the Fig. 6.3); iii) solution is not unique at a certain interval. This means that the self-focusing is prevented by a distance where the beam is unstable and can decay into several filaments (curve *c* at the Fig. 6.3). Let us study the cases above in detail.

The function $z(I)$ in Eq. (6.24) has only one critical point $\partial_I z(I) = 0$ if $\beta = \beta_c \sim 0.175$. For $\beta < 0.175$, two critical points z_1 and z_2 exist and a region of beam instability before the self-focusing appears. For $\beta > 0.175$, the Eq. (6.24) has no special points, the on-axial intensity monotonically increases approaching a saturation value I_{sat} . The self-focusing position z_{sf} as a function of β for various

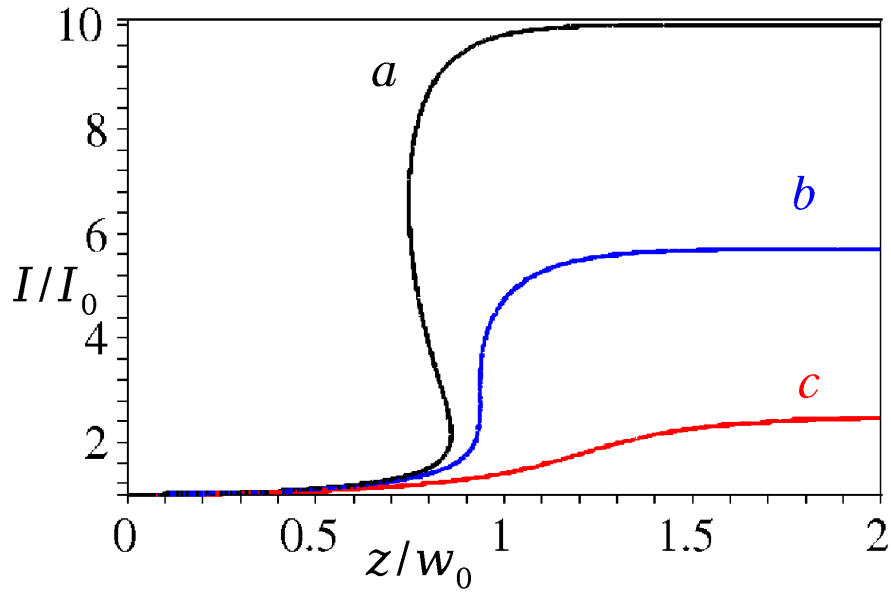


Figure 6.3: (Color online.) On-axial intensity distribution versus the propagation distance obtained for the refractive index $n = n_2 I - n_4 I^2$, $\beta = 2n_4 I_0 / n_2$, $\alpha = n_2 I_0 = 0.4$: black curve (a) $\beta = 0.1$; blue curve (b) $\beta = 0.125$; red curve (c) $\beta = 0.4$.

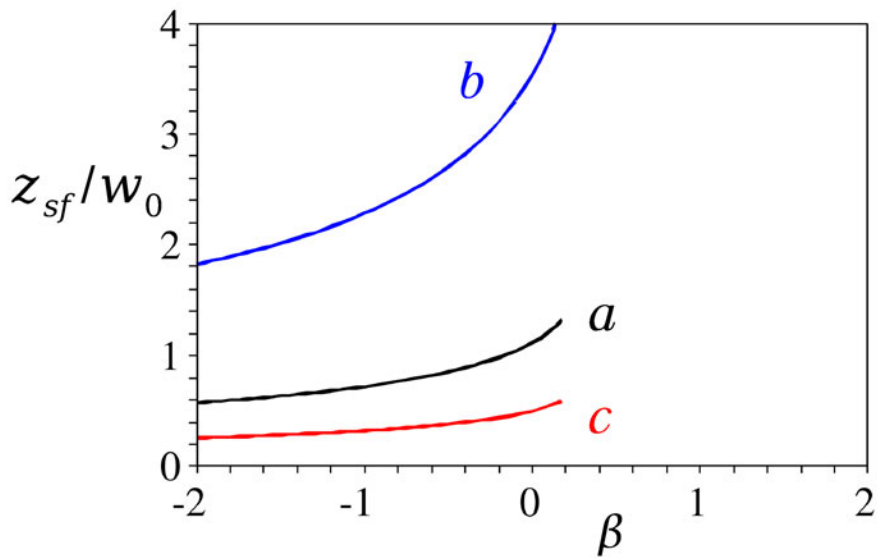


Figure 6.4: (Color online.) The self-focusing position as a function of $\beta = 2n_4 I_0 / n_2$ for various $\alpha = n_2 I_0$: black curve (a) $\alpha = 0.2$; blue curve (b) $\alpha = 0.02$; red curve (c) $\alpha = 1$. All curves end at the point $\beta_c = 0.175$, for the value of β bigger then β_c there is no self-focusing collapse: derivatives $\partial_z I$ does not turn into infinity.

α is presented in Fig. 6.4. We see that for the value of β bigger then β_c the is no self-focusing collapse: derivatives $\partial_z I$ does not turn into infinity.

By studying the asymptotic behavior of $I = I(z)$ one finds that $I_{\text{sat}} = 1/\beta$. Note that the saturated value fulfills the condition $1 - \beta I_{\text{sat}} = \varphi(I_{\text{sat}}) = 0$.

Another case for which an explicit expression for $I = I(\Psi_2)$ can be found at the boundary corresponds to the third power dependence of the refractive index on intensity $n(I) = n_2 I - n_6 I^3$. We have $\varphi = 1 - \beta I^2$, $\beta = 3n_6 I_0^2/n_2$ and

$$\begin{aligned}\Psi_2 &= \frac{\operatorname{arctanh}(\sqrt{\beta}I)}{\sqrt{\beta}} - \alpha\tau^2, \\ \Psi_1 &= \chi(1 - \beta I^2)\end{aligned}\tag{6.26}$$

whose solution reads

$$\begin{aligned}\tanh\left(\operatorname{arctanh}(\sqrt{\beta}I) - \alpha I^2 z^2 \sqrt{\beta}\right) &= \\ \sqrt{\beta} \exp\left(\frac{-\chi^2(1 - \beta I^2)^2}{(1 - \tanh[\operatorname{arctanh}(\sqrt{\beta}I) - \alpha I^2 z^2 \sqrt{\beta}])^2}\right), \\ v &= -2\alpha I z X(1 - \beta I^2),\end{aligned}$$

where $X = x(1 - 2\alpha I z^2(1 - \beta I^2)^{-1})$, with the on-axial intensity

$$2 \operatorname{arctanh}(\sqrt{\beta}I) - \alpha I^2 z^2 \sqrt{\beta} = 2 \operatorname{arctanh}(\sqrt{\beta}).\tag{6.27}$$

The features of these solutions are similar to the cases considered before. The value of the saturating intensity is equal to $I_{\text{sat}} = 1/\sqrt{\beta}$.

Notice that the values of I_{sat} for $K = 2$ and 3 obtained here are different from previous theoretical estimates [30, 15, 112], which were obtained assuming that the intensity in the filament saturates when the nonlinear terms in $n(I)$ compensate each other [30]. From the present results we see, however, that this is not the case. Upon propagation the beam tends to reach the on-axial value of the intensity which *maximizes* the index of refraction at the beam axis. In other words, not the nonlinear refractive index itself but its variation should be zero:

$$\partial_I n(I)|_{I_{\text{sat}}} = 0.\tag{6.28}$$

This condition on the saturated filament intensity is general, and independent of the nonlinear medium. It can serve as a basis for future calculations. Note that such a general mathematical condition cannot be obtained from the numerical simulations.

6.2 An example: influence of the Taylor series truncation

Taylor series expansion in the power of a small parameter is one of the basic techniques in theoretical physics. In this context, the nonlinear optics is not an exception

[21, 34]. Since in real physical situations the refractive index can be a rather complicated function if the intensity, one construct solution only for the first term of the Taylor series expansion $n(I) = n_2 I$. In the present section, based on the approach developed above, we construct analytical solutions for the eikonal equation with refractive index given by function $n = 1 - e^{-n_s I}$, afterwards, we assume that n_s is small enough to give rise a Taylor expansion in its power. We construct analytical solutions with this form of the refractive index. Further, we construct series of solutions to this equation with refractive indexes, $n_0 = n_s I$, $n_1 = n_s I - n_s^2 I^2/2$, $n_2 = n_s I - n_s^2 I^2/2 + n_s^3 I^3/6$, which are Taylor approximations to the original function.

For the present form of the refractive index we have $\varphi = e^{-\beta I}$. For the initial Gaussian shape, integration of Eq. (3.17-3.18) gives:

$$\begin{aligned} \ln(e^{\beta I} - \tau^2 \beta^2) &= \beta \exp(-\chi^2(1 - \tau^2 \beta^2 e^{-\beta I})^2), \\ \tau &= \frac{-w}{2\chi} e^{\beta I}. \end{aligned}$$

Returning to the original variables, we arrive at the result

$$\begin{aligned} \ln(e^{\beta I} - z^2 \beta^2 I^2) &= \beta \exp\left(\frac{-x(1 - z^2 I^2 \beta^2 e^{\beta I})}{1 - 2z^2 I \beta e^{\beta I}}\right)^2, \\ v &= \frac{-2zxI\beta e^{-\beta I}}{1 - 2z^2 I \beta e^{-\beta I}}. \end{aligned} \quad (6.29)$$

On-axial intensity distribution for this form of the refractive index as a function of the propagation distance is given by the implicit expression:

$$e^{\beta I} - \beta^2 z^2 I^2 = e^\beta. \quad (6.30)$$

and is presented in Fig. 6.5. We see that around certain point the intensity sharply increases and, afterwards, tends to infinity. Physically, this unrestricted intensity increase can be arrested by the diffraction or dispersion which are not included into the eikonal equations (3.7-3.8). The point where the beam stops to compress due to these processes can be estimated from the condition that the beam radius cannot be smaller than the wave length. A rough estimate for real physical parameters gives that intensity should increase in this point about 20 times. From the Fig. 6.5, we see that the solution is not everywhere unique. Such a behavior is similar to the case of a saturating nonlinearity considered in the previous section. In order to find z_{sf} , it is more convenient to investigate the inverse function $z(I)$

$$z = \pm \sqrt{e^{\beta I} - e^\beta} \frac{1}{\beta I}.$$

Investigating extremum of this function in a standard way, we get

$$z_{sf} = \frac{-1}{\sqrt{L(-e^{\beta-2})}} [L(-2e^{\beta-2}) + 2]^{3/2},$$

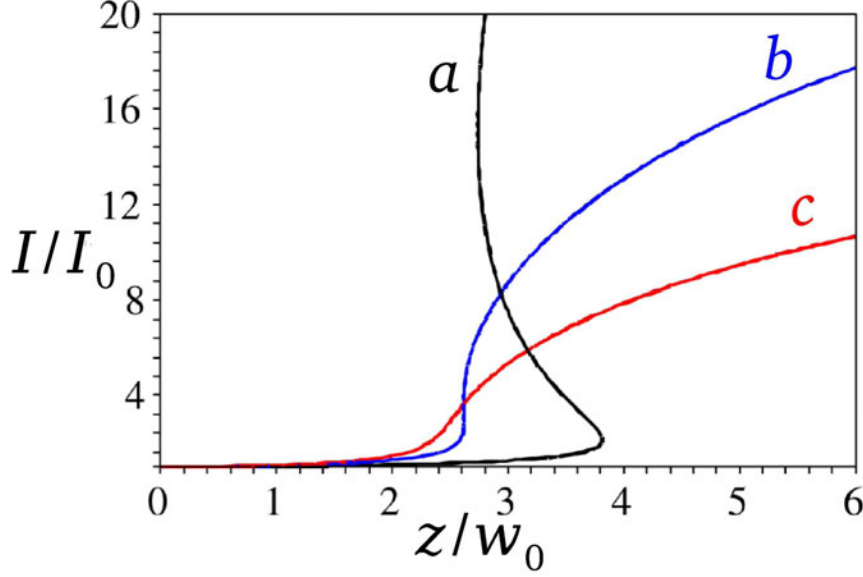


Figure 6.5: (Color online.) On-axis intensity distribution versus the propagation distance obtained for the refractive index $n = n_2 I - n_4 I^2$, $\beta = 2n_4 I_0 / n_2$, $\alpha = n_2 I_0 = 0.4$: black curve (a) $\beta = 0.1$; blue curve (b) $\beta = 0.125$; red curve (c) $\beta = 0.4$.

where $L(h)$ denotes the Lambert function satisfying the equation $L(h)e^{L(h)} = h$.

Let us now investigate a convergence of the Taylor series to the obtained results.

First order approximation. This case corresponds to the well-studied Kerr non-linearity, $\varphi = 1$. For the Gaussian beam the result was obtained in Ref. [69]. In particular, the on-axis intensity and the self-focusing positions are given by formulae

$$I[1 - \beta z^2 I] = 1, \quad z_{\text{sf}} = 1/(2\sqrt{\beta}). \quad (6.31)$$

Second order approximation. $\varphi = 1 - \beta I$. Substituting φ into (5.33) one gets

$$1 - (1 - \beta I)e^{\beta^2 I^2 z^2} = \beta \exp\left(-\chi^2 e^{-2\beta^2 I^2 z^2}\right),$$

$$v = -\frac{2\beta I z x(1 - \beta I)}{(1 - 2\beta I z^2(1 - \beta I))}.$$

On-axis intensity distribution is given by the implicit expression:

$$\beta^2 I^2 z^2 = \ln \left[\frac{1 - \beta}{1 - \beta I} \right], \quad (6.32)$$

then for the self-focusing we obtain

$$z_{\text{sf}} = \sqrt{(-4L(h) - 2)} \frac{L(h)}{2L(h) + 1} \quad (6.33)$$

where $h \equiv e^{-1/2}/(2\beta - 2)$, and $L(h)$ denotes the Lambert function.

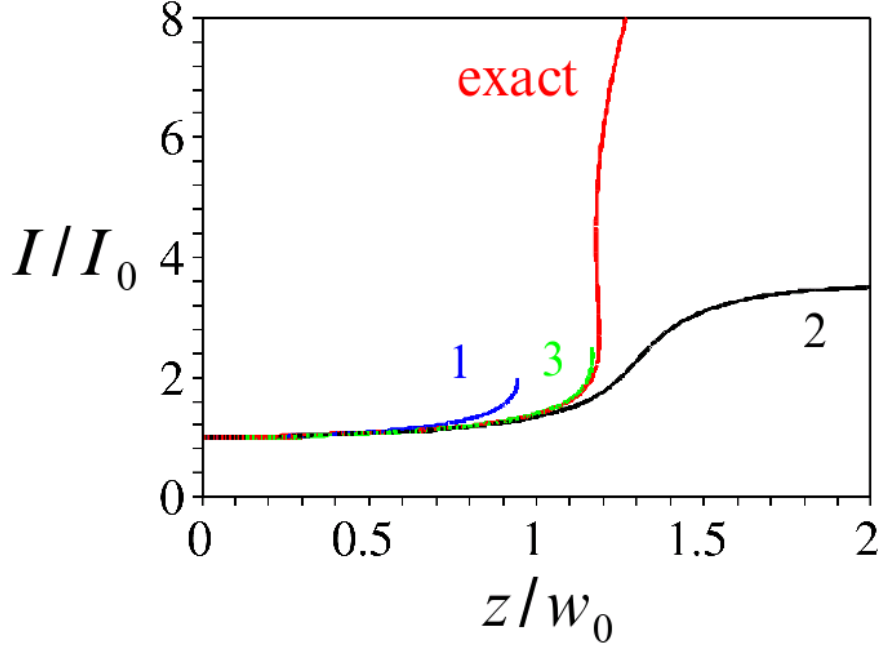


Figure 6.6: (Color online.) Comparison solutions obtained for exact refractive index and its Taylor approximations. On-axial intensity distribution constructed for exact (red curve) refractive index. Blue curve is the first, black curve is the second, and green curve is the third approximation to $n(I)$, respectively.

Third order approximation. To this order of approximation we have $\varphi = 1 - \beta I + \beta^2 I^2/2$. Thus, the approximate analytical solution reads

$$\beta \exp \left(\frac{\tan(\arctan(\beta I - 1) - \beta^2 I^2 z^2/2) + 1}{[\tan^2(\arctan(\beta I - 1) + \beta^2 I^2 z^2/2) + 1]^2} \right),$$

$$v = -\frac{2\beta x I z (1 - \beta I + \beta^2 I^2/2)}{1 - 2\beta(1 - \beta I + \beta^2 I^2/2) I z^2} \quad (6.34)$$

Consequently, at the beam axis intensity distribution is given by the implicit expressions:

$$\arctan(\beta I - 1) - \beta^2 I^2 z^2/2 = \arctan(\beta - 1) \quad (6.35)$$

Let us now compare and discuss the obtained results. Comparison between obtained solutions is presented in Fig. 6.6 for $\beta = 0.2$. On-axial intensity distribution obtained for the original function $n(I)$ is presented by the red curve. We see that around $z = 1.3w_0$ intensity sharply increases and, afterwards, tends to infinity.

Solution corresponding to the first order Taylor approximation of the refractive index is presented in Fig. 6.6 with the blue curve. This is a collapsing solution: the beam propagate no longer that $z_{sf} \simeq 1.1w_0$, the maximal value of intensity is

achieved in this point and equals to $I_{\max} \simeq 2I_0$. Before the point z_{sf} , one can observe an intensity fluctuation due to the fact that the solution is not unique at the interval from $z = 0$ to $z = z_{\text{sf}}$. We see that the first order approximation to $n(I)$ provides the shorter value of z_{sf} in comparison with the value obtained for the original function $n(I)$.

The next order approximation consists of "defocusing" term, $-n_s^2 I^2/2$, and, as a result increases the self-focusing distance. This is represented by the black curve in Fig. 6.6. This curve starts to significantly increase around $z \approx 1.4w_0$ and goes to the saturating value $I_{\max} = 5I_0$. For this particular value β , the solution is unique and increases monotonically.

The third order approximation is presented by the green curve. It provides already very close value of z_{sf} with respect to the original one, presented by the turning of the red curve. However, we have to notice that beyond the self-focusing point, behavior of the solutions obtained for different order of approximation are very different.

We summarize. From the results presented in this section, we see that the Taylor series expansion of the refractive index provides the magnitude of the self-focusing position within a good accuracy. Moreover, increase of the order of approximation leads to a convergence of the value z_{sf} to the value obtained for the original function $n(I)$. However, beyond the positions where intensity increases significantly, even if the beam intensity reminds finite, the behaviors of the curves, found for different order of the Taylor power expansion, become completely different. In such a way, several term Taylor expansion of $n(I)$ cannot serve for a decision on the asymptotic intensity distribution for long distances.

6.3 Propagation on the laser pulse with arbitrary initial intensity distribution

One of the physical situations which is modeling with the nonlinear Schrödinger equation in (1+1) dimensions is propagation of the laser pulse of a certain profile and duration in fiber. It is known that the temporal beam shape can be easily varied in experiments (see e.g. [35]). Therefore this is interesting to get analytical expressions for the intensity distribution in a general case: in case of arbitrary initial beam profile.

As before, we start from equations (3.17,3.18):

$$\partial_w \tau - \frac{I}{\varphi(I)} \partial_I \chi = 0, \quad (6.36)$$

$$\partial_w \chi + \alpha \partial_I \tau = 0, \quad (6.37)$$

with the boundary conditions $\tau(0, I) = 0$, and assume that the intensity distribution

at the boundary is defined as $I = \exp(F(\chi))$, where F is an arbitrary function. Evidently, $H(I)$ is the inverse function to F . As usually, due to smallness of α , we construct an approximate solution to the system (6.36-6.37) in two steps.

At the first step we assume that $\partial_w \chi = 0$. Differentiate the boundary condition $I = \exp(F(\chi))$ with respect to I , we get $\chi_I = 1/(F_\chi I)$, where F_χ means $\partial_\chi F(\chi)$. Substituting χ_I into Eq. (6.36), we get

$$\tau = wF_\chi^{-1}. \quad (6.38)$$

Substituting this function into Eq. (6.37) after integration and taking boundary conditions into account, we get

$$\frac{\alpha\tau^2}{2}F_{\chi\chi} + I = \exp(F).$$

In such a way, returning to the original variables, we get the result:

$$\begin{aligned} \frac{\alpha I^2 z^2}{2} F_{\chi\chi} + I &= \exp(F), \\ v &= \alpha I z F_\chi. \end{aligned} \quad (6.39)$$

We notice that, if $F(\chi)$ is a polynomial function, and for physical reasons is a convex and positive, the highest term should be negative.

Expressing I from both of Eqs. (6.39), we arrive at the implicit expression for v :

$$\frac{-1 - \sqrt{1 + 2\alpha z^2 F_{\chi\chi} \exp(F)}}{z F_{\chi\chi}} = \frac{v}{F_\chi}. \quad (6.40)$$

Let at the boundary we have a two-peak profile $I = \exp(-x^4 + bx^2)$. Then in new variables, we get an approximation

$$\tau = w/(2b\chi - 4\chi^3), \quad (6.41)$$

Substituting this approximation into Eq. (3.18), after integration, we get

$$\begin{aligned} I + aI^2 z^2 (b - 6(x - vz)^2) &= \exp(-x^4 + bx^2), \\ v &= 2aIz(b(x - vz) - 2(x - vz)^3). \end{aligned}$$

Function $I(x)$ has three extremes for $x = 0$, $x = \pm\sqrt{b/2}$. For $x = 0$ the intensity distribution is given by an implicit expression $at^2 I^2 b = 1 - I$, and on-axial value of the intensity monotonically decreases. At the points $x = \pm\sqrt{b/2}$ the intensity increases up to the point

$$z_{\text{sf}} = \frac{e^{b/8}}{2\sqrt{2\alpha b}}, \quad (6.42)$$

where the singularity arrears. We see that if initial intensity distribution exhibits several maxima, each of these maxima collapse independently. Moreover, the functional dependence of the collapse position Eq. (6.42) for each peak is $1/\sqrt{I_0}$, and, in such a way, the scaling law does not depend on the initial beam shape.

6.4 Generalization in (1+1) dimensions

In the previous section we suggested a general approach for construction of analytical solution, and discussed many particular cases of dependence of the refractive index on intensity. The problem however remains: the system of equations (6.5-6.6) cannot be resolved explicitly for any nonlinear function $n(I)$, in other words, we cannot construct an explicit function $I = I(\Psi_2)$ at the boundary for any desired nonlinearity. As a way to overcome this difficulty, one can try to use any approach to construct an approximate expression for I , e.g. construct a resolvable approximation to the integral in Eq. (6.6). As another way, in Ref. [112], an approximate RG symmetries admitted by Eqs. (3.17-3.18) were constructed.

First, we find the Lie symmetry group

$$X = f\partial_\tau + g\partial_\chi, \quad (6.43)$$

where f and g are unknown functions of n, w, χ, τ , and their derivatives: $\partial\chi/\partial n$, $\partial\tau/\partial n$, etc. admitted by Eqs. (3.17-3.18).

In case of Eq. (3.17-3.18), determining equation reads:

$$\begin{aligned} D_w(g) + \alpha D_I(f) &= 0, \\ D_w(f) - \frac{I}{\varphi(I)} D_I(g) &= 0, \end{aligned} \quad (6.44)$$

where

$$D_I \equiv \partial_I + \sum_{s=0}^{\infty} (\tau_{I^{s+1}} \partial_{\tau_{I^s}} + \chi_{I^{s+1}} \partial_{\chi_I^s}), \quad (6.45)$$

$$D_w \equiv \partial_w + \sum_{s=0}^{\infty} (\tau_{w^{s+1}} \partial_{\tau_{w^s}} + \chi_w^{s+1} \partial_{\chi_w^s}) \quad (6.46)$$

are total derivatives. Here, the index s stands for the order of the derivatives: $\tau_I^s \equiv \partial^s \tau / \partial I^s$, etc. Derivatives with respect to w in Eq. (6.46) in brackets should be excluded in accordance with Eqs. (3.17-3.18): $\tau_w^1 = I/\varphi\chi_I^1$, $\tau_w^2 = I/\varphi\chi_{Iw}^1 = -\alpha I/\varphi\tau_I^2$ and so on. As a result, the operator of Eq. (6.46) takes form of a series in powers of the small parameter α .

To determine f and g we propose formal series in powers of α as well:

$$f = \sum_{i=0}^{\infty} \alpha^i f^i, \quad g = \sum_{i=0}^{\infty} \alpha^i g^i, \quad (6.47)$$

Substituting Eqs. (6.47) into Eqs. (6.44) and collecting terms with the same power of α , we obtain up to the first order in α :

$$\partial_w f^0 - \frac{I}{\varphi} D_I(g^0) = 0, \quad (6.48)$$

$$\partial_w g^1 - D'_w(g^0) + D_I(f^0) = 0, \quad (6.49)$$

$$\partial_w f^1 - D'_w(f^0) - \frac{I}{\varphi} D_I(g^1) = 0, \quad (6.50)$$

where $D'_w = \sum_{s=0}^{\infty} \tau_{I^{s+1}} \partial_{\chi_{I^s}}$. The system of differential equations (6.48-6.50) can be solved sequentially starting from a given g^0 . The requirement that the symmetry group fulfills the boundary conditions means that f and g vanish under substitution of Eqs. (3.21) in each order of approximation. Therefore, the natural choice for the first step in solving Eqs. (6.48-6.50) is to put $g^0 = 0$. However, in Ref. [102], it was demonstrated that, for initial Gaussian beam, the choice

$$g^0 = 1 + 2I\chi\chi_I. \quad (6.51)$$

provides the better result, since it corresponds to a further iteration in the renormalization procedure.

Substituting Eq. (6.51) into Eq. (6.48), and solving Eqs. (6.48-6.50) step by step, after some calculations, we obtain

$$g^1 = 1 + 2I\chi\chi_I + 2\alpha \left(1 + I\frac{\varphi_I}{\varphi}\right) \chi\chi_\alpha - 2\alpha\varphi\tau\tau_I - 2\alpha\varphi_I\tau^2, \quad (6.52)$$

$$f^1 = 2I \left(\chi_I\tau + \chi\tau_I + \frac{\varphi_I}{\varphi}\chi\tau\right) + 2\alpha\chi\tau_\alpha \left(1 + I\frac{\varphi_I}{\varphi}\right). \quad (6.53)$$

Based on these symmetries, one can write an approximate solution to Eqs. (3.7-3.8) as follows

$$\begin{aligned} \frac{-x^2}{(1 - 2\alpha z^2 I\varphi)^2} &= \ln(I[1 - \alpha z^2 I\varphi]), \\ v &= -\frac{2\alpha z x I\varphi}{1 - 2\alpha z^2 I\varphi}. \end{aligned} \quad (6.54)$$

where, as everywhere above, φ is related to the arbitrary refractive index as $\varphi \equiv \partial_I n(I)$.

A comparison between the exact (Eq. (6.24)) and the approximate (Eq. (6.54)) solutions for $\varphi = 1 - \beta I$ is shown in Fig. 6.7. It is easy to see that the expressions (6.54) lead to exactly the same conditions for the saturating filament intensity Eq. (6.28) and the self-focusing position $z_{\text{sf}} \simeq 1.2$. The solutions are slightly different at the finite interval where the exact solution increases more sharply in contrast to the approximate one.

6.5 Nonlinear models in $(1+\nu)$ dimensions

6.5.1 Analytical solutions. Search for the best approximation

We see from Eqs. (3.19,3.20) that in case of $(1+\nu)$ dimensions, the hodograph transformation is no longer convenient: it does not turn the initial equations into a linear system. Nevertheless, an approximate solution can be constructed in a similar

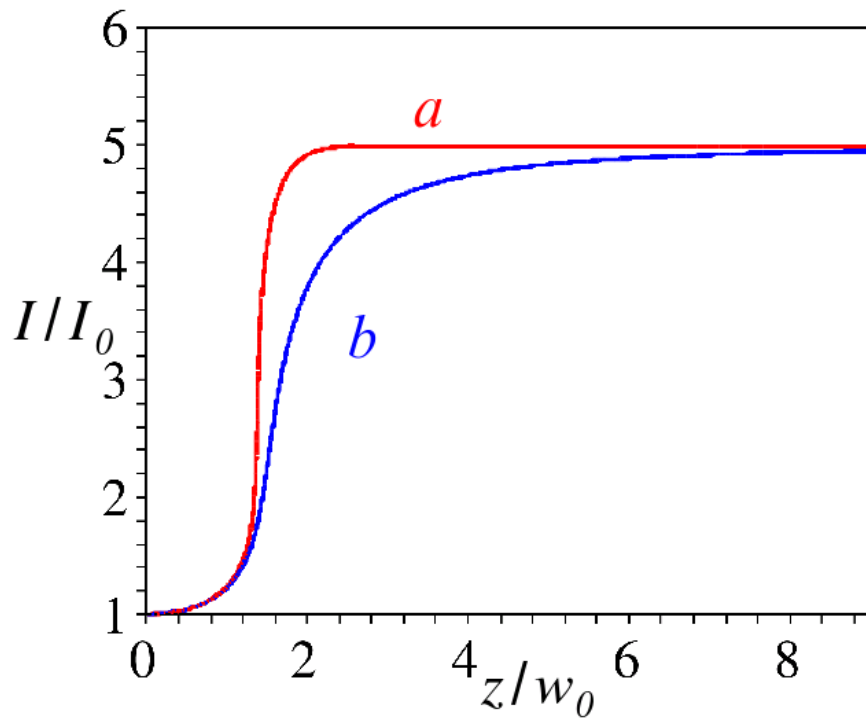


Figure 6.7: (Color online.) Comparison of the exact (red curve *a*) and the approximate (blue curve, *b*) solutions. On-axial intensity distribution versus the propagation distance in case of the nonlinear refractive index $n = n_2 I - n_4 I^2$, $\alpha = n_2 I_0 = 0.2$, $\beta = 2n_4 I_0/n_2 = 0.1$.

way. We consider several approaches to construct solutions in this case. Fortunately, several analytical solutions for the Kerr nonlinearity are known. We will use them as test examples in order to find the best approximation.

Notice that the equation (3.17) does not depend on the dimension of the problem. Thus, an approximation (6.3) can be used not only in case of (1+1) but in (1+ ν) dimensions as well. Therefore, we rewrite (6.3) in original variables and substitute the obtained function $v(x, z, I)$ into Eq. (3.8).

6.5.2 The parabolic beam profile

We start from the Kerr nonlinearity and the parabolic beam, because in this case an exact analytical solution is known (see Chapter 4).

At the first stage we assume that χ does not depend on w . At the boundary we have $I = 1 - \chi^2$. Differentiating the initial distribution with respect to time, we get $\chi_I = -1/2\chi$. Substituting this expression into Eq. (3.19), we get $\partial_w \tau = -I/2\chi$ and integrating

$$\tau = -\frac{nw}{2\chi} \quad (6.55)$$

returning to the original variables, we get

$$v = \frac{-2\alpha xz}{1 - 2\alpha z^2}. \quad (6.56)$$

For derivatives of v we have

$$\partial_x v = \frac{-2\alpha z}{1 - 2\alpha z^2}. \quad (6.57)$$

Substituting (6.57) into Eq. (6.62), we get

$$(1 - 2\alpha z^2)\partial_z I - 4\alpha I z - 2\alpha z x \partial_x I = 0. \quad (6.58)$$

Integration of Eq. 6.58) gives

$$I = \frac{1}{1 - 2\alpha z^2} \left(1 - \frac{x^2}{1 - 2\alpha z^2} \right) \quad (6.59)$$

that is indeed coincides with solution Eq. (4.4) of Chapter 4 from Ref. [4].

6.5.3 Gaussian beam profile. First consideration

Applying the same idealogy to the case of the Gaussian beam $1 = -2I\chi\partial_I\chi$, we find an approximation

$$\tau = -\frac{w}{2\chi} \quad (6.60)$$

From Eq. (6.60) one obtains

$$v = \frac{-2\varphi Izx}{1 - 2\varphi Iz^2}. \quad (6.61)$$

Differentiating Eq. (6.61) with respect to x , and keeping only main terms of the power of φ one obtains the first order partial differential equation

$$(1 - 2\alpha\varphi Iz^2)\partial_z I = 2\alpha Izx(2\varphi + \varphi_I I)\partial_x I + 4\alpha\varphi I^2 z. \quad (6.62)$$

Eq. (6.62) can be integrated in a standard way for each particular form of nonlinear refractive index.

Kerr nonlinearity. First of all, we are going to check the accuracy of the solutions which we construct based on the suggested approach in (1+2) dimensions. To do this, we consider case of Kerr nonlinear refractive index and compare the solutions with already constructed in Ref. [68].

Substituting (6.61) into (3.8) and keeping only main terms in powers of φ we obtain the following characteristic equation

$$\frac{dz}{1 - 2\varphi Iz^2} = \frac{-dx}{4Izx} = \frac{dI}{4I^2 z}. \quad (6.63)$$

Integration of Eq. (6.63) gives

$$\Psi_1 = 2I\alpha z^2 - \ln I, \quad \Psi_2 = Ix$$

what provides the intensity distribution

$$Ie^{-2I\alpha z^2} = \exp\left(\frac{-x^2}{e^{-4I\alpha z^2}}\right) \quad (6.64)$$

and the self-focusing position given by

$$z_{\text{sf}} = 1/\sqrt{2\alpha e}. \quad (6.65)$$

This is an approximate result different from the exact expression $z_{\text{sf}} = 1/\sqrt{2\alpha}$ obtained on the basis of the renormalization group analysis in Ref. [68]. One can see that the approximate value of z_{sf} is about two times shorter than the exact one. However, from Ref. [12] one can see that our formula still yields significantly better results than the ones provided by the variational approach.

6.5.4 Two-term nonlinearity

Let us consider the case of the cubic-quintic nonlinearity. Then $\varphi = 1 - \beta I$, $\varphi_I = -\beta$. Substituting these expressions into Eq. (6.62) after integration one obtains

$$\Psi_1 = -\ln\left(\frac{I}{\beta I - 1}\right), \quad \Psi_2 = x^2 I^2 (\beta I - 1).$$

Accounting for the boundary conditions, we obtain the intensity distribution

$$\frac{e^{-2\alpha z^2 I}}{\beta I e^{-2\alpha z^2 I} + 1 - \beta I} = \exp\left(-x^2(\beta I e^{-\alpha z^2 I} + 1 - \beta I)^3 e^{4\alpha z^2 I}\right).$$

Consequently, the on-axial intensity is given by the approximate formula

$$2\alpha z^2 I = \ln\left(\frac{I - \beta I}{1 - \beta I}\right). \quad (6.66)$$

which provides

$$z_{\text{sf}} = \sqrt{\frac{-\beta}{2\alpha L(h)}}(L(h) - 1),$$

where $L(h)$ is the Lambert function and $h = \beta e/(\beta - 1)$.

In general, the expression (6.66) is approximate. However, one can see that it provides the same value of the saturated intensity $I_{\text{sat}} = 1/\beta$ as Eq. (6.24) in (1+1) dimensions. Therefore, we conclude that the general condition for the saturated intensity given by Eq. (6.28) does not depend on the dimension of the problem.

6.5.5 Gaussian beam profile. Second consideration

Let us now use an another approximation $\partial_I \chi = -1/2\chi e^{-\chi^2}$. Then, substituting this approximation into Eq. (3.19) we get

$$\tau = -\frac{Iw}{2\varphi\chi e^{-\chi^2}}. \quad (6.67)$$

Now we assume that χ in the exponent is a parameter. Then for v we get

$$v = \frac{-2\alpha x z \varphi e^{-\chi^2}}{1 - 2\alpha z^2 \varphi e^{-\chi^2}}. \quad (6.68)$$

Now, neglecting high order terms with in the power of α , we get an approximate expression ¹

$$\partial_x v = \frac{-2\alpha z \varphi e^{-\chi^2}}{1 - 2\alpha z^2 \varphi e^{-\chi^2}}. \quad (6.69)$$

Substituting this approximation into Eq. (3.8), we get the characteristic equation

$$(1 - 2\alpha\varphi z^2 e^{-\chi^2})\partial_z I - 2\alpha x z(\varphi + \varphi_I I)e^{-\chi^2}\partial_x I - 2(\nu + 1)\alpha\varphi I z e^{-\chi^2} = 0. \quad (6.70)$$

¹Advantage of the analytical approach is we can use any convenient approximation and afterwards check accuracy of the obtained result.

Integration of Eq. (3.8) gives

$$I\varphi x^\nu = \Psi_1, \quad 2\alpha z^2 e^{-x^2} = \Psi_2 I^{-\frac{2}{\nu}} + \frac{2I^{-\frac{2}{\nu}}}{\nu} \int \frac{I^{\frac{2-\nu}{\nu}}}{\varphi} dI \quad (6.71)$$

The desired solution for the boundary value problem can be found in a standard way: i) we express I and x as functions of integration invariants $I = I(\Psi_1, \Psi_2)$ and $x = x(\Psi_1, \Psi_2)$ at the boundary $t = 0$, and construct the following relation between the integration invariants $I(\Psi_1, \Psi_2) = \exp(-x(\Psi_1, \Psi_2)^2)$; ii) substituting expressions (6.71) into this relation, we arrive at the desired solution to the boundary value problem.

Kerr nonlinearity in (1+2) dimensions. In this case $\varphi = 1$ $\nu = 2$ and from Eq. (6.71) we have

$$Ix^2 = \Psi_1, \quad I + \Psi_2 = 0.$$

After taking the boundary conditions into account, the solution reads

$$\begin{aligned} v &= \frac{-2\alpha x z e^{-x^2}}{1 - 2\alpha z^2 e^{-x^2}}, \\ I(1 - 2\alpha z^2 e^{-x^2}) &= \exp\left(\frac{-x^2}{(1 - 2\alpha z^2 e^{-x^2})}\right) \end{aligned} \quad (6.72)$$

At the beam axis this solutions

$$2\alpha I z^2 + I - 1 = 0 \quad (6.73)$$

becomes singular at the point $z_{\text{sf}} = 1/\sqrt{2\alpha}$. This result coincides with the Kovalev formula for the propagation of a Gaussian beam in the media with Kerr nonlinearity.

In contrast to the case of (1+1) dimensions, we see that in the collapsing point z_{sf} not the derivatives $\partial_z I$, but the intensity goes to the infinity.

By the direct substitution of the constructed solutions into the original equations, we can see that the second approach to find the solution in (1+2) dimensions provides a better accuracy in comparison with the previous one. At the moment we are not able to emplane why one approximation is better then an another one. We can only check its accuracy by the direct substitution.

Let us now to extend this approach into more complicated nonlinear models and higher dimensions.

6.5.6 Power nonlinearity

Let us start consideration from the power nonlinearity $\varphi = kI^{k-1}$, $k \neq 2$. In accordance with Eqs. (6.71), we get

$$kI^k x^2 = \Psi_1, \quad 2\alpha I z^2 e^{-x^2} + \frac{I^{2-k}}{k(k-2)} = \Psi_2. \quad (6.74)$$

The solution reads

$$\begin{aligned}
v &= \frac{-2\alpha x z k I^{k-1} e^{-\chi^2}}{1 - 2\alpha z^2 k I^{k-1} e^{-\chi^2}}, \\
&\quad (2\alpha I z^2 k (k-2) e^{-\chi^2} + I^{2-k})^{1/(2-k)} \\
&= \exp\left(\frac{-x^2 I^k}{(2\alpha I k (k-2) z^2 e^{-\chi^2} + I^{2-k})^{k/(2-k)}}\right)
\end{aligned} \tag{6.75}$$

The on-axial intensity is given by expression

$$2\alpha I k (k-2) z^2 + I^{2-k} = 1, \tag{6.76}$$

which, evidently, for $k = 1$ turns into Eq. (6.73) obtained for the Kerr nonlinearity. The self-focusing position is defined as

$$z_{\text{fs}} = \sqrt{\frac{(k-1)^{\frac{-1}{k-2}} - (k-1)^{\frac{1-k}{k-2}}}{2\alpha k (k-2)}} \tag{6.77}$$

Similar to the case of (1+1) dimensions, we see that the higher is the power of nonlinearity k , the shorter is the propagation distance.

6.5.7 Saturating nonlinearity

Let us consider a saturating nonlinearity with the refractive index $n = 1 - e^{-\beta I}$. Then, we put $\varphi = e^{-\beta n}$, $\alpha = \beta$. Substituting the present form of φ into Eqs. (6.71), we get the solution

$$\begin{aligned}
v &= \frac{-2\alpha x z e^{-\beta I} e^{-\chi^2}}{1 - 2\alpha z^2 e^{-\beta I} e^{-\chi^2}}, \\
\ln(F) + \beta I - 2\alpha \beta z^2 e^{-\chi^2} &= \beta \exp\left(\frac{-\beta x^2 I F}{\ln(F) + \beta I - 2\alpha \beta z^2 I e^{-\chi^2}}\right).
\end{aligned}$$

where $F = 1 - e^{-\beta I} + e^{-\beta I + 2\alpha \beta I e^{-\chi^2}}$. Thereafter, at the beam axis we have

$$2\alpha \beta I z^2 - \beta I = \ln\left(\frac{1 - e^{\beta I}}{e^\beta - 1}\right). \tag{6.78}$$

The onaxial intensity distribution as a function of the propagation distance is similar to the case of (1+1) dimensions.

6.5.8 Two-term nonlinearity

Firstly we consider the cubic-quintic model $n = n_2 I - n_4 I^2$. Then $\varphi = 1 - \beta I$, where $\beta = n_4 I_0 / n_2$. Substituting this function into Eq. (6.71), we obtain

$$2\alpha z^2 I + \frac{1}{\beta} \ln(1 - \beta I) = \Psi_2, \quad x^2 I (1 - \beta I) = \Psi_1 \tag{6.79}$$

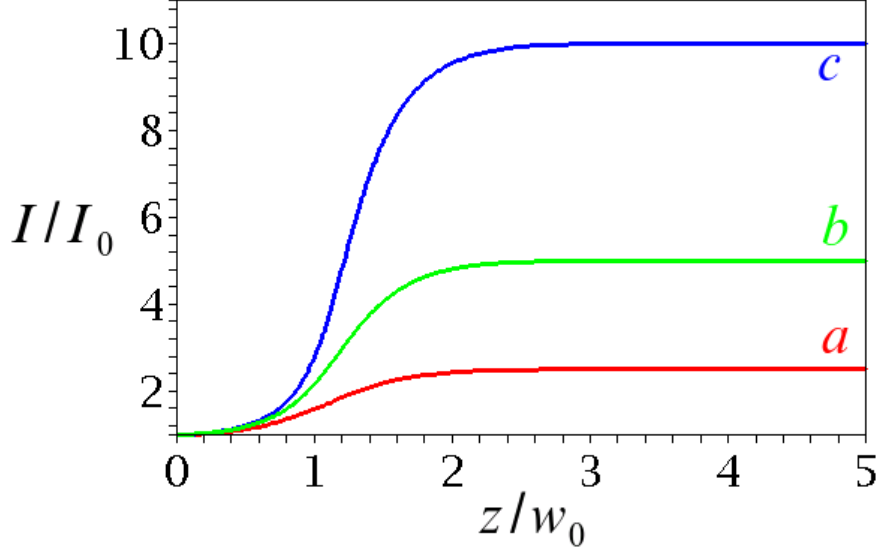


Figure 6.8: (Color online.) On-axial intensity distribution versus the propagation distance obtained for the refractive index $n = n_2I - n_4I^2$, $\beta = 2n_4I_0/n_2$, $\alpha = n_2I_0 = 0.4$: red curve (a) $\beta = 0.4$; green curve (b) $\beta = 0.2$; blue curve (c) $\beta = 0.1$.

The solution reads

$$1 - (1 - \beta I)e^{2\alpha\beta z^2 I e^{-x^2}} = \beta \exp\left(\frac{-\beta I x^2}{(1 - (1 - \beta I)e^{2\alpha\beta z^2 I e^{-x^2}})e^{2\alpha\beta z^2 I e^{-x^2}}}\right) \quad (6.80)$$

At the beam axis we have the intensity distribution given by the formula:

$$2\alpha\beta z^2 I = \ln\left(\frac{1 - \beta}{1 - \beta I}\right). \quad (6.81)$$

Analyzing Eq. (6.81) in a usual way, we get

$$z_{\text{sf}} = \sqrt{-L\left(\frac{e^{-1}}{\beta - 1}\right) \frac{1}{2\alpha}}, \quad (6.82)$$

where L is the Lambert function (satisfying the equation $L(h)e^{L(h)} = h$). Evidently, under the limit $\beta \rightarrow 0$, Eq. (6.82) turns into $z_{\text{sf}} = 1/\sqrt{2\alpha}$. On-axial intensity distribution as a function of the propagation distance is presented in Fig. 6.8. It exhibits the similar behavior as in case of (1+1) dimensions.

Let us consider case of $n = n_2I - n_6I^3$. Then $\varphi = 1 - \beta I^2$, where $\beta = n_6I_0^2/n_2$. Substituting this function into Eq. (6.71), we obtain

$$2\alpha z^2 I + \frac{1}{\sqrt{\beta}} \arctan(\sqrt{\beta} I) = \Psi_2, \quad x^2 I (1 - \beta I^2) = \Psi_1. \quad (6.83)$$

The solutions reads

$$\tanh(\Theta) = \sqrt{\beta} \exp\left(\frac{-I(1 - \beta I^2)\sqrt{\beta} x^2}{\tanh(\Theta)(1 - \tanh^2(\Theta))}\right), \quad (6.84)$$

where $\Theta = \operatorname{arctanh}(\sqrt{\beta}I) - 2\alpha\sqrt{\beta}z^2I \exp(-\chi^2)$. At the beam axis we have

$$\operatorname{arctanh}(\sqrt{\beta}I) - 2\alpha Iz^2 + \tanh(\sqrt{\beta}) = 0.$$

Under limit $z \rightarrow \infty$, this expression gives us $I_{\text{sat}} = 1/\sqrt{\beta}$.

To summarize this part of the work, we discuss here some general results. Explicit/implicit expressions for the self-focusing position for different form of the refractive index were obtained. In case of (1+1) dimensions and (1+2) dimensions for the same form of the refractive index, we got different results. This fact is in agreement with results obtained previously by another authors (see e.g. Refs. [102, 67, 69]). In contrast, achieved by us law for the single filament intensity Eq. (6.28) is general, and does not depend on the dimensionality of the problem.

6.6 Comparison with results of experiments and numerical simulations

As an example, let us consider here problem of femtosecond pulse propagation in air which is relevant due to a large number of applications and whose description is still a subject of discussion (see, e. g. Refs. [30, 15] and Refs. therein). The nonlinear refractive index of air is taken in the following widely used form (see. e.g. reports. [30, 15])

$$n = n_2[I + R(I)] + n_4I^2 - \frac{\rho(I)}{2\rho_c}, \quad (6.85)$$

where the first term describes the Kerr response involving a delayed (Raman) contribution $R(I) = \tau_K^{-1} \int_{-\infty}^t e^{-(t-t')/\tau_K} I(t') dt'$. n_2 and τ_K are known to be equal to $3.2 \times 10^{-19} \text{ cm}^2/\text{W}^2$ and 70 fs [14], respectively. $n_4 \equiv \chi^{(5)}/2n_0$, where $\chi^{(5)}$ is the fifth order nonlinear susceptibility its exact value is a subject of some controversy [15]. The most accepted estimates lie around $\sim 10^{-32} \text{ cm}^4/\text{W}^2$ [30]. In the last term of Eq. (6.85), $\rho(I)$ refers to the density of free electrons and ρ_c denotes the critical density above which the plasma becomes opaque. A rough estimate yields $\rho(I) \sim \sigma_K I^K \rho_{\text{at}} t_p$, where ρ_{at} is the atom density $\rho_{\text{at}} = 2 \times 10^{19} \text{ cm}^{-3}$ and t_p the pulse duration. $K = 8$ for the MPI with a pulse of 800 nm, and $\sigma_8 = 3.7 \times 10^{-96} \text{ cm}^{16}/\text{W}^8/\text{s}$ [30].

A numerical solution of the NLSE for the focused beam with $f = 2 \text{ m}$, $P_{\text{in}} \sim 0.08 \text{ TW}$ and $w_0 = 3 \text{ mm}$ using $n(I)$ given by Eq. (6.85) with $n_2 = 3.2 \times 10^{-19} \text{ cm}^2/\text{W}^2$, $n_4 = 0$ and $R = 0$ gives $z_{\text{sf},f} = 128.2 \text{ cm}$ Ref. [115]. Note that if $n(I) = n_2I$, the self-focusing distance is given by the Kovalev formula [68, 67] $z_{\text{sf}} = w_{\text{in}}/\sqrt{2n_2I_0}$, which is exact under the geometrical optics approximation and for initially Gaussian beam shape. For the experimental conditions of Ref. [115] it

Table 6.1: Comparison of the predictions for z_{sf} and the filament fluence in air calculated using Eq. (6.81) and Eq. (6.28) with the results of experiments and numerical simulations.

pulse duration	z_{sf} (m)		Fluence (J/cm ²)
	50fs	450fs	50fs
experiment [24]	3	5.5	0.6
numerical [24]	3	6.5	0.6 – 1.4
this work	3	6.2	0.66

yields $z_{\text{sf},f} = 127.6$ cm. This confirms our initial statement that for many experiments diffraction (and in this case also the plasma defocusing) can be neglected.

Now we compare our results with the recent experiment and numerical results of Refs. [24], where a collimated beam with FWHM diameter of $d \sim 4 - 5$ mm ($w_0 = d/\sqrt{2 \ln 2}$), with a pulse energy $E_{\text{in}} \sim 20$ mJ and different pulse durations (FWHM) was used. In Ref. [24], n_2 was taken to be $n_2 = 2.5 \times 10^{-19} \text{ cm}^2/\text{W}$ for the pulse duration 50 fs, and $n_2 = 6 \times 10^{-19} \text{ cm}^2/\text{W}$ for 450 fs, $n_4 = -2.5 \times 10^{-33} \text{ cm}^4/\text{W}$ were fixed and independent on the pulse duration. Substituting this set of parameters into Eq. (6.81) and estimating the delayed response as an integral over the pulse duration, we obtain z_{sf} and the on-axial fluence F ($F = \int I(t) dt$) which are presented in Table 6.1.

From the Table 6.1, one can see that in spite of used simplifications, our results are in a good agreement with experimental and numerical results.

Recently reported experimental results on air clearly indicate that z_{sf} scales as $1/\sqrt{P_{\text{in}}}$ for a relatively low initial pulse power P_{in} . However, for powers above 500 GW ($I_0 \sim 5 \times 10^{12} \text{ W/cm}^2$) a qualitative change is observed and z_{sf} depends on the power as $\sim 1/P_{\text{in}}$ [48]. This behavior was attributed by authors to noise effects in the beam. However, as we saw from our studies of the collapse of the beam with arbitrary initial intensity distribution, each intensity peak collapsed independently with scaling law $1/\sqrt{I_0}$. Moreover, on the other hand one can notice that the value of 500 GW in the experiment of Ref. [48] corresponds to the case where the terms $n_2 I_0 = 1.7 \times 10^{-6}$ and $n_4 I_0^2 \sim 3.1 \times 10^{-7}$ in the refractive index (6.85) become comparable. Therefore, we believe that the change in the power dependence is mainly driven by the contribution of the highly nonlinear terms (fifth order susceptibility). Moreover, from the analysis of the experiment of Ref. [48] within our theoretical scheme we can draw important conclusions regarding the form of the nonlinear refractive index.

Using the value of I_0 given in Ref. [48], and assuming $n_4 \sim \mp 10^{-32} \text{ cm}^4/\text{W}^2$ [30], we get $\beta \simeq \pm 0.35$. Comparing this value with $\beta_c \sim 0.175$, we see that, if $n_4 < 0$, then no self-focusing would be observed. Since self-focusing is indeed observed, we conclude that $n_4 > 0$. The behavior of z_{sf} as a function of the initial beam intensity

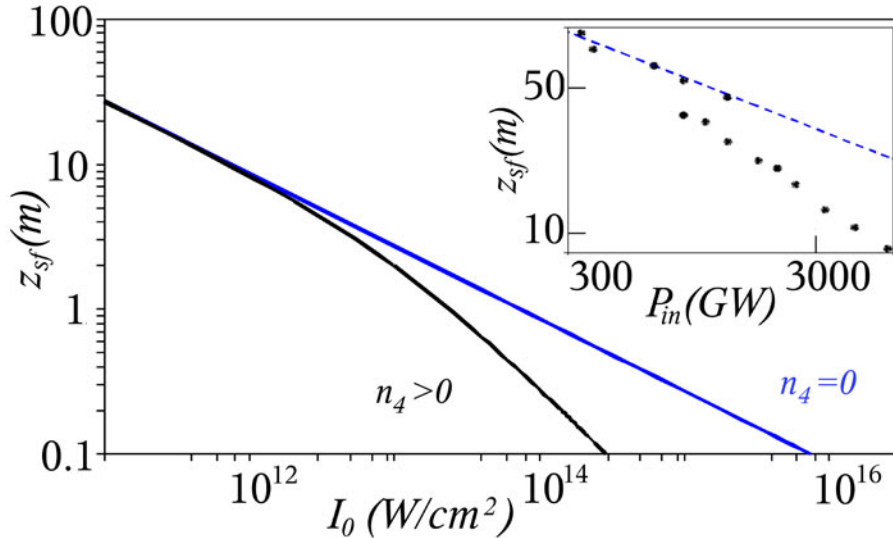


Figure 6.9: (Color online.) Dependence of the self-focusing position on the beam intensity. The blue curve refers to the dependence $1/\sqrt{I}$ (obtained for low intensities), whereas the black curve shows the deviation for high intensities due to influence of the fifth-order nonlinearity $n_4 = 10^{-32} \text{cm}^4/\text{W}^2$. Inset: Experimental points for $z_{\text{fs}}(P_{\text{in}})$ from Ref. [48].

obtained from our theory is shown in Fig. 6.9 and is qualitatively compared to the measured z_{sf} . Note that one could use our results to find an accurate value of n_4 by performing a similar experiment with a controlled initial Gaussian beam profile (i.e., without noise) and fitting the measured curve $z_{\text{sf}}(I_0)$ to the solution of Eq. (6.82).

It is important to point out that the values of all parameters in Eq. (6.85) are subject of controversy. For example the magnitude of n_2 is taken as $n_2 = 3.2 \times 10^{-19} \text{cm}/\text{W}^2$ in Refs. [30] and as $n_2 = 4 \times 10^{-19} \text{cm}/\text{W}^2$ in Ref. [15]. The value $\sigma_8 = 2.9 \times 10^{-99} \text{cm}^{16}/\text{W}^8/\text{s}$ from Ref. [15] is three orders of magnitude larger than the one used in Ref. [30]. With such an uncertainty in these parameters and fluctuations of the experimental data, a single experiment is probably not sufficient in order to adjust all the parameters of the refractive index Eq. (6.85).

Therefore, and based on Eq. (6.81), we suggest the following scaling measurement. In Fig. 6.9 we show our results for the dependence of z_{sf} on the initial pulse intensity. We obtain considerable qualitative (and quantitative) differences depending on the sign and magnitude of n_4 . One can use this result to design an experiment with varying beam power to find accurate values of n_2 and n_4 by fitting the measured experimental curve $z_{\text{sf}}(I_0)$ with z_{sf} obtained from Eq. (6.81). Afterwards, the Eq. (6.28) derived from the first principles can be used for determining the plasma response by fitting the value of I_{sat} .

Summarizing this part, we can conclude that our approach provides a good accuracy for theoretical analysis of experimental data and can therefore, in some

situations, replace an extensive numerical simulations. Obtained by us simple analytical expressions can serve as as a tool for determination of the highly nonlinear media response parameters from comparison theoretical predictions with results of experiments.

Chapter 7

Theoretical study of the fused silica ablation

The present chapter of the dissertation is devoted to a theoretical explanation of the experimental results obtained in fused silica ablation by Englert and co-workers and published in Refs. [35, 36].

A considerable interest to ablation in the modern scientific literature is based on two related problems: a wide range of existing applications including micro-machining of materials, thin film production, nanoparticle production etc; and the necessity to understand the physics of laser-material interactions at the extremely short time and high intensity when some usual approximations do not work. From the application point of view it is very important to get a clean ablation with minimal debris and thermal damage such as melting and cracking to the surrounding area. For this goal, it is important to have a solid knowledge about influence of the laser pulse parameters on the final ablation crater. From the fundamental point of view, a necessity to model the ablation will lead to construction of new theoretical models for systems far from equilibrium and without small parameters.

7.0.1 Short review of the ablation results

Because of a huge number of publications devoted to ablation, we can mention here only some of them.

One of the first papers on the ablation was published by Stuart *et al.* Ref. [107, 108]. The authors reported extensive laser-induced damage threshold measurements on dielectric materials at wavelengths of 1053 and 526 nm for pulse durations t_p ranging from 140 fs to 1 ns.

They observed a qualitative differences in the morphology of the ablated area for $t_p < 10$ ps and for $t_p > 50$ ps. A decreasing threshold fluence associated with a gradual transition from the long-pulse, thermally dominated regime to an ablative regime dominated by collisional and multiphoton ionization, and plasma formation

was mentioned in the paper. A theoretical model based on electron production via multiphoton ionization, Joule heating, and collisional (avalanche) ionization was put forward in order to explain experimentally observed features. This model provided a quantitative agreement with the experimental results.

Later, in Ref. [83] Lenzner *et al.* presented measurements of the optical breakdown threshold and ablation depth in dielectrics with different band gaps for laser pulse durations ranging from 5 ps to 5 fs at a carrier wavelength of 780 nm. The authors pointed out that for the pulse duration $t_p < 100$ fs, the dominant channel for free electron generation was found to be either impact or multiphoton ionization depending on the size of the band gap. Observed multiphoton ionization rates turned out to be substantially lower than the ones predicted by the Keldysh theory. The sub-10-fs laser pulses investigated in this paper opened up the way to reversible nonperturbative nonlinear optics (at intensities greater than 10^{14} W/cm² slightly below damage threshold) and to nanometer-precision laser ablation (slightly above threshold) in dielectric materials.

Glezer *et al.* in Ref. [54] first demonstrated that sub-micron dimensional microexplosions could take place in fused silica and other materials using 100 fs pulses. These voxels (volume pixels) could be formed in a range from threshold energy to three times above it. They appeared to consist of spherical damage regions with diameter increasing with the increase of laser energy in this fluence range. Self-focusing is believed to also contribute to the small voxel size. For higher energies, a head and filament structure was described with a length of 20-40 microns. No cracking was observed at energies up to 100 times threshold. In contrast, 200 ps and 10 ns pulses produced more cracking and larger damaged areas.

In Refs. [58, 51], a group of authors presented the experimental and theoretical studies of a single femtosecond laser pulse interaction inside a bulk of transparent media. Sapphire, glass, polymer were taken as media examples. Such interaction lead to drastic transformations in a solid resulting in a void formation inside a dielectric. The laser pulse energy was absorbed within a volume of approximately $\sim 0.15 \mu\text{m}^3$ creating a pressure and temperature comparable to that in the core of a strong multi-kilo-tons explosion. The material within this volume was rapidly atomized, ionized, and converted into a tiny super-hot dense cloud of expanding plasma that generated strong shock and rarefaction waves which resulted in the formation of a void, whose diameter was about 200 nm for a 100 nJ pulse in sapphire.

In order to model the process of these small voids formation, the authors suggested a theoretical model based on high-temperature plasma hydrodynamics equations. This model confirmed the fact that unique states of matter characterized by temperatures 10^5 K, heating rates up to the 10^{18} K/s, and pressures more than 100 times the strength of any material were created using a standard table-top laser in well-controlled laboratory conditions.

Laser induced damage was noted in fs laser cutting and drilling of glasses in Ref. [117]. Varel *et al.* in Ref. [118] have investigated the drilling of channels through quartz samples. A lens with 75 mm focal length was used with 120 fs pulses at 790 nm to obtain channels with 21 micron diameter through 1 and 2 mm thick quartz samples. These narrow channels were observed in vacuum but not in atmospheric pressure N_2 . More cracking was observed around the entrance hole than the exit hole with relatively little observable damage within the bulk. An increase of the peripheral damage around the entrance was also mentioned.

In parallel to the experimental results on the ablation features, theoretical models were constructed and developed as well.

Strictly speaking, a model describing electron-lattice energy transfer should be based on the system of kinetic (Boltzmann) equations. Such model would take into account the electron-lattice energy exchange by a set of collision integrals and the heat-mass flux by the gradient terms. However, because of the extreme difficulty of these equations from the mathematical point of view, up to now the problem was not researched as a whole. Based only on properties of the collision integral (without proper account of the transfer processes) the solutions were found by Rethfeld with collaborators in Refs. [62, 96, 97].

In Ref. [96] the author developed a new model describing the free-electron generation in transparent solids under high-intensity laser irradiation. The multiple rate equation model unified key points of detailed kinetic approaches and simple rate equations to a widely applicable description, valid on a broad range of time scales. This model provided us with a nonstationary energy distribution of electrons on ultrashort time scales as well as the transition to the asymptotic avalanche regime for longer irradiation.

Mass and energy transfer with the use of hydrodynamic equations was modeled by Bulgakova *et al.* in Refs. [23]. In this paper the authors theoretically studied the role of rapid electron transport in defining the characteristics of material removal with ultrashort laser pulses. A strong electrostatic ion repulsion force caused the break-up of the surface of charged dielectric materials, while for semiconductors and metals due to efficient neutralization the ablation received a more thermal appearance.

Finally, we have to notice that when studying ablation in transparent materials, not only the thermodynamical properties of material have to be taken into account but its optical properties as well. Position of the beam (nonlinear) focus in the material, its dependence on the intensity, temporal profile of the beam etc, can dramatically change the ablation picture. It is exactly the problem of influence of the nonlinear self-focusing on the results of ablation that we devote ourselves to in this part of dissertation. Our research is based on the experimental ablation results produced in Baumert AG and published in Refs. [35, 36].

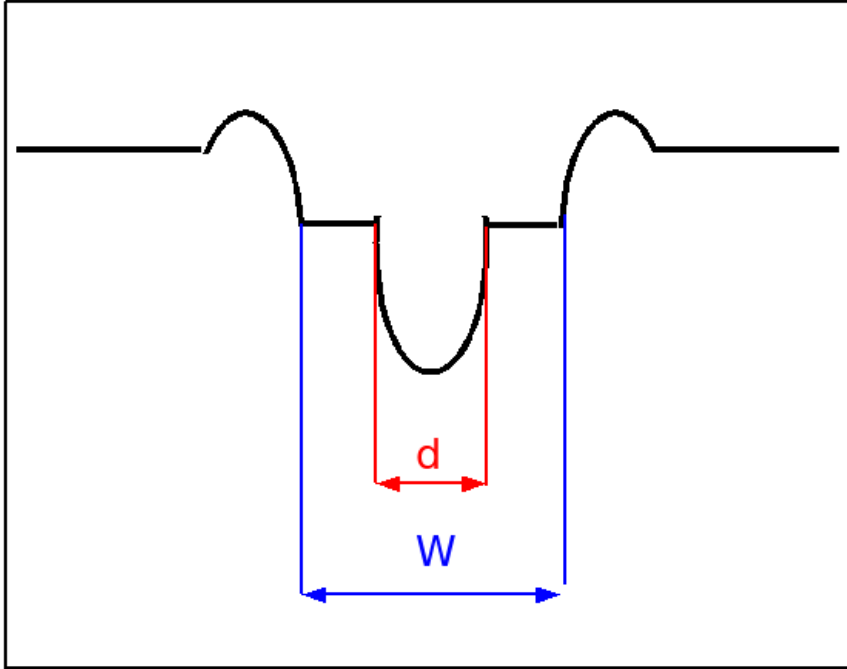


Figure 7.1: (Color online) Scheme of the crater profile observed in experiments in Ref. [35]. One can observe a small hole with diameter d inside of the bigger one with diameter denoted as W .

7.0.2 Material processing below the diffraction limit with the help of the femtosecond laser pulse

In the experiment of Ref. [35] the femtosecond pulse shaping techniques [120] were combined with a microscope setup for material processing [9]. Laser pulses with $\Delta t = 35$ fs full width at half maximum (FWHM) pulse duration (measured in the interaction region) and a central wavelength of 790 nm were provided by an amplified Ti:Sapphire laser system.

For material processing phase shaped femtosecond pulses were focused onto fused silica. The single shot pulse energy was adjusted by a motor driven gradient neutral density filter and recorded with a calibrated photodiode. The sample was translated by a 3-axis piezo table to a new position for each shot. In a typical measurement pattern the authors varied the spectral phase mask, energy and focal z -position. The threshold for material damage was determined visually from the scanning electron microscopy (SEM) images.

In Ref. [35] the authors reported observation of the ablation craters. The typical profile of a crater is schematically presented in Fig. 7.1. Its most unusual feature is a reported presence of a small inner hole inside the crater.

The authors observed the expected increase of the damage threshold energy

due to a reduction of intensity caused by the increase of cubic phase. For a vanishing cubic phase the damage threshold of the bandwidth limited pulse was obtained. The observed threshold energy for fused silica was about 30 nJ that was consistent with the values reported in the literature [107, 83, 84, 33, 114]. Comparing thresholds for positive and negative cubic phase parameters the authors found out that the threshold for positive cubic phase was always lower than for negative one in case their absolute values were identical. Because the pulses had identical fluence, spectrum and pulse durations the authors concluded that the different asymmetric temporal shapes, i.e. the energy distribution in time, have a significant influence on the material damage threshold.

7.0.3 Theoretical model

Let us now discuss the experimental results obtained for a single laser pulse and suggest a possible explanation. First of all, we have to understand a physical nature of the small hole formation in the ablation crater.

Because of insufficient experimental evidence that the experiment was actually performed with a pulse focused at the surface, we have to theoretically describe two distinct cases: *i) with the focus situated at the surface* and *ii) with the focus situated under the surface*. In the first case, the (nonlinear) beam propagation effects are neglectable due to both relatively small n_2 in air and a small distance between the laser lens and the sample surface. In this case formation of the smaller hole can be attributed to the electrons generation at the surface and the subsequent Coulomb explosion. In the second case, the smaller hole appearance is related to the thermodynamical processes: material heating inside the bulk followed by a formation of the void due to extremely high pressures in the focal point. The focus position in this case is affected by the nonlinear optics effects (i.e. defocusing due to material ionization).

The laser beam is focused exactly at the surface

Let us assume that the laser beam generates at the surface the electron density with a narrow peak over a Gaussian distribution (see Fig. 7.2) due to the effects of avalanche ionization when light intensity is high. We assume that, in this case, the central region of the beam (where density of excited electrons is big) provides a small inner hole. Here we are using a standard model describing the process of glass ionization (see e.g. Ref. [30, 103])

$$\partial_t \rho = \sigma_K \rho_{\text{nt}} I^K + \eta \rho I \quad (7.1)$$

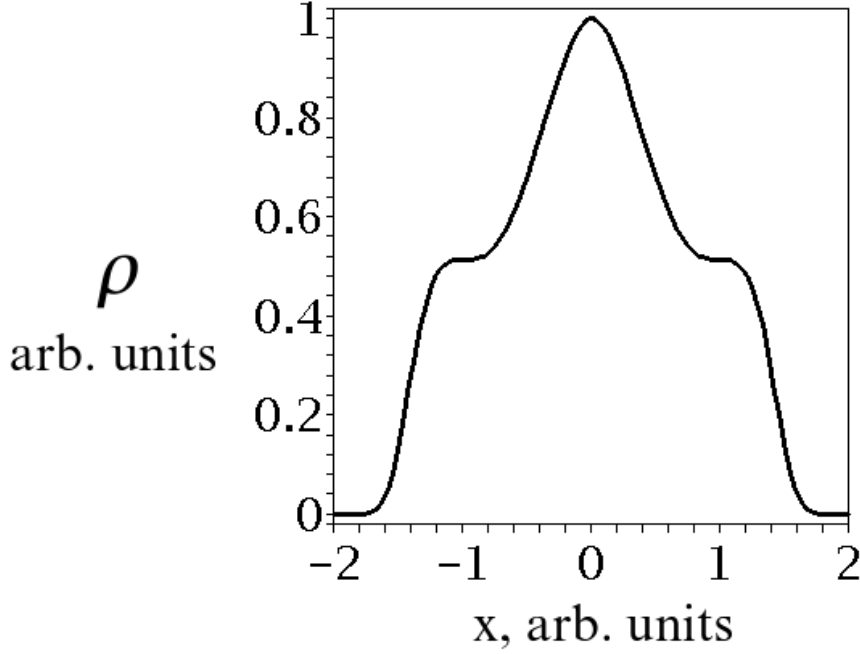


Figure 7.2: (Color online.) A suggested electron distribution which could hypothetically lead to a double-hole crater shape.

Integrating this equation with initial conditions $\rho(0) = 0$ one arrives at the solution

$$\rho(t, x) = \int_0^t (A \exp((-5t_1^2 - 1/2B\pi^{1/2}t_p^3 \text{erf}(t_1/t_p))/t_p^2)) dt_1 \exp(1/2B\pi^{1/2}t_p \text{erf}(t/t_p)) \quad (7.2)$$

where erf is the error function and t_p is the pulse duration, $A = \sigma_K \rho_{\text{nt}} I_0^K e^{-Kx^2/w_0}$, $B = \eta I_0 e^{-x^2/w_0}$.

The electron density as a function of time and space is presented in Fig. 7.3. We see that the electron density manifests a super-Gaussian spatial shape that is different from the profile in Fig. 7.2. It implies that the avalanche ionization and the Coulomb explosion from the surface cannot provide formation of the inner hole with the diameter observable diameter (see Fig. 1.3).

The laser beam is focused under the surface

Let us now consider the case when the pulse is focused on a certain point below the surface of the sample.

Outer hole. We shall first describe the formation of the outer hole with the object of obtaining a relation between parameters of the beam and the damage area. For the Gaussian beam the fluence is given by a formula:

$$F(r) = F_0 \exp\left(\frac{-2r^2}{r_0^2}\right), \quad (7.3)$$

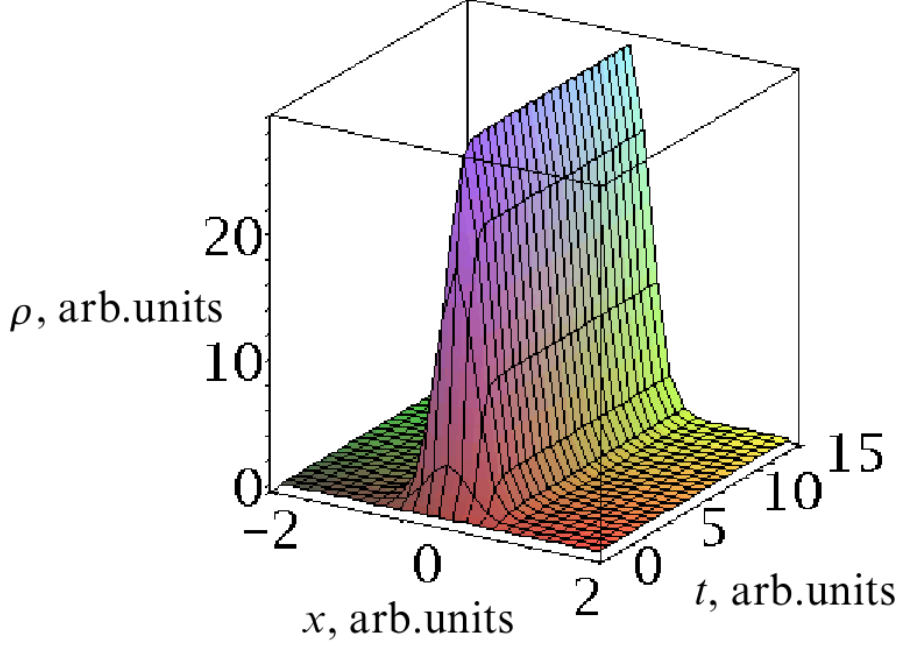


Figure 7.3: (Color online.) Density of the excited electrons at the surface as a function of the space x , and the time t , obtained from the solution of Eq. (7.1).

where r_0 is the beam radius. For the circular Gaussian beam the fluence F is related to the pulse energy as $F = 2E/(\pi r_0^2)$. Assuming that the threshold energy E_{th} exists, the damage area shall expand to the radius r_{th} in case the local fluence exceeds E_{th} . So Eq. (7.3) can be rewritten as

$$E_{th} = E_0 \exp\left(\frac{-2r_{th}^2}{r_0^2}\right). \quad (7.4)$$

Inverting this relations one can express the diameter of damage/ablation crater as a function of the pulse energy for spatially Gaussian beam:

$$W_{out}(E) = \frac{d_0}{\sqrt{2}} \sqrt{\ln\left(\frac{E}{E_{th}}\right)}, \quad (7.5)$$

where d_0 is the beam diameter, and E_{th} is the pulse threshold energy. Experimentally measured outer hole diameter W is presented in Fig. 7.4 by blue circles. Analytical blue curve is constructed on the basis of Eq. (7.5). Coincidence of the theoretical and experimental results are obtained for $E_{th} = 31$ nJ, that is in accordance with result of Ref. [35].

Inner hole. The formation of the inner hole can be attributed to the mechanisms responsible for the void formation in Refs. [58, 51] (as in the previous paragraph we are assuming that the beam was focused under the surface of the bulk of silica). This void appears as a result of the laser pulse energy concentration in a small closed

volume what leads to ionization and a strong heating of the glass in this volume followed by a propagation of the shock and rarification waves from the center of irradiated volume to the peripheral areas. This small void becomes observable in *post mortem* electronic microscope photos due to the common ablation from the surface discussed above. For the first time this simulation was described in Refs. [58, 51]. Let us now, following to these papers, consider this process in more detail.

First of all, we have to notice that one can produce some detectable structure inside the material with the following properties: i) absorption length should be large enough to provide an energy deliver to the focal space in the bulk ii) the energy needs to be focused to the smallest possible volume, with dimensions of the order of the laser wavelength, where the optical properties should be changed (absorption increased) under the laser action. Two particular properties of transparent dielectrics, the large absorption length and the low thermal conductivity, make them very suitable for that purpose.

The major mechanism of absorption in the low-intensity laser-solid interaction is the interband electron transition. Since the photon energy is smaller than the band-gap energy, the electron transitions are forbidden in linear approximation, which corresponds to a large real and small imaginary part of the dielectric function. The optical parameters in these conditions are only slightly changed during the interaction in comparison to those of the cold material. The absorption can be increased for shorter wavelengths if the incident light intensity increases to the level where the multiphoton (and avalanche) processes become important. Under such conditions the properties of the material and the laser-material interaction change rapidly during the pulse. As the intensity increases above the ionization threshold, the neutral material transforms into plasma, which absorbs the incident light very efficiently. A localized deposition of the laser light creates a region of high energy density. A void in the bulk of material is created if the pressure in absorption volume significantly exceeds the Young's modulus of a solid.

A detailed description of the laser-matter interaction process and laser-induced material modification from the first principles is a very difficult task even for modern supercomputers. Therefore, we present here a theoretical analysis which is split into a sequence of simpler interconnected problems: the absorption of laser light, the ionization and energy transfer from electrons to ions, the heat conduction, and hydrodynamic expansion, which we are describing below.

Absorbed energy. The absorbed laser energy per unit time and per unit volume, E_{abs} , is related to the divergence of the Poynting vector $E_{abs} = -c \operatorname{div} \mathbf{E} \times \mathbf{H}/4\pi$. Replacing the magnetic field in accordance with the Maxwell equations, calculating averaging over the laser period, expression for the absorbed energy density through

the incident laser field intensity reads (see. Ref. [51]):

$$E_{abs} = \frac{4n}{(n+1)^2 + \kappa^2} \frac{2\omega\kappa}{c} I(t) \equiv AI(t), \quad (7.6)$$

where $n+i\kappa$ is the complex refractive index, and I is the incident laser flux intensity I .

Since duration of the pulse 35 fs in Ref. [35] is shorter than the usual electron-phonon and electron-ion collision times Ref. [51], the single electron energy ϵ_e as a function of time can be found from equation:

$$\frac{d(\rho_e \epsilon_e)}{dt} = AI(t),$$

its integration gives

$$\epsilon_e = \frac{a}{\rho_e} \int_0^t I(t) dt. \quad (7.7)$$

Electron density must be found from the kinetic equation that taking into account the electron-ion recombination processes reads

$$\partial_t \rho_e = W_{ion} \rho_e - \beta_e \rho_e^2 \rho_i, \quad (7.8)$$

where ρ_i is the ion density and assumed that the recombination proceeds mainly by three-body collisions with one electron acting as a third body [51]. Equation (7.8) gives value $\rho_e \sim 3 \times 10^{23} \text{ cm}^{-3}$. Magnitudes of other parameters in Eq. (7.7) for $\lambda = 800 \text{ nm}$ are $n = 1.20$, $\kappa = 1.16$, $A = 0.014 \text{ nm}^{-1}$.

Now we are in a position to estimate both the electron temperature and pressure at the end of the laser pulse. Taking integral over the pulse duration in Eq. (7.7), we get the energy deposited into the focal volume. The latest can be estimated in accordance with Refs. [58, 51] $V_{abs} = l_s \pi r_0^2$, where $l_s = c/\omega k$, finally $V_{abs} \sim 10^{-2} \mu\text{m}^3$. Then for 150 nJ pulse we get $Q_{dep} \simeq 6 \text{ MJ/cm}^3$ and for 240 nJ, the absorbed energy is $Q_{dep} \simeq 10 \text{ MJ/cm}^3$. Electron thermal energy $\rho_e T_e$ is difference between the deposited energy Q_{dep} and the energy required for the ionization $\rho_i (Q_{Si} + 2Q_0)$. Taking the last values from Refs. [51], we get the pressure $P_e = \rho_e T_e$ varied from $\sim 6 \text{ TPa}$ to $\sim 12 \text{ TPa}$ dependently on the pulse energy.

Energy transfer from electrons to ions. The hydrodynamic motion can start after the electrons transfer the absorbed energy to ions. The following processes are responsible for the energy transfer from electrons to ions: recombination, electron-to-ion energy transfer in Coulomb collisions, ion acceleration in the field of charge separation gradient of electronic pressure, and electronic heat conduction.

In Ref. [51] there was noted that in the dense plasma created by the tight focusing inside a bulk solid the major processes responsible for the electron-to-ion

energy transfer are different from those in the laser ablation. The fastest process of the energy transfer from hot electrons to the ions is the electron-ion recombination by three-body collisions with one electron acting as a third body. This process takes 1 fs. The ion acceleration by the gradient of the electron pressure and the electron-to-ion energy transfer by the Coulomb collisions both comprise 1 ps. This is the time of hydrodynamic motion. The electronic nonlinear heat conduction becomes important much later, about 15 ps after the pulse end.

Hydrodynamical stage of the dynamics. The hydrodynamic motion starts, that is, the shock wave emerges from the energy deposition zone, when the electrons have transferred their energy to ions. The total deposited energy builds up the pressure that drives the shock wave. This pressure in several order of magnitude exceeds the Youngs modulus for the majority of materials for example, $Y = 400$ GPa for sapphire, and $Y = 75$ GPa for the fused silica. Therefore, a strong shock wave emerges that compresses the material up to the density $\rho \simeq \rho_0(\gamma + 1)/(\gamma - 1)$, where γ is the adiabatic constant for the majority of cold solids is 3.

The compressed material behind the shock wave front can then be transformed to another phase state in such highpressure conditions. After unloading the shock-affected material undergoes transformation into a final state at normal pressure. The final state may possess properties different from those in the initial state. We consider in succession the stages of compression and phase transformation, pressure release, and material transformation into a postshock state.

The shock wave propagating in a cold material loses its energy due to dissipation, and it gradually transforms into the sound wave due to the work done against the internal pressure, Y that resists material compression. Let us consider for simplicity a spherically symmetric motion. The distance at which the shock front effectively stops defines the shock-affected volume. Actually at this point the shock wave converts into a sound wave, which propagates further into the material without inducing any permanent changes to a solid. This stopping distance, r_{stop} , can be estimated from the condition that the internal energy in the volume inside the shock front is comparable to the absorbed pulse energy: $4\pi r_{stop}^3 Y/3 \approx E_{abs}$. Then the stopping distance reads

$$r_{stop} \approx (3E_{abs}/4\pi Y)^{1/3}. \quad (7.9)$$

The void formation inside a solid is only possible if the mass initially contained in the volume of the void was pushed out and compressed. Thus after the microexplosion the whole mass initially confined in a volume with radius r_{stop} resides in a layer in between r_{stop} and d , which has a density $\rho = \rho_0\delta$ with a compression factor $\delta > 1$. The inner hole radius can be expressed through the compression ratio $d_{in} = r_{stop}/C$, $C = (1 - 1/\delta)^{-1/3}$. In such a way, we arrive at expressions for the

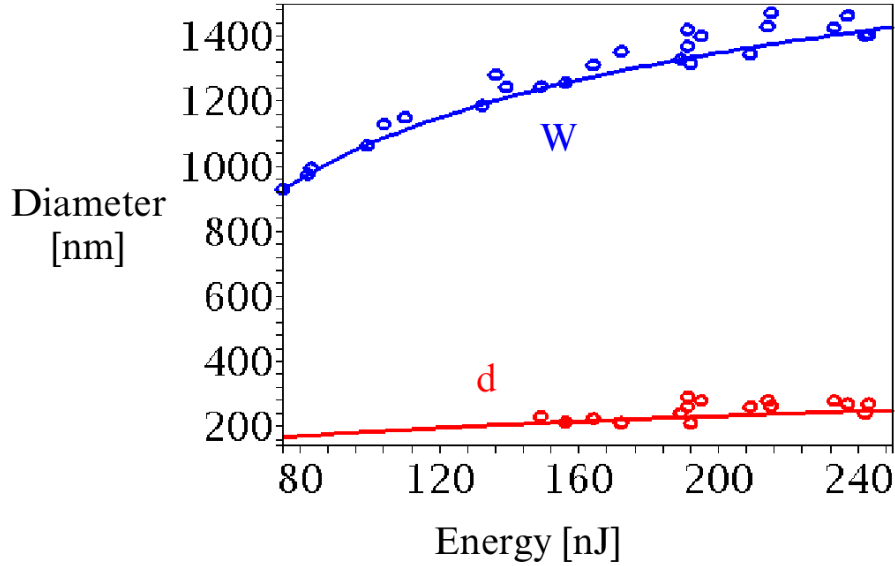


Figure 7.4: (Color online.) Diameter of outer and inner holes versus the pulse energy. Blue points represent experimentally measured diameters of the inner holes from Ref. [35], blue curve is the theoretical prediction according to the Eq. (7.5); red points denote radiuses of the inner holes from Ref. [35], the red curve is given by Eq. (7.10).

diameter of the inner hole:

$$d_{\text{in}}(E) = l_a(E(1 - 1/\delta))^{1/3}, \quad (7.10)$$

where parameters δ should be found from numerical solution to the hydrodynamic equations $\delta = 1.14$; and $l_a \simeq 80$ nm for sapphire and $l_a \simeq 140$ nm for fused silica.

Comparison of the analytical (red) curve with experimental points is presented in Fig. 7.4. One can see that experimentally measured diameters of the inner holes as a function of the pulse energy display a reasonable agreement with the analytical curve. Additional details related to the temporal pulse shape can slightly change the analytical prediction. For example, change the threshold energy

We have to notice that formation of the inner hole is possible only in case when the pressure achievable in the focal volume is greater than the Yung's modulus of the dielectric under consideration. In case of fused silica it means that the deposited energy must be greater than 1 nJ.

Summarizing this chapter of the dissertation, we can conclude that a successful explanation of the experimental results of Ref. [35] is suggested. Constructed by us curves, based on analytical expressions (7.10,7.5), are in a good agreement with results of experiments. As a further prolongation of this work a temporal laser pulse shape manipulation can be included into the analytical model that can give a promising opportunity for the inner hole parameters manipulations.

Chapter 8

Conclusions

The present dissertation was devoted to the construction of analytical solutions to the problem of light propagation in media with a highly nonlinear response.

- We presented in detail the derivation and the range of the applicability of the model equations. We noticed that the model can be significantly simplified under the geometrical optics approximation. Accuracy of this approximation was estimated and experimental conditions capable to provide us with a satisfactory accuracy were discussed.
- In the presented work, for the first time, an exact analytical solution Eqs. (5.51,5.56) for the eikonal equations with refractive index being a saturating function of the electric field intensity was constructed. We demonstrated that, in this particular case, the fact that the refractive index is a saturating function of the intensity, cannot arrest the beam collapse. An explicit analytical formula (5.58) for the beam collapse position was presented.
- In the case when the analytical solution cannot be found exactly, we formulated an alternative approach which allowed us to construct approximate analytical solutions for arbitrary nonlinearity and boundary conditions. The advantages of our approach in comparison to previous ones are the follows: i) it is applicable to the light propagation equations with arbitrary refractive index and boundary conditions; ii) it does not require any assumptions about fixed beam profile in the media. It was demonstrated that the approximate solutions to the eikonal equations constructed in this part of the dissertation are exact at the beam axis, and only give a small error on the distance.
- Several particular cases of the nonlinear refractive indices were considered. We constructed an analytical solution to the eikonal equation for the refractive index being a power-type function of the intensity $n(I) = n_{2K}I^K$. We derived an explicit formula Eq. (6.17) for the self-focusing position and demonstrated

that propagation distance is decreasing with the increase of the power of the nonlinearity. Different forms (saturating, polynomial) of the refractive index were studied as well. For a saturating form of the refractive index $n(I) = 1 - e^{-n_s I}$ analytical solutions were obtained as well. These results were compared with the ones received by making use of the Taylor series expansion. The problem of the Taylor series convergence for self-focusing position was also discussed.

- The advantages of the obtained analytical expressions for the self-focusing position over empirical Marburger formula Eq. (2.57) traditionally used as an estimate of the nonlinear self-focusing position (see e.g. the latest reviews [15, 30]) are as follows: our results are deduced from the analytical solutions whose accuracy can be easily evaluated via direct substitution into the light propagation equations; the obtained formulae explicitly demonstrate the influence of the higher order nonlinear terms in the refractive index on the self-focusing position.
- A general rule for calculation of the single filament intensity Eq. (6.28) in case of arbitrary refractive index is formulated.
- Analytical expressions describing intensity and phase distributions for Kerr-type refractive index and arbitrary initial intensity distribution were obtained. It was demonstrated that if the initial intensity distribution has several local maxima, the initial beam splits into several light channels. The expression for the self-focusing positions for each light channel (filament) was obtained. It scales as $1/\sqrt{I_0}$ as a function of the initial beam intensity I_0 . Summarizing, in such a way, we demonstrated that the scaling law is determined by the form of the refractive index $n(I)$ but not the initial shape of the beam.
- Applicability of the obtained analytical results to concrete experimental conditions is discussed. Comparing our analytical expressions with results of detailed numerical simulations of the nonlinear Schrödinger equations from Refs. [115, 24] we observed that both approaches yield the same magnitudes of the self-focusing distance and the filament intensity. In such a way, the rather simple analytical expressions obtained in the dissertation can, in some cases, replace tedious numerical simulations.
- The last chapter of the dissertation was devoted to the theoretical explanation of the experimental results obtained in Ref. [35]. It was demonstrated that the observed "hole-in-hole" crater structure can be described within the frame of the theory suggested in Refs. [58, 51]. From the Fig. 7.4 one can see that the experimental results are in good agreement with theoretical prediction.

Most important formulas of the dissertation

- The eikonal equation with refractive index $n = \int_0^I n_2 I e^{-bI} dI$, where I is the light intensity, n_2 and b are constants, in (1+1) dimension has an exact analytical solution:

$$x - vz = \frac{1}{\sqrt{2}} \sqrt{\left(2e^{1-bI} - 1 + \frac{b^2 e v^2}{2\alpha}\right) + \sqrt{\left(2e^{1-bI} - 1 + \frac{b^2 e v^2}{2\alpha}\right)^2 + \frac{2b^2 e v^2}{\alpha}}},$$

$$Iz = \sqrt{\frac{e}{2\alpha}} \ln \left(e^{bI-1} ((x - vz)^2 + 1) - 1 + \sqrt{(e^{bI-1} ((x - vz)^2 + 1) - 1)^2 - 1} \right).$$

Here, and throughout the dissertation, $\alpha = n_2 I_0$, where I_0 is an initial beam intensity, z denotes the propagation distance, x is a coordinate orthogonal to the propagation distance, v is a eikonal derivative $v \equiv \partial_x S$.

- In case of arbitrary refractive index and initial collimated beam, the eikonal equations in (1+1) dimensions have approximate analytical solutions:

$$\chi\varphi = \Psi_1, \quad \int \frac{dI}{\varphi} - \alpha I^2 z^2 = \Psi_2, \quad I(\Psi_1, \Psi_2) = \exp(-\chi(\Psi_1, \Psi_2)^2)$$

where $\chi \equiv x - vz$, $\varphi \equiv \partial_I n(I)$, and Ψ_1, Ψ_2 are constants. $n(I)$ is a nonlinear part of the refractive index.

- Under the same boundary conditions but in (1+2) dimensions, the solutions reads

$$I\varphi x^2 = \Psi_1, \quad 2\alpha I z^2 e^{-x^2} = \Psi_2 + \int \frac{dI}{\varphi}, \quad I(\Psi_1, \Psi_2) = \exp(-\chi(\Psi_1, \Psi_2)^2).$$

- For arbitrary refractive index $n(I)$, the single filament intensity I_{sat} is defined by the formula:

$$\partial_I n(I)|_{I_{\text{sat}}} = 0.$$

Bibliography

- [1] F. Abdullaev, S. Darmanyan, P. Khabibullaev, *Optical Solitons* (Springer-Verlag, Berlin, Heidelberg, New York, 1993).
- [2] G. P Agrawal, *Nonlinear Fiber Optics* (Academic Press, San Diego, third edition, 2001).
- [3] S. A. Akhmanov, R. V. Khokhlov, A. P. Sukhorukov, On the self-focusing and self-channelling of intense laser beams in nonlinear medium, *Sov. Phys. JETP* **23**, 1025-1033 (1966).
- [4] S. A. Akhmanov, A. P. Sukhorikov, R. V. Khokhlov, Self-focusing and diffraction of light in a nonlinear medium, *Sov. Phys. Usp.* **10**, 609-636 (1968).
- [5] N. Aközbeke, C. M. Bowden, A. Talebpour, S. L. Chin, Femtosecond pulse propagation in air: Variational analysis, *Phys. Rev. E* **61**, 4540-4549 (2000).
- [6] M. V. Ammosov, N. B. Delone, and V. P. Krainov, Tunnel ionization of complex atoms and atomic ions by an alternating electromagnetic field, *Sov. Phys. JETP* **64**, 1191-1194 (1986).
- [7] D. Anderson, Variational approach to nonlinear pulse propagation in optical fibers, *Phys. Rev. A* **27**, 3135-3145 (1983).
- [8] E. Arévalo, A. Becker, Variational analysis of self-focusing of intense ultrashort pulses in gases, *Phys. Rev. E* **72**, 026605(1-8) (2005).
- [9] A. Assion, M. Wollenhaupt, L. Haag, F. Mayorov, C. Sarpe-Tudoran, M. Winter, U. Kutschera, and T. Baumert, Femtosecond laser-induced breakdown spectrometry for Ca_2^+ analysis of biological samples with high spatial resolution, *Appl. Phys. B* **77**, 391397 (2003).
- [10] R. S. Bennink, V. Wong, A. M. Marino, D. L. Aronstein, R. W. Boyd, C. R. Stroud, S. Lukishova, D. J. Gauthier, Honeycomb Pattern Formation by Laser-Beam Filamentation in Atomic Sodium Vapor, *Phys. Rev. Lett.* **88**, 113901(1-4) (2002).

- [11] L. Bergé, A. Couairon, Gas-Induced Solitons, *Phys. Rev. Lett.* **86**, 1003-1006 (2001).
- [12] L. Bergé, A. Couairon, Nonlinear propagation of self-guided ultra-short pulses in ionized gases, *Phys. Plasmas* **7**, 210-230 (2000).
- [13] L. Bergé, and S. Skupin, Self-channeling of ultrashort laser pulses in materials with anomalous dispersion, *Phys. Rev. E* **71**, 065601(R) (2005).
- [14] L. Bergé, S. Skupin, F. Lederer, G. Méjean, J. Yu, J. Kasparian, E. Salmon, J. P. Wolf, M. Rodriguez, L. Wöste, R. Bourayou, R. Sauerbrey, Multiple Filamentation of Terawatt Laser Pulses in Air, *Phys. Rev. Lett.* **92**, 225002(1-4) (2004).
- [15] L. Bergé, S. Skupin, R. Nuter, J. Kasparian, J.-P. Wolf, Ultrashort filaments of light in weakly-ionized, optically-transparent media, *Rep. Prog. Phys.* **70**, 1633-1684 (2007).
- [16] L. Bergé, Wave collapse in physics: principles and applications to light and plasma waves, *Phys. Rep.* **303**, 259-370 (1998).
- [17] F. Bloom, *Mathematical Problems of Classical Nonlinear Electromagnetic Theory*, Chapman & Hall/CRC, New York, 1993.
- [18] N. N. Bogoliubov, and D. V. Shirkov, Charge Renormalization Group in Quantum Field Theory, *Nuovo Cim.* **3**, 845-863 (1956).
- [19] N. N. Bogoliubov and D. V. Shirkov, On Renormalization Group in Quantum Electrodynamics, *Dokl. Akad. Nauk. SSSR* **103**, 203-206 (1955); *ibid.*, **103**, 391-394 (1955) (in Russian).
- [20] A. B. Borisov, A. V. Borovskiy, O. B. Shiryayev, V. V. Korobkin, A. M. Prokhorov, J. C. Solem, T. S. Luk, K. Boyer, C. K. Rhodes, Relativistic and charge-displacement self-channeling of intense ultrashort laser pulses in plasmas, *Phys. Rev. A* **45**, 5830-5845 (1992).
- [21] R. W. Boyd, *Nonlinear Optics*, (Academic Press, Amsterdam, Tokyo, 2003).
- [22] T. Brabec and F. Krausz, Nonlinear Optical Pulse Propagation in the Single-Cycle Regime, *Phys. Rev. Lett.* **78**, 3282(1-4) (1997).
- [23] N. M. Bulgakova, R. Stoian, A. Rosenfeld, I. V. Hertel, and E. E. Campbell, Electronic transport and consequences for material removal in ultrafast pulsed laser ablation of materials, *Phys. Rev. B* **69**, 054102(1-6) (2004).

- [24] S. Champeaux, L. Bergé, D. Gordon, A. Ting, J. Peñano, P. Sprangle, (3+1)-dimensional numerical simulations of femtosecond laser filaments in air: Toward a quantitative agreement with experiments, *Phys. Rev. E* **77** 036406(1-6) (2008).
- [25] S. Chávez Cerda, S. B. Cavalcanti, J. M. Hickmann, A variational approach of nonlinear dissipative pulse propagation, *Euro. Phys. J. D* **1**, 313-316 (1998).
- [26] C.-C. Cheng, E. M. Wright, and J. V. Moloney, Generation of Electromagnetic Pulses from Plasma Channels Induced by Femtosecond Light Strings, *Phys. Rev. Lett.* **87**, 213001(1-4) (2001).
- [27] C.-C.Cheng, E. M. Wright, and J. V. Moloney, Cheng, Wright, and Moloney Reply: *Phys. Rev. Lett.* **89**, 139302 (2002).
- [28] R. Y. Chiao, E. Garmire, and C. H. Townes. Self-trapping of optical beams. *Phys. Rev. Lett.* **13**, 479482 (1964).
- [29] A. Chiron, B. Lamouroux, R. Lange, J.-F. Ripoche, M. Franco, B. Prade, G. Bonnaud, G. Riazuelo, and A. Mysyrowicz, Numerical simulations of the nonlinear propagation of femtosecond optical pulses in gases, *Eur. Phys. J. D* **6**, 383-396 (1999).
- [30] A. Couairon, A. Mysyrowicz, Femtosecond filamentation in transparent media, *Phys. Rep.* **441**, 47-189 (2007).
- [31] A. Couairon, L. Sudrie, M. Franco, B. Prade, A. Mysyrowicz, Filamentation and damage in fused silica induced by tightly focused femtosecond laser pulses, *Phys. Rev. B* **71**, 125435(1-11) (2005).
- [32] C. Degoulet, R. Perrinaud, A. Ajdari, J. Prost, H. Benoit, and M. Bourrel, Self-Focusing in Gradient Liquid Adsorption Chromatography of Polymers, *Macromolecules* **34**, 2667-2672 (2001).
- [33] Y. P. Deng, X. H. Xie, H. Xiong, Y. X. Leng, C. F. Cheng, H. H. Lu, R. X. Li, and Z. Z. Xu, Optical breakdown for silica and silicon with double femtosecond laser pulses, *Opt. Express* **13**, 30963103 (2005).
- [34] J.-C. Diels, W. Rudolph, *Ultrashort Laser Pulse Phenomena*, (Elsevier, Amsterdam, 2006).
- [35] L. Englert, B. Rethfeld, L. Haag, M. Wollenhaupt, C. Sarpe-Tudoran and T. Baumert, Control of ionization processes in high band gap materials via tailored femtosecond pulses, *Opt. Express* **15**, 17855 (2007).

- [36] L. Englert, B. Rethfeld, L. Haag, M. Wollenhaupt, C. Sarpe-Tudoran and Th. Baumert, Tailored femtosecond pulses for nanoscale laser processing, Presentation, Aachen 2007.
- [37] European XFEL, <http://www.xfel.eu/>
- [38] P. A. Franken, J. F. Ward, Optical Harmonics and Nonlinear Phenomena, Rev. Mod. Phys. **35**, 23-39 (1963).
- [39] G. Fibich, Some Modern Aspects of Self-Focusing Theory in Self-Focusing: Past and Present, R.W. Boyd, S.G. Lukishova, Y.R. Shen, editors, (Springer Series: Topics in Applied Physics , Vol. 114, 605p. 2009).
- [40] G. Fibich, Self focusing in the damped nonlinear Schrodinger equation, SIAM Journal on Applied Mathematics **61**, 1680-1705, (2001).
- [41] G. Fibich and B. Ilan, Optical light bullets in a pure Kerr medium, Optics Letters **29**, 887-889 (2004).
- [42] G. Fibich and B. Ilan, Self focusing of elliptic beams: An example of the failure of the aberrationless approximation, J. Opt. Soc. A B **17**, 1749-1758, (2000).
- [43] G. Fibich, B. Ilan, and S. Tsynkov, Computation of Nonlinear Backscattering Using a High-Order Numerical Method, J. Sci. Comput. **17**, 351-364. (2002).
- [44] G. Fibich and G. C. Papanicolaou, Self-focusing in the perturbed and unperturbed nonlinear Schrodinger equation in critical dimension SIAM Journal on Applied Mathematics **60**, 183-240, (1999).
- [45] G. Fibich and G. C. Papanicolaou, A modulation method for self-focusing in the perturbed critical nonlinear Schrodinger equation, Phys. Lett. A **239**, 167-173, (1998).
- [46] G. Fibich and G. C. Papanicolaou, Self-focusing in the presence of small time dispersion and nonparaxiality, Optics Letters **22**, 1379-1381, (1997).
- [47] G. Fibich, W. Ren and X. P. Wang, Numerical simulations of self focusing of ultrafast laser pulses, Physical Review E **67**, 056603 (2003).
- [48] G. Fibich, Sh. Eisenmann, I. Boaz, Y. Erlich, M. Fraenkel, Z. Henis, A. Gaeta, A. Zigler, Self-focusing distance of very high power laser pulses, Opt. Express **13**, 5897-5903 (2005).
- [49] L. Gagnon and P. Winternitz, Lie symmetries of a generalised nonlinear Schrodinger equation: I. The symmetry group and its subgroups, J. Phys. A: Math. Gen. **21**, 1493-1511 (1988).

- [50] L. Gagnon and P. Winternitz, Lie symmetries of a generalised non-linear Schrodinger equation. II. Exact solutions. *J. Phys. A: Math. Gen.* **22**, 469-497 (1989).
- [51] E. G. Gamaly, S. Juodkazis, K. Nishimura, H. Misawa, B. Luther-Davies, L. Hallo, Ph. Nicolai, and V. T. Tikhonchuk, Laser-matter interaction in the bulk of a transparent solid: Confined microexplosion and void formation, *Phys. Rev. B* **73**, 214101(1-10) (2006).
- [52] N. Gavish, G. Fibich, L. T. Vuong, A. L. Gaeta, Predicting the filamentation of high-power beams and pulses without numerical integration: A nonlinear geometrical optics method, *Phys. Rev. A* **78**, 043807(1-16) (2008).
- [53] M. Gell-Mann and F. Low, Quantum Electrodynamics at Small Distances, *Phys. Rev.* **95**, 1300-1312 (1954).
- [54] E. N. Glezer, L. Huang, R. J. Finley, T.-H. Her, J. P. Callan, C. Schaer, and E. Mazur, Ultrafast laser-induced microexplosions in transparent materials, *Laser-Induced Damage in Optical Materials* **2966**, of Proc. SPIE, 392403 (1996).
- [55] A. N. Gorban, I. V. Karlin, A. Yu. Zinoviev, Constructive methods of invariant manifolds for kinetic problems, *Phys. Rep.* **396**, 197-403 (2004).
- [56] S. Henz, J. Herrmann, Two-dimensional spatial optical solitons in bulk Kerr media stabilized by self-induced multiphoton ionization: Variational approach, *Phys. Rev. E* **53**, 4092-4097 (1996).
- [57] N. H. Ibragimov, *CRC Handbook of Lie Group Analysis of Differential Equations* (CRC Press, Boca Raton, 1994).
- [58] S. Juodkazis, K. Nishimura, S. Tanaka, H. Misawa, E. G. Gamaly, B. Luther-Davies, L. Hallo, P. Nicolai, and V. T. Tikhonchuk, Laser-Induced Microexplosion Confined in the Bulk of a Sapphire Crystal: Evidence of Multimegabar Pressures, *Phys. Rev. Lett.* **96**, 166101(1-4) (2006).
- [59] V. P. Kandidov, O. G. Kosareva, I. S. Golubtsov, W. Liu, A. Becker, N. Aközbeck, C. M. Bowden, and S. L. Chin, Self-transformation of a powerful femtosecond laser pulse into a white-light laser pulse in bulk optical media (or supercontinuum generation), *Appl. Phys. B: Lasers & Optics* **77**, 149-165. (2003).
- [60] J. Kasparian, M. Rodriguez, G. Méjean, J. Yu, E. Salmon, H. Wille, R. Bourayou, S. Frey, Y. B. André, A. Mysyrowicz, R. Sauerbrey, J. P. Wolf, *Science* **301**, 61-64 (2003).

- [61] W. L. Kath, N. F. Smyth, Soliton evolution and radiation loss for the nonlinear Schrödinger equation, *Phys. Rev. E* **51**, 1484-1892 (1995).
- [62] A. Kaiser, B. Rethfeld, M. Vicanek, and G. Simon, Microscopic processes in dielectrics under irradiation by subpicosecond laser pulses, *Phys. Rev. B* **61**, 1143711450 (2000).
- [63] L. V. Keldysh, Ionization in the Field of a Strong Electromagnetic Wave, *Sov. Phys. JETP* **20**, 1307-1314 (1965).
- [64] P. L. Kelley, Self-Focusing of Optical Beams, *Phys. Rev. Lett.* **15**, 1005-1008 (1965).
- [65] M. Kitzler, J. Zanghellini, Ch. Jungreuthmayer, M. Smits, A. Scrinzi, and T. Brabec, Ionization dynamics of extended multielectron systems, *Phys. Rev. A* **70**, 041401(1-4) (2004).
- [66] N. E. Kosmatov, V. F. Shvets, V. E. Zakharov, Computer simulation of wave collapses in the nonlinear Schrödinger equation, *Physica D* **52**, 16-35 (1991).
- [67] V. F. Kovalev, V. Yu. Bychenkov, V. T. Tikhonchuk, Renormalization-group approach to the problem of light-beam self-focusing, *Phys. Rev. A* **61**, 033809(1-10) (2000).
- [68] V. F. Kovalev, Renormalization group analysis for singularities in the wave beam self-focusing problem, *Theor. Math. Phys.* **113**, 719-730 (1990).
- [69] V. F. Kovalev, Renormgroup symmetries in problems of nonlinear geometrical optics, *Theor. Math. Phys.* **111**, 686-702 (1997).
- [70] V. F. Kovalev, and V. V. Pustovalov, Group and renormgroup symmetry of a simple model for nonlinear phenomena in optics, gas dynamics and plasma theory, *Mathem. Comp. Modelling* **25**, 165-179 (1997).
- [71] V. F. Kovalev, and V. V. Pustovalov, Functional self-similarity in a problem of plasma theory with electron nonlinearity, *Theor. Math. Physics* **81**, 1060-1071 (1990).
- [72] V. F. Kovalev, V. V. Pustovalov, Strong nonlinearity and generation of high harmonics in laser plasma, in *Proceedings contributed papers (of the Int. Conf. on Plasma Physics, Kiev, USSR, April 6-12, 1987)*, Ed. A.G. Sitenko (Naukova Dumka, Kiev, 1987), **1**, 271-273.
- [73] V. F. Kovalev, V. V. Pustovalov, D. V. Shirkov, Group analysis and renormgroup, *Comm. JINR, Dubna* (1995), P5-95-447 (in Russian).

- [74] V. F. Kovalev, V. V. Pustovalov and D. V. Shirkov, Group analysis and renormgroup symmetries, *J. Math. Phys.* **39**, 1170-1188 (1998).
- [75] V. F. Kovalev, and V. V. Pustovalov, Lie algebra of renormalization group admitted by initial value problem for Burgers equation, *Lie Groups and their Applications* **1**, No 2, 104-120 (1994).
- [76] V. F. Kovalev, V. V. Pustovalov, Functional self-modeling in a nonlinear plasma theory, *Soviet Physics – Lebedev Institute Reports*, No. 3, 54-57 (1989).
- [77] V. F. Kovalev, V. V. Pustovalov, Symmetry group of nonlinear one-dimensional equations of electron plasma, *Soviet Physics – Lebedev Institute Reports*, No. 2, 28-31 (1991).
- [78] V. F. Kovalev and D. V. Shirkov, Renorm-group symmetry for functionals of boundary value problem solutions, *J. Phys. A: Math. Gen.* **39**, 8061-8073 (2006).
- [79] V. F. Kovalev and D. V. Shirkov, Renormgroup symmetries for solutions of nonlinear boundary value problems, *Physics Uspekhi*, **51**, 815 (2008).
- [80] Y. Kuramoto, *Chemical oscillations, waves, and turbulence* (Springer, Berlin, 1984).
- [81] N. Kuriyama and Y. Ito, Third international symposium on laser precision microfabrication, vol. 4830 of *Proceedings of SPIE*, (Bellingham, WA), pp. 567572, SPIE, 2003.
- [82] M. Lenzner, J. Krüger, S. Sartania, Z. Cheng, C. Spielmann, G. Mourou, W. Kautek, and F. Krausz, Femtosecond Optical Breakdown in Dielectrics, *Phys. Rev. Lett.* **80**, 40764079 (1998).
- [83] M. Lenzner, J. Krger, S. Sartania, Z. Cheng, Ch. Spielmann, G. Mourou, W. Kautek, and F. Krausz *Phys. Rev. Lett.* **80**, 4076 (1998).
- [84] M. Li, S. Menon, J. P. Nibarger, and G. N. Gibson, Ultrafast Electron Dynamics in Femtosecond Optical Breakdown of Dielectrics, *Phys. Rev. Lett.* **82**, 23942397 (1999).
- [85] V. N. Lugovoi, and A. M. Prokhorov, Theory of the propagation of high-power laser radiation in a nonlinear medium, *Sov. Phys. Usp.* **16**, 658-679 (1974).
- [86] J. H. Marburger, Self-focusing: Theory, *Prog. Quant. Electron.* **4** 35-110 (1975).

- [87] F. Merle. On uniqueness and continuation properties after blow-up time of self-similar solutions of nonlinear Schrödinger equation with critical exponent and critical mass. *Comm. Pure Appl. Math.* **45**, 203254 (1992).
- [88] F. Merle. Determination of blow-up solutions with minimal mass for nonlinear Schrödinger equation with critical power. *Duke Math. J.* **69**, 427454, (1993).
- [89] E. T. J. Nibbering, P. F. Curley, G. Grillon, B. S. Prade, M. A. Franco, F. Salin, and A. Mysyrowicz, Conical emission from self-guided femtosecond pulses in air, *Opt. Lett.* **21**, 62-65 (1996).
- [90] P. J. Olver, *Applications of Lie groups to differential equations*, (Springer-Verlag, N. Y., 1986).
- [91] L. V. Ovsiannikov, *Group analysis of differential equations*, (Academic Press, N.-Y., 1982).
- [92] G. Paltauf and P. E. Dyer, Photomechanical Processes and Effects in Ablation, *Chem. Rev.* **103**, 487-518 (2003).
- [93] J. R. Peñano, P. Sprangle, B. Hafizi, A. Ting, D. F. Gordon, and C. A. Kapetanakos, Propagation of ultra-short, intense laser pulses in air, *Phys. Plasmas* **11**, 2865 (2004).
- [94] A. M. Perelomov, V. S. Popov, and M. V. Terentev, Ionization of atoms in alternating electric field, *Sov. Phys. JETP* **23**, 924-934 (1966).
- [95] J. J. Rasmussen, K. Rypdal, Blow-up in Nonlinear Schroedinger Equations-I A General Review, *Phys. Scripta* **33**, 481-497 (1986).
- [96] B. Rethfeld, Unied model for the free-electron avalanche in laser-irradiated dielectrics, *Phys. Rev. Lett.* **92**, 187401(1-4) (2004).
- [97] . B. Rethfeld, Free-electron generation in laser-irradiated dielectrics, *Phys. Rev. B* **73**, 035101(1-6) (2006).
- [98] J. F. Ripoche, G. Grillon, B. Prade, M. Franco, E. Nibbering, R. Lange, and A. Mysyrowicz, Determination of the time dependence of n_2 in air, *Opt. Commun.* **135**, 310-314 (1997).
- [99] W. Sellmeier, Theorie der anomal Licht-Dispersion, *Annalen der Physik und Chemic* **143**, 272-8 (1871).
- [100] D. V. Shirkov, The renormalization group, the invariance principle, and functional self-similarity, *Sov. Phys. Doklady*, **27**, 197-203 (1982).

- [101] D. V. Shirkov, Renormalization Group Symmetry and Sophus Lie Group Analysis, *Intern. J. Mod. Physics C* **6**, 503-512 (1995).
- [102] D. V. Shirkov, V. F. Kovalev, The Bogoliubov renormalization group and solution symmetry in mathematical physics, *Phys. Rep.* **352**, 219-249 (2001).
- [103] S. Skupin, L. Bergé, Self-guiding of femtosecond light pulses in condensed media: Plasma generation versus chromatic dispersion, *Physica D: Nonlinear Phenomena*, **220**, 14-30 (2006).
- [104] P. Sprangle, J. R. Peñano, and B. Hafizi, Propagation of intense short laser pulses in the atmosphere, *Phys. Rev. E* **66**, 046418(1-22) (2002).
- [105] P. Sprangle, J. R. Peñano, B. Hafizi, and C. A. Kapetanacos, Ultrashort laser pulses and electromagnetic pulse generation in air and on dielectric surfaces, *Phys. Rev. E* **69**, 066415(1-18) (2004).
- [106] K. Stelmaszczyk, Ph. Rohwetter, G. Méjean, Jin Yu, E. Salmon, J. Kasparian, R. Ackermann, J.-P. Wolf, and L. Wöste, Long-distance remote laser-induced breakdown spectroscopy using filamentation in air, *Appl. Phys. Lett.*, **85**, 3977-3981 (2004).
- [107] B. C. Stuart, M. D. Feit, A. M. Rubenchik, B. W. Shore, and M. D. Perry, Laser-Induced Damage in Dielectrics with Nanosecond to Subpicosecond Pulses, *Phys. Rev. Lett.* **74**, 22482251 (1995).
- [108] B. C. Stuart, M. D. Feit, S. Herman, A. M. Rubenchik, B. W. Shore, and M. D. Perry, Nanosecond-to-femtosecond laser-induced breakdown in dielectrics, *Phys. Rev. B* **53**, 1749-1761 (1996).
- [109] E. E. C. Stueckelberg and A. Petermann, La normalisation des constantes dans la theorie des quanta, *Helv. Phys. Acta* **22**, 499-520 (1953) (in French).
- [110] L. Sudrie, A. Couairon, M. Franco, B. Lamourpux, B. Prade, S. Tzortzakis, A. Mysyrowiez, Femtosecond Laser-Induced Damage and Filamentary Propagation in Fused Silica, *Phys. Rev. Lett.* **89** 186601(1-4) (2002).
- [111] V. I. Talanov. Focusing of light in cubic media. *JETP Lett.* **11**, 199201 (1970).
- [112] L. L. Tatarinova, M. E. Garcia, Analytical theory for the propagation of laser beams in nonlinear media, *Phys. Rev. A* **76**, 043824(1-8) (2007).
- [113] L. L. Tatarinova, M. E. Garcia, Exact solutions of the eikonal equations describing self-focusing in highly nonlinear geometrical optics, *Phys. Rev. A* **78**, 021806(R)(1-4) (2008).

- [114] V. V. Temnov, K. Sokolowski-Tinten, P. Zhou, A. El-Khamhawy, and D. von der Linde, Multiphoton Ionization in Dielectrics: Comparison of Circular and Linear Polarization, *Phys. Rev. Lett.* **97**, 237403 (2006).
- [115] S. Tzortzakis, L. Bergé, A. Couairon, M. Franco, B. Prade, and A. Mysyrowicz, Breakup and Fusion of Self-Guided Femtosecond Light Pulses in Air, *Phys. Rev. Lett.* **86**, 5470-5473 (2001).
- [116] S. Tzortzakis, L. Sudrie, M. Franco, B. Prade, A. Mysyrowicz, A. Couairon, L. Bergé, Self-Guided Propagation of Ultrashort IR Laser Pulses in Fused Silica, *Phys. Rev. Lett.* **87**, 213902(1-4) (2001).
- [117] E. Vanagas, J. Kawai, D. Tuzhilin, I. Kudryashov, A. Mizuyama, K. Nakumara, K. Kondo, S. Koshihara, M. Takesada, K. Matsuda, S. Joudkakis, V. Jarutis, S. Matsuo, and H. Misawa, Glass cutting by femtosecond pulsed irradiation, *J. Microlith., Microfab., Microsyst.*, **3**, 358363 (2004).
- [118] H. Varel, D. Ashkenasi, A. Rosenfeld, M. Wähmer, and E. E. B. Campbell, Micromachining of quartz with ultrashort laser pulses, *Appl. Phys. A* **65**, 367373 (1997).
- [119] A. Vinçotte, L. Bergé, Femtosecond Optical Vortices in Air, *Phys. Rev. Lett.* **95**, 193901(1-4) (2005).
- [120] A. M. Weiner, Femtosecond pulse shaping using spatial light modulators, *Rev. Sci. Instrum.* **71**, 19291960 (2000).
- [121] M.I. Weinstein. Nonlinear Schrödinger equations and sharp interpolation estimates. *Comm. Math. Phys.* **87**, 567576 (1983).
- [122] K. Wilson, Renormalization Group and Critical Phenomena, *Phys. Rev. B* **4**, 3184-3205 (1971).
- [123] O. C. Wright, M. G. Forest, K. T.-R. McLaughlin, On the exact solution of the geometric optics approximation of the defocusing nonlinear Schrödinger equation, *Phys. Lett. A* **257**, 170-174 (1991).
- [124] T.-T. Xi, X. Lu, J. Zhang, Interaction of Light Filaments Generated by Femtosecond Laser Pulses in Air, *Phys. Rev. Lett.* **96** 025003(1-4) (2006).
- [125] V. E. Zakharov, A. B. Shabat, Exact theory of two-dimensional self-focusing and one-dimensional self-modulation of waves in nonlinear media, *Sov. Phys. JETP* **34**, 62-79 (1971).

- [126] J. Zhang, K. Kasala, A. Rewari, and K. Saravanamuttu, Self-Trapping of Spatially and Temporally Incoherent White Light in a Photochemical Medium, *J. Am. Chem. Soc.* **128**, 406-407 (2006).
- [127] A. A. Zozulya, S. A. Diddams, A. G. Van Engen, and T. S. Clement, Propagation Dynamics of Intense Femtosecond Pulses: Multiple Splittings, Coalescence, and Continuum Generation, *Phys. Rev. Lett.* **82**, 1430-1433 (1999).
- [128] D. Zubarev, V. Morosov, and G. Röpke, *Statistical Mechanics of Nonequilibrium Processes*, (Akademie Verlag, Berlin, Vol. 1. 1996).

List of Publications

During the period of this thesis work, I finished four papers which have been published and submitted for publication. A list of these publications is shown below.

1. L. L. Tatarinova and M. E. Garcia, *Analytical theory for the propagation of laser beams in nonlinear media*, Phys. Rev. A **76** 043824 (2007).
2. L. L. Tatarinova and M. E. Garcia, *Exact solutions of the eikonal equations describing self-focusing in highly nonlinear geometrical optics*, Phys. Rev. A **78** 021806(R) (2008).
3. L. L. Tatarinova and M. E. Garcia,
Light propagation in media and materials with highly nonlinear response: an analytical study,
Physica D, submitted (2009).
4. L. L. Tatarinova and M. E. Garcia,
Nonlinear beam collapse studied using different degrees of approximation to the refractive index,
Phys. Lett. A, submitted (2009).

The publications which did not contribute to the thesis

1. A. G. Szykh, E. A. Tarakanova, L. L. Tatarinova, *Laser-induced reduction of a dye characterized by a high triplet-state yield and dissolved in a polymer*, Quantum Electronics, **30** (1), 40-44, (2000).
2. A. N. Gorban, I. V. Karlin, H. C. Öttinger, and L. L. Tatarinova, *Ehrenfest's argument extended to a formalism of nonequilibrium hermodynamics*, Phys.Rev.E **63**, 066124(1-6) (2001).
3. I. V. Karlin, L. L. Tatarinova, A. N. Gorban and H. C. Öttinger, *Irreversibility in the short memory approximation*, Physica A **327** 399-424 (2003).
4. E. S. Zijlstra, L. L. Tatarinova, and M. E. Garcia, *Laser-induced phonon-phonon interactions in bismuth*, Phys. Rev. B **74**, 220301 (2006).

5. E. S. Zijlstra, L. L. Tatarinova, and M. E. Garcia, *Ab-initio study of coherent phonons excited by femtosecond laser pulses in Bismuth*, Proc. SPIE **6261**, 62610R (2006).

Acknowledgments

First of all I would like to express my deepest gratitude to my supervisor Prof. Dr. Martin E. Garcia for unique opportunity to fulfill this work. Without his advice and support I would not be able to obtain results presented in the dissertation.

I am deeply indebted to Prof. Dr. Vladimir F. Kovalev for the joint work, whose results formed a basis for Chapter 5 and scientific correspondence that deepened my understanding of the renormalization group symmetry analysis and other methods of mathematical physics.

I thank Prof. Dr. Thomas Baumert and Lars Englert for useful discussions and the tolerance they manifested concerning the time I required for the acquaintance with the material.

Taking the opportunity I would like to express my gratitude to Prof. Dr. Alexander N. Gorban, Dr. Iliya Karlin and Prof. Dr. Hans Christian Öttinger for their contribution to my life on both scientific as well as everyday levels, my education and the general perception of modern theoretical physics that was formed during communications with them.

I am thankful to the Theoretical Physics Group of Uni-Kassel for the benevolent and helpful atmosphere that surrounded me throughout these years and my special thanks to Dr. Josef Anton, Prof. Dr. Burkhard Fricke, Dr. Dima Gridnev, Prof. Dr. Gustavo Pastor, Dr. Alexander Uvarov for the interest in my work and useful comments.

I am grateful to my husband Dr. Kirill M. Shekhter, whose love and care were an invaluable support for me during all the years of our acquaintance. Special thanks are also to my parents, parents-in-law, and friends for their love and support.

Erklärung

Hiermit versichere ich, daß ich die vorliegende Dissertation selbständig und ohne unerlaubte Hilfe angefertigt und andere als die in der Dissertation angegebenen Hilfsmittel benutzt habe. Alle Stellen, die wörtlich oder sinngemäß aus veröffentlichten oder unveröffentlichten Schriften entnommen sind, habe ich als solche kenntlich gemacht. Kein Teil dieser Arbeit ist in einem anderen Promotions- oder Habilitationsverfahren verwendet worden.

Juli 2009, Kassel

Larisa Tatarinova

Curriculum Vitae

Personal Data

Name Larisa Tatarinova
Date of Birth January 23, 1973
Place of Birth Barnaul, Russia

School education

Sep. 1980 – May. 1983 Primary school, Krasnoyarsk
Sep. 1983 – May. 1988 Secondary school, Krasnoyarsk
Sep. 1988 – Jun. 1990 Higher school, Krasnoyarsk

University education

Sep. 1991 – Jun. 1996 Physics Department, Krasnoyarsk State University
Jun. 1996 Diploma (*with honor*), speciality "Physics"
major "Quantum Electronics"

Employment

Dez. 1995 – Nov. 1998 engineer, Krasnoyarsk State University,
Krasnoyarsk, Russia
Dez. 1998 – Mar. 2000 engineer-researcher, Institute
of Computational Modeling, Krasnoyarsk, Russia
Apr. 2000 – Jun. 2001 assistant, Institute of Polymer, ETH Zürich,
Switzerland
Jul. 2001 – Nov. 2004 engineer-researcher, Kirensky
Institute of Physics, Krasnoyarsk, Russia
Dez. 2004 – Jul. 2009 PhD student, University of Kassel,
Kassel, Germany